

April 2020

A Data-Driven Model for Multiphase Flow in Pipes

Francisco Bruno Xavier Teles

Louisiana State University and Agricultural and Mechanical College

Follow this and additional works at: https://digitalcommons.lsu.edu/gradschool_theses



Part of the [Other Engineering Commons](#)

Recommended Citation

Xavier Teles, Francisco Bruno, "A Data-Driven Model for Multiphase Flow in Pipes" (2020). *LSU Master's Theses*. 5110.

https://digitalcommons.lsu.edu/gradschool_theses/5110

This Thesis is brought to you for free and open access by the Graduate School at LSU Digital Commons. It has been accepted for inclusion in LSU Master's Theses by an authorized graduate school editor of LSU Digital Commons. For more information, please contact gradetd@lsu.edu.

A DATA-DRIVEN MODEL FOR MULTIPHASE FLOW IN PIPES

A Thesis

Submitted to the Graduate Faculty of the
Louisiana State University and
Agricultural and Mechanical College
in partial fulfillment of the
requirements for the degree of
Master of Science in Petroleum Engineering

in

The Craft & Hawkins Department of Petroleum Engineering

by

Francisco Bruno Xavier Teles
B.S., Universidade Federal do Ceara, 2017
May 2020

Acknowledgments

I would like to express my gratitude to my advisor Dr. Paulo Waltrich for providing me the great opportunity of joining the Petroleum Engineering Graduate Program at LSU. I feel honored to have him as an advisor. His support, patience, and encouragement were important to me and are highly appreciated.

I appreciate Dr. Ipsita Gupta and Dr. Richard Hughes for serving as committee members. Their time, feedback and suggestions along my thesis project are appreciated. I also thank Jeanette Wooden and Janet Dugas for the administrative support during the past couple of years.

Special thanks to my parents, Solange X Aragão and Antônio A Teles; grandmother Alice J Aragão, my sister, Rafaela Xavier, for supporting and always believing in me. My family's care and efforts to provide me good education were essential for me and are greatly appreciated. I am very grateful for the love and support of my fiancée, Ligia Tornisiello. I am glad to have had her on this journey with me and shared many great experiences.

I would like to thank my research group colleagues and all the great friends that I met in Baton Rouge for making my past years more enjoyable. Special thanks to Renato Coutinho and Erika Pagan for all support and great friendship.

Table of Contents

Acknowledgments.....	ii
List of Tables	v
List of Figures	vi
Abstract	ix
1. Introduction.....	1
1.1. Aspects of the Problem.....	1
1.2. Objectives	3
1.3. Thesis Outline.....	4
2. Literature Review.....	5
2.1. Flow Regimes	5
2.2. Liquid Holdup	9
2.3. Superficial and Phase Velocities	9
2.4. Pressure Gradient	10
2.5. Empirical Models for Multiphase Flow in Pipes.....	12
2.6. Mechanistic Models for Multiphase Flow in Pipes.....	15
2.7. Drift-Flux Models for Two-Phase Flow in Pipes.....	20
2.8. Future of Multiphase Flow Modeling	22
3. Evaluation of Multiphase Flow Models.....	26
3.1. Summary of Models Evaluation Results	27
3.2. Possible Causes of the Models Inaccuracies	34
3.3. Possible Solutions for Models Shortcomings.....	36
4. Fully Automated Flow Loop for Two-Phase in Pipes	37
4.1. Introduction	37
4.2. Test Sections and Instrumentation	38
4.3. Pressure and Temperature Measurements	43
4.4. Flow Regime Visualizations	48
4.5. Control and Data Acquisition System	49
4.6. Direct Experimental Simulation and Data-Driven Approach	50
5. Results and Discussion	56
5.1. Experimental Test Matrix.....	56
5.2. Entrance Effect Evaluation.....	57
5.3. Flow Regime Validation	59
5.4. Data-Driven Approach Applied to Liquid Holdup Followed by Pressure Gradient Predictions	63
5.5. Data-Driven Approach for Direct Calculation of Pressure Gradient	80
6. Conclusions and Recommendations for Future Work.....	85

Appendix. Teles and Waltrich (2018) Model Description.....	88
References.....	90
Vita.....	97

List of Tables

Table 2.1. Models and their applicability. Rao (1998); and Brill and Mukherjee (1999).	14
Table 3.1. Source and main characteristics of the database.....	27
Table 4.1. Flow Measurement Devices Specification.	39
Table 4.2. Pressure measurement instrumentation.	44
Table 5.1. Summary of the flow conditions of the experiments carried in this study.	56
Table 5.2. Training data for upward vertical (90°) and inclined (45°) flow performed in the short test section.....	66
Table 5.3. Drift-flux parameters obtained for vertical (90°) and inclined (45°) two-phase flow.	67
Table 5.4. Testing cases for vertical (90°) and inclined (45°) upward flow.....	69
Table 5.5. Testing cases for direct estimation of pressure gradient at vertical (90°) and inclined (45°) flow at different gas and liquid superficial velocities.....	82

List of Figures

Figure 2.1. Flow regimes for different inclination angles. Adapted from Shoham (2006).	6
Figure 2.2. Four main flow regimes for upward flow in a vertical pipe. Guet and Ooms (2005). 6	
Figure 2.3. Flow regimes map for vertical upward flow. Taitel et al. (1980).....	8
Figure 2.4. Pressure gradient curve for a constant liquid flow rate. (A) Represents vertical flow and typically flow regimes; (B) represents horizontal flow and typically flow regimes. ...	11
Figure 2.5. Minimum diameter for bubbly existence for water and air. Large diameter transition zone for Taylor bubbles existence.	17
Figure 2.6. Minimum diameter for bubbly existence for oil and natural gas. Large diameter transition zone for Taylor bubbles existence.	18
Figure 2.7. Evolution of flow models Shippen (2012).	23
Figure 3.1. Comparison of field bottomhole pressure and simulated bottomhole pressure for Reinicke et al. (1987) Field Data.	28
Figure 3.2. Average absolute error and standard deviation of the errors for Reinicke et al. (1987) Field Data. Error bars represent the standard deviation.	29
Figure 3.3. Average Absolute Error of pressure gradient in % for Flow Models for the LSU/PERTT Lab experimental data reported by Waltrich et al. (2017).	30
Figure 3.4. Overall average absolute error of pressure gradient in % for Flow Models for the LSU/PERTT Lab experimental data reported by Waltrich et al. (2017). Error bars represent the standard deviation.	30
Figure 3.5. Average absolute error of the simulated bottomhole pressure of the three different wells for Petrobras data.	31
Figure 3.6. Overall average absolute error of the simulated bottomhole pressure for Petrobras data. Error bars represent the standard deviation.	32
Figure 3.7. Average absolute error of the simulated bottomhole pressure for Asheim (1986) field data. Error bars represent the standard deviation.	33
Figure 3.8. Average absolute error of the simulated bottomhole pressure for Fancher and Brown (1963) field data. Error bars represent the standard deviation.	34
Figure 4.1. Inclined short test section (A) and long test section (B) illustration.	38
Figure 4.2. Short test section in the vertical position.	41

Figure 4.3. Short test section in the horizontal position.	42
Figure 4.4. Hoist system for the short test section.	42
Figure 4.5. Long test section description.	43
Figure 4.6. Example of a calibration curve representation for a pressure measurement device..	46
Figure 4.7. Snapshot of video recorded during experimental runs for Slug, Churn, and Annular for flow in a vertical pipe (90°).	48
Figure 4.8. Snapshot of video recorded during experimental runs for Plug, Slug, Stratified- wavy, Wavy-annular for flow in an inclined pipe (45°).	49
Figure 4.9. Snapshot of the control and data acquisition panel in LabVIEW 2017.	50
Figure 4.10. Pipe segmentation illustration.	51
Figure 4.11. Workflow for direct experimental simulation based on a data-driven approach. ...	52
Figure 4.12. Flowcharts of drift-flux and direct estimations of dp/dL approaches.	53
Figure 4.13. Drift-flux plot illustration.	54
Figure 5.1. Entrance effect analysis for flow regime and pressure gradient at different liquid and gas superficial velocities.	58
Figure 5.2. Validation of experimental flow regimes observation with Taitel et al. (1980) Aziz et al. (1972) vertical flow regime map.	60
Figure 5.3. Validation of experimental flow regimes observation with Duns and Ros (1963) empirical vertical flow regime map.	61
Figure 5.4. Validation of experimental flow regime observation at 45° with Barnea et al. (1985) empirical flow regime map for inclined pipes. This is a modification of Taitel et al. (1980) to account for pipe inclination.	63
Figure 5.5. Drift-flux plot for experimental runs on short flow section for vertical (90°) and inclined (45°) two-phase flow, Region I (1 – 4ft/s), Region II (4 – 20ft/s), Region III (20 – 40ft/s), All Ranges (1 – 40ft/s).....	65
Figure 5.6. Liquid holdup errors for each model in upward vertical (90°) flow having constant liquid superficial velocity ($v_{sl}=1.3\text{ft/s}$).	71
Figure 5.7. Liquid holdup errors for each model in upward inclined (45°) flow having constant liquid superficial velocity ($v_{sl}=1.17\text{ ft/s}$).....	71

Figure 5.8. Average absolute error of the liquid holdup for vertical (90°) and $vsl=1.3$ ft/s; inclined (45°) and $vsl=1.17$ ft/s. Error bars represent the standard deviation of liquid holdup calculation of all cases for each model and pipe inclination.	73
Figure 5.9. Pressure gradient errors in each model for upward vertical (90°) flow having constant liquid superficial velocity ($vsl=1.3$ ft/s).....	74
Figure 5.10. Pressure gradient errors in for each model for upward inclined (45°) flow having constant liquid superficial velocity ($vsl=1.17$ ft/s).....	75
Figure 5.11. Average absolute error of the pressure gradient for vertical (90°) and $vsl=1.3$ ft/s; inclined (45°) and $vsl=1.17$ ft/s. Error bars represent the standard deviation of pressure gradient calculation of all cases for each model and pipe inclination.	77
Figure 5.12. Results summary for liquid holdup calculation of all cases for all models in vertical (90°) and inclined (45°) two-phase flow. Dashed lines represent the $\pm 20\%$ error region.	78
Figure 5.13. Results summary for pressure gradient calculation of all cases for all models in vertical (90°) and inclined (45°) two-phase flow. Dashed lines represent the $\pm 20\%$ error region.	78
Figure 5.14. Flowchart for simplified transient multiphase flow model algorithm from Tornisiello (2020). Red box represents the step in which the data-driven approach can be implemented.....	80
Figure 5.15. Pressure gradient versus Ngv for constant NLv in vertical (90°) and inclined (45°) two-phase flow.....	81
Figure 5.16. Results summary for direct estimation of pressure gradient for all cases and other models in vertical (90°) and inclined (45°) two-phase flow. Dashed lines represent the $\pm 15\%$ error region.	82
Figure 5.17. Average absolute error of pressure gradient for the Data-Driven Approach, Beggs and Brill (1973), Duns and Ros (1965), Bhagwat and Ghajar (2014), Hagedorn and Brown (1965)	84
Figure A. Teles and Waltrich model workflow. The model uses Pagan et al. (2017) approach for churn and annular flow. The chosen sub model for bubbly and slug flow in this study is Duns and Ros (1963).	89

Abstract

Steady-state models commonly used to determine pressure gradient in wells are either empirical correlations or are dependent on empirical parameters correlated to specific flow conditions such as pressures, temperatures, fluid types, and pipe inclinations. The empirical nature of these models leads to limitations in predicting cases in a wide range of conditions. Established models may be delivering inaccurate results when applied at conditions beyond those which they were derived from. For instance, models available in the literature have shown to have limitations when used in large diameter pipes and high-velocity scenarios.

This work aims to evaluate different flow models with field and laboratory data and propose a data-driven modeling technique to determine liquid holdup and pressure gradient for a wide range of flowing scenarios. This methodology can be implemented either using drift-flux concepts or direct estimation of pressure gradient through data analytics techniques. A fully automated flow loop was designed and built to demonstrate how data can be generated in real-time to cover a wide range of pipe inclinations, and different liquid and gas velocities, without the need of flow regime estimation to accurately predict liquid holdup and pressure gradient.

The results from this work were compared with drift-flux and empirical models from the literature. Liquid holdup prediction using the data-driven approach resulted in errors at least 15% lower than the other models including in the comparison. While the estimation of pressure gradient based on existing data provided errors on average 10% lower than the other models evaluated.

This study showed that empirical and mechanistic models have limitations when are applied in flow conditions beyond their range of application. The drift-flux approach showed improvements but is not feasible to determine the pressure gradient for a wide range of flow

velocities. It was evident that the application of dimensionless numbers that account for the dynamics of two-phase flow to determine pressure gradient has the potential to improve multiphase flow modeling. The integration of automated flow loops, as the one built in this work, can improve data-driven models like the one proposed in this work.

1. Introduction

In the past seven decades, significant resources have been invested in multiphase flow modeling studies. A better understanding of how mixed phases flow inside wells, risers, and pipelines, and the determination of pressure drop along those are crucial for the petroleum, nuclear, and chemical industry. Given the significance of such studies, it is important that multiphase flow modeling be further improved due to its economic and environmental impact in several aspects, such as equipment design, drilling, production, flow assurance, and leak contention as in the case of blowouts. One specific example is the use of multiphase flow in pipes modeling on the prevention and remediation of blowouts in the oil and gas exploration and production in offshore environments. For instance, since the Macondo accident in 2010, the US Bureau of Ocean Energy Management (BOEM) requires Worst Case Discharge (WCD) reports from operators prior to drilling wells in several offshore locations in the United States. Such reports provide the calculations performed to determine the single highest liquid flow rate that would occur during an expected event, as defined by SPE (2015). The use of modeling tools for multiphase flow in pipes is one of the key components in the preparation of such reports.

1.1. Aspects of the Problem

Most of the empirical multiphase flow models currently available were developed back in the 1970s and 1980s, and rely mainly on curve fitting of large amount of data obtained with certain degree of accuracy (Duns & Ros, 1963; Orkiszewski, 1967; Hagedorn & Brown, 1965; Beggs & Brill 1973; Mukherjee & Brill, 1985). These models are based on correlations derived from experiments performed in limited flow conditions, such as type of fluids, pressure, temperature, diameters, inclinations, and flow rates. The other class of models, called mechanistic models, first predicts the occurring flow regime (or flow pattern) and then accounts for its mechanisms in order

to calculate the fluid fractions and the pressure gradient (Brill & Mukherjee, 1999; Ansari et al., 1994). Although improvements have been achieved in the last seven decades, these mechanistic models are also dependent on experiment-derived parameters. Very often these mechanistic models are used outside the range of flow conditions in which these experiment-derived parameters are derived from (Waltrich et al., 2014). Consequently, the empirical nature of these mechanistic models implies that unpredictable errors are expected when they are applied for this flow conditions beyond their range of application.

Moreover, flow regimes determination is still up-to-this-date a subjective field that relies mainly on visual observations of flow regime in laboratory experiments. The subjective nature of flow regime observations can lead to inaccuracies on flow modeling due to misinterpretations of flow regimes, and frequently, it has caused discordances regarding the existence of some flow regimes. For instance, according to Govier and Aziz (2008), churn flow has not been the subject to an extensive experimental study, and it has usually not been treated as a separate flow regime. Instead, churn flow regime is often treated as a modified form of slug flow regime.

Both empirical and mechanistic multiphase flow models are used daily in the field by engineers in a wide range of scenarios. Therefore, it is essential to address the existing gaps in multiphase flow modeling caused by the empirical nature of parameters in the models.

In recent years, the application of advanced analytic techniques in gas-liquid two-phase flow has tried to overcome some of these limitations. Efforts have increased on the implementation of predictive methods to determine flow regime and liquid holdup, such as the work from Osman (2004), Al-Naser et al. (2015), and Al-Naser et al. (2016).

Kanin et al. (2019) developed a model that, besides flow regime and liquid holdup, can also predict the pressure gradient based on existing data using Machine Learning algorithms. However, their model still needs liquid holdup and flow regimes derived from laboratory data (which consequently limits the range of application of models). The application of data-driven modeling in multiphase flow in pipes is believed to have a considerable potential to overcome challenges in this area of study when applied appropriately.

Motivated by the fact that up to this date there is no model suitable for a wide range of conditions as the ones encountered in the oil and gas industry, this work will focus on evaluating existing models and employing a data-driven methodology that can improve multiphase flow modeling. This work will investigate the performance of some models under large diameters and high velocities scenarios and evaluate how an inaccurate prediction of flow regimes can impact the results of the pressure gradient. In addition to that, experimental data generated in a fully automated experimental flow-loop (described in Chapter 4) will be used to evaluate the flow regime independent data-driven modeling method proposed in this study.

A literature review of the mechanistic and empirical models which were briefly mentioned in this chapter along with the description of other types of models, so-called drift-flux approach, will be described in the next chapter as well.

1.2. Objectives

The objective of this work is to develop and evaluate a data-driven modeling approach to estimate liquid holdup and pressure gradient for multiphase flow in pipes. In order to achieve this objective, the following tasks are carried out:

- Literature review on the current limitations of the models applied to multiphase flow in pipes.
- Gather experimental and field data to evaluate several multiphase flow models widely used in the oil and gas industry for a wide range of flowing scenarios. The data will be used to evaluate the current deficiencies of the models available in the literature and commercial packages.
- Design and construction of an automated experimental flow section capable of performing experiments from fully horizontal to fully vertical upward two-phase flow. This experimental setup is used to demonstrate how a fully automated facility for two-phase flow in pipes can be used to generate high-quality data in a continuous manner.
- Compare the performance of the data-driven approach with models found in the literature.

1.3. Thesis Outline

This thesis is divided into six chapters. Chapter 1 presents a brief introduction to the problem, motivations, and objectives of this research. Chapter 2 consists of the literature review of the main multiphase flow concepts, models and their limitations. Chapter 3 describes the main results of an extensive study of several multiphase flow models using several field and laboratory data. Chapter 4 describes the main features of the fully automated experimental flow loop, capable of determining pressure drop at all inclinations, which was built to prove the concept of continuous data acquisition for data-driven modeling of two-phase flow in pipes. Chapter 5 presents the results and discussion for the experiments carried out at the flow loop facility described in Chapter 4. Chapter 6 presents the conclusions and recommendations for future work.

2. Literature Review

This chapter is subdivided into nine sections. The first section describes the main flow regime (patterns) for gas-liquid two-phase flow in vertical pipes and addresses the main challenges on the flow regimes determination for multiphase flow modeling. Important flow parameters, such as liquid holdup, superficial and phase velocities, and pressure gradient are defined in Sections 2.2, 2.3, and 2.4. Sections 5 and 6 outline the steady-state empirical and mechanistic models available in the literature. The focus of these two sections is to provide a summary of the main models and their limitations. A description of the drift-flux models is included in Section 7. Finally, Section 8 reviews the main perspectives for the future of multiphase flow modeling and describes what has been done in terms of the applicability of advanced data-driven techniques towards this area.

2.1. Flow Regimes

Since mechanistic and many empirical flow models are flow regime dependent, the appropriate flow regime determination is a crucial part of two-phase flow modeling. Two-phase flow regimes are described by Shoham (2006) as a group of similar geometrical distribution of the gas and liquid phases in a pipe during a two-phase flow. The phase's distribution is determined by the main forces governing multiphase flow, which are: buoyancy, inertia, gravity, and surface tension. The axial distribution of gas and liquid phases can be considerably affected by pipe inclinations and phase velocities. Figure 2.1 illustrates flow regimes for different inclinations.

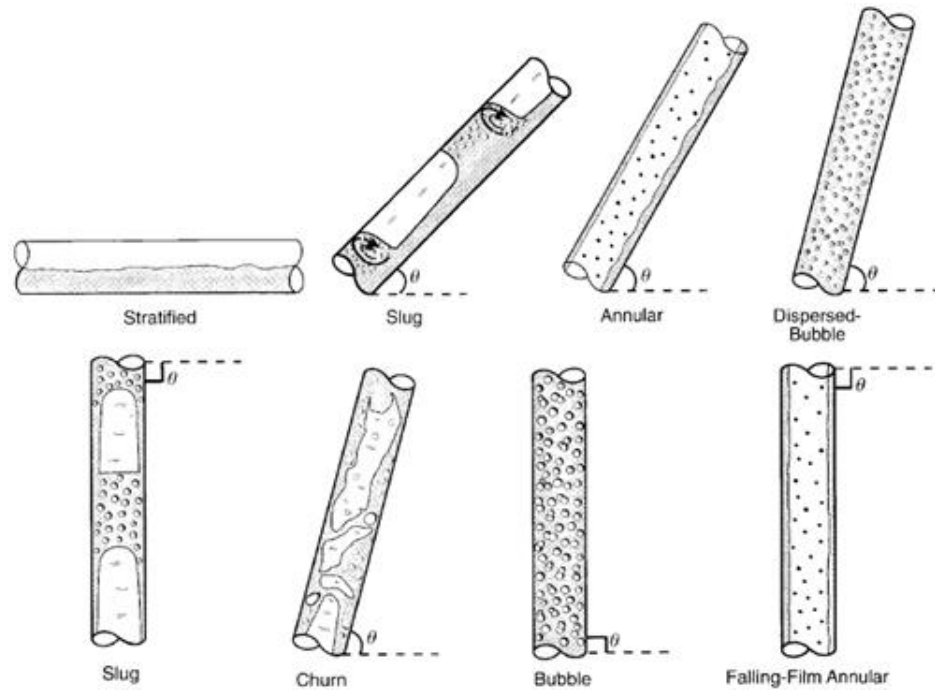


Figure 2.1. Flow regimes for different inclination angles. Adapted from Shoham (2006).

Although it is possible to find several different classifications of flow regimes throughout the literature, there are four classical flow regimes for vertical upward gas-liquid two-phase flow in pipes, namely bubbly, slug, churn, and annular. Figure 2.2 summarizes the representation of the typical flow regimes for upward vertical flow.

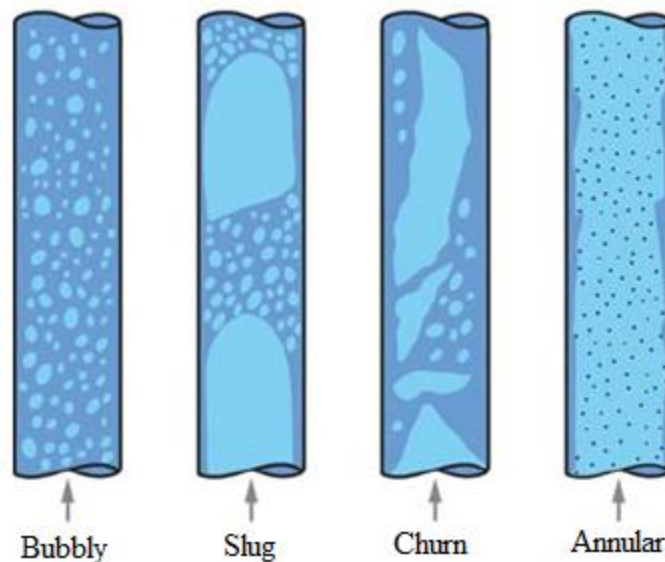


Figure 2.2. Four main flow regimes for upward flow in a vertical pipe. Guet and Ooms (2005).

- Bubbly flow: this flow regime occurs for relatively low gas velocities and high liquid velocities. The continuous liquid phase flows upward carrying the dispersed gas bubbles. Both phases move upward.
- Slug flow: this flow regime is characterized by a higher gas velocity and by the event of bubbles getting closer and coalescing, forming a series of slug units. These slug units consist of bullet-shaped bubbles called Taylor bubbles with small gas bubbles dispersed in the liquid within the units. They are axially symmetrical and occupy almost the entire diameter of the pipe. There is a thin liquid film moving downward between the Taylor bubbles and the pipe wall as the gas flows upwards.
- Churn flow: for higher gas velocities, large gas bubbles become unstable and there is a chaotic movement of both gas and liquid in the downward and upward directions. There is no clear boundary between the phases.
- Annular flow: this flow regime occurs for very high gas velocities and it is characterized by a continuous fast-moving gas core with some liquid droplets entrained, and a continuous and thin liquid layer on the pipe wall flowing upwards.

Throughout the years, empirical and mechanistic flow regime maps were developed to graphically represent the boundaries between flow regimes (Duns & Ros, 1963; Aziz et al. 1972, Beggs & Brill, 1973; Taitel et al. 1980; Barnea 1987). These maps are based on visual observations of the phase distribution inside pipes under specific flow conditions, mostly based on experimental and field data with small diameters (up to 6 inches). An example of a flow regime map is illustrated in Figure 2.4, which is the mechanistic flow regime map from Taitel. et al. (1980).

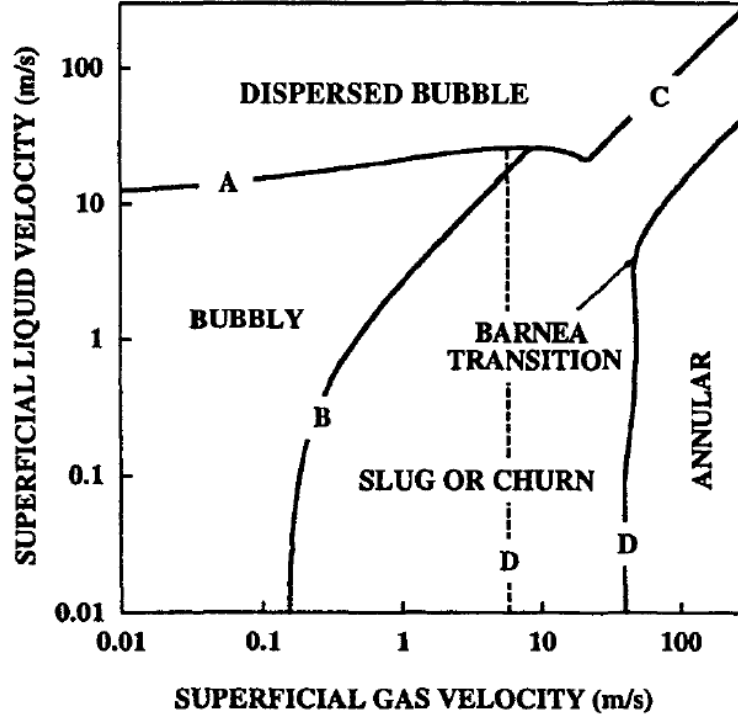


Figure 2.3. Flow regimes map for vertical upward flow. Taitel et al. (1980).

Fluid phase distribution and flow regimes transitions depend on several flow properties and can vary significantly with changes in diameter, inclination, pressure, velocity, type of fluids, and flow direction. When flow regimes are predicted inaccurately, important flow parameters will be erroneously obtained, consequently affecting the calculation of the pressure gradient. Flow regimes consideration is subjective and this has resulted in some flow regimes, such as churn flow, been treated differently among some models, as it will be further discussed in Section 2.6.

Waltrich et al. (2017) have noticed that one of the possible sources of errors in pressure drop calculations is the inaccurate prediction of flow regimes when flow conditions differ from those in which flow regime maps were developed. The flow regime consideration is assumed by many investigators as the central problem in the field of multiphase flow in pipes (Shoham, 2006).

2.2. Liquid Holdup

This parameter represents the fraction of the pipe occupied by the liquid in a two-phase gas-liquid flow. Liquid holdup estimation is important when modeling two-phase flow since the fraction of the phases should be known in order to determine the mixture fluid properties, such as mixture density, effective viscosities, and in-situ phase velocities. On the other hand, the void fraction is the portion of gas-phase contained in a section of pipe. Equation 2.1 and Equation 2.2 represent the liquid holdup and the void fraction, respectively.

$$H_L = \frac{V_l}{V} = (1 - \alpha) \quad 2.1$$

$$\alpha = \frac{V_g}{V} \quad 2.2$$

where V_l and V_g are the volumes of the liquid and gas phase present in a pipe segment, and V is the total volume of the pipe segment.

Liquid holdup is closely related to the flow regime. Empirical and mechanistic models determine liquid holdup based on specific correlations for each flow regime. An inaccurate prediction of flow regimes can result in erroneous liquid holdup, which in turn will affect the pressure gradient calculation.

2.3. Superficial and Phase Velocities

Superficial velocity is defined as the velocity a given phase would have if it occupies the entire pipe, therefore only this phase would be moving in the pipe. The superficial velocity of the liquid or the gas phase is determined by the ratio of the volumetric flow rate of that phase by the total cross-sectional area of the pipes as shown by Equation 2.3

and Equation 2.4

$$V_{sl} = \frac{q_l}{A} \quad 2.3$$

$$V_{sg} = \frac{q_g}{A} \quad 2.4$$

where q_l is the liquid volumetric flow rate, q_g is the gas volumetric flow rate, and A is the cross-sectional area of the pipe.

The summation of gas and liquid superficial velocities result in the mixture velocity (v_m). The average phase velocities for liquid (V_L) and gas (V_G) can be calculated by the ratio of the phase's superficial velocity by their respective fractions as shown in Equation 2.5 and Equation 2.6:

$$V_L = \frac{V_{sl}}{H_L} \quad 2.5$$

$$V_G = \frac{V_{sg}}{1 - H_L} \quad 2.6$$

2.4. Pressure Gradient

Based on the application of the conservation of mass, momentum, and energy in multiphase flow in pipes, the steady-steady pressure gradient consists of the three components shown in the expression below (Mukherjee & Brill, 1999),

$$-\left(\frac{dp}{dl}\right) = -\left[\left(\frac{dp}{dl}\right)_f + \left(\frac{dp}{dl}\right)_g + \left(\frac{dp}{dl}\right)_{acc}\right] \quad 2.7$$

where (dp/dl) is total pressure gradient, $(dp/dl)_f$ is the frictional component, $(dp/dl)_g$ is the gravitational component, and $(dp/dl)_{acc}$ is the acceleration component.

The gravitational component represents the hydrostatic head caused by elevation changes in the pipe and depends on the densities of the two-phase mixture. In most of the cases, in vertical flow, the resulting pressure gradient is dominated by the gravitational component. The friction

component is dominant in very high velocities and/or horizontal flow scenarios. This component accounts for the friction losses through the pipe. The pressure gradient resulting from the acceleration component is often neglected in most of the two-phase flow models. Figure 2.4 shows a typical representation of how the pressure gradient is affected by the mentioned components in a two-phase flow scenario for vertical (A) and horizontal (B) flow, in which the liquid volumetric flow rate (q_l) is kept constant and the gas volumetric flow rate (q_g) is increased.

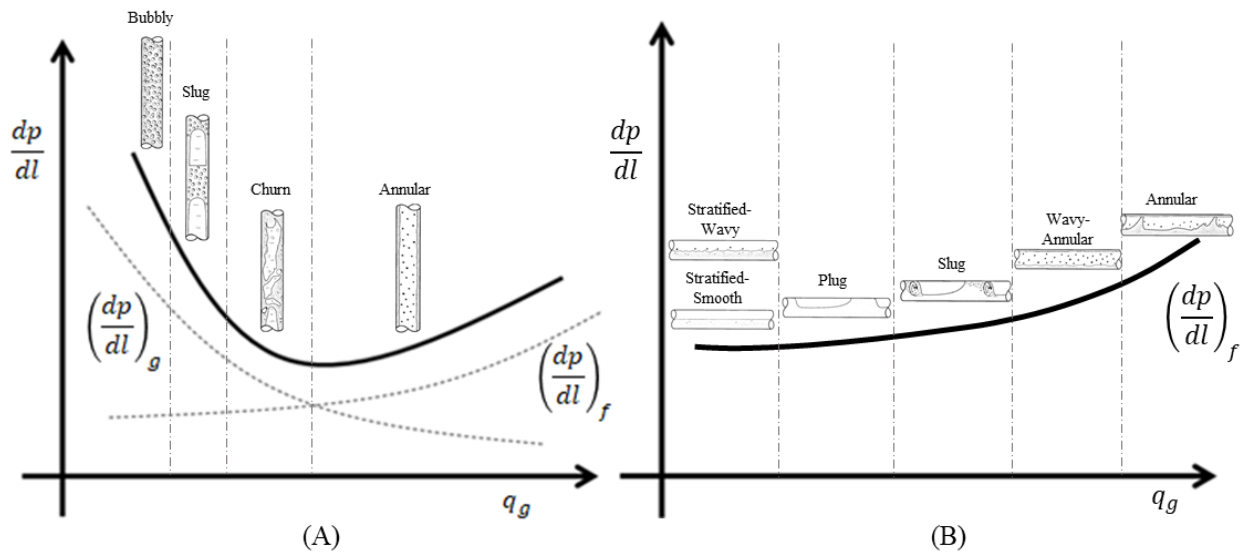


Figure 2.4. Pressure gradient curve for a constant liquid flow rate. (A) Represents vertical flow and typically flow regimes: bubbly, slug, churn, and annular flow; (B) represents horizontal flow and typically flow regimes: stratified-smooth, stratified-wavy, plug, slug, wavy-annular, and annular flow.

In the plot (A) above, initially, for a low gas flow rate, the gravitational component dominates, due to this component be highly dependable of the mixture fluid properties, and the liquid (heavier) phase being more present. The flow regimes present in gravitational dominated flow are bubbly, slug, and chun. As the gas flow rate increases, the gravitational component decreases and the total pressure gradient reaches a minimum point, and then the friction component becomes dominant due to the higher velocities of gas and presence of lighter phase. Annular is the flow regime predominant in the latter region. In the plot (B), for horizontal flow, the gravitational

component is not considered. As seen in the picture, as gas flow rates increase and more turbulence is present, flow regimes changes from initially stratified to annular flow. As shown in Equation 2.7, if the pressure drop caused by the acceleration component is neglected, the resulting pressure gradient is the summation of the friction and gradient components.

2.5. Empirical Models for Multiphase Flow in Pipes

The traditional empirical models consist on mathematical correlations based on curve fitting of large amounts of experimental data, which are commonly used in field applications where multiphase flow in pipes occur (Duns & Ros, 1963; Orkiszewski, 1967; Hagedorn & Brown, 1965; Beggs & Brill, 1973; Mukherjee & Brill, 1985).

For instance, the study conducted by Duns and Ros (1963) resulted in a model for three different flow regimes: bubbly, plug, and mist flow. These flow regimes are represented in the Duns and Ros (1963) flow regime map, which presented some improvements in comparison to previous flow regime maps. This model is a result of 4,000 two-phase flow laboratory tests carried out in vertical pipes with diameters ranging from 1.26 to 5.60 inches, being one of the first empirical models also derived from experiments containing hydrocarbons fluids.

Ros (1961) developed the first dimensionless analysis for two-phase flow in pipes. Out of twelve dimensionless groups, four were said to dominate the two-phase flow behavior and are important for the prediction of the liquid holdup. These four groups are the liquid velocity number, the gas velocity number, the pipe diameter number, and the liquid viscosity number, represented by the equations below:

Liquid velocity number:

$$N_{Lv} = V_{sl} \sqrt[4]{\frac{\rho_L}{g \sigma_L}} \quad 2.8$$

$$\text{Gas velocity number:} \quad N_{gv} = V_{sg} \sqrt[4]{\frac{\rho_L}{g\sigma_L}} \quad 2.9$$

$$\text{Pipe diameter number:} \quad N_d = d \sqrt{\frac{\rho_L g}{\sigma_L}} \quad 2.10$$

$$\text{Liquid viscosity number:} \quad N_L = \mu_L \sqrt[4]{\frac{g}{g\sigma_L^3}} \quad 2.11$$

where V_{sl} is the liquid superficial velocity, V_{sg} is the gas superficial velocity, d is the tubing diameter, σ_L is the surface tension, ρ_L is the liquid density, and g is the gravity acceleration.

Table 2.1 summarizes the models commonly used in the oil and gas industry. Due to their empirical nature, these models have several limitations and are most accurate only for the particular range of flow conditions which the experimental data were generated to develop such empirical models.

Studies such as Ahmed and Ayoub (2014) have shown that when empirical models are applied in conditions beyond those which the correlations were derived, it can lead to several inaccuracies, often underestimating the pressure gradient.

Table 2.1 summarizes recommendations and the main limitations of the empirical models mentioned in this section. Most of the models are mainly recommended for low gas-liquid-ratios (lower than 5,000 SCF/STB), and a limited range of pipe diameters and inclinations.

Table 2.1. Models and their applicability. Rao (1998); and Brill and Mukherjee (1999).

Model	Applicability
Beggs and Brill	Recommend for inclined wells. GLR lower than 5,000 SCF/STB. Good for water-cut up to 10%.
Duns and Ros	GLR lower than 5,000 SCF/STB. Not recommended when water is present.
Hagedorn and Brown	GLR lower than 5,000 SCF/STB. Accurate prediction for tubing sizes between 1 and 1.5 in. Recommended for vertical wells.
Mukherjee and Brill	This is model is an attempt to overcome some of the limitations of Beggs and Brill (1973) model. No GLR and water-cut ranges of applicability were found for this correlation.
Orkiszewski	GLR lower than 5,000 SCF/STB. Good for oil °API higher than 30. Good for slug flow condition. This model contains a discontinuity for velocities higher than 10 ft/s (mist/annular flow).

For instance, Hagedorn and Brown (1965) model is recommended only for vertical pipes and small diameters, while Beegs and Brill (1973) is recommended mainly for inclined pipes. Both models have been frequently used in the oil and gas industry. As it will be discussed in the next section, pipe diameter plays an important role in the stability of certain flow regimes, which is not accounted for in empirical correlations.

The limitations of these models are one of the main motivations of the data-driven approach proposed in this work, which aims to directly determine two-phase flow parameters without the use of empirically-derived correlations that are outside the range of flowing conditions to be modeled.

2.6. Mechanistic Models for Multiphase Flow in Pipes

These models use mathematical modeling approaches to account for the mechanisms of the flow regimes and then predict the liquid holdup and pressure gradient. For instance, Ansari et al. (1994) developed a model to predict liquid holdup and pressure gradient in upward vertical two-phase flow in pipes. Their model predicts the existing flow regimes using the flow regime map proposed by Taitel et al. (1980), which is represented in Figure 2.3. Ansari et al. (1994) model presented better results when compared to other models available in the literature for a database gathered from five different sources, such as TUFFP database; Asheim (1986); Govier & Fogarasi (1972); Chierici et al. (1974), Prudhoe Bay. Mechanistic models are dependent on some empirical parameters as closure relationships, and then become somewhat similar to the empirical models presented in the previous section. Mechanistic models also have a limited range of application in which they provide reliable results (Qi et al., 2018). For instance, Ansari et al. (1994) did not consider the presence of churn flow but enclosed it as a transition zone between slug and annular flow regimes. Although some studies (Jayanti & Brauner, 1994; Zabaras et al., 2013) have investigated this chaotic flow regime and supported its existence and the need for an independent modeling approach for churn flow regime, there are still limitations in the models found in the literature to accurately predict and model churn flow. Therefore, treating it as a transition or as part of slug flow will fail to capture the proper flow behavior of this flow regime and can possibly result in erroneous outcomes.

Furthermore, studies such as the work from Omebere-Iyari and Azzopardi (2007), showed that the pipe diameter can significantly impact the existence of certain flow regimes, such as bubbly and slug flow, which only exists in certain diameter ranges and pressure/temperature conditions. Taitel et al. (1980) developed an expression that determines the minimum diameter

necessary for bubbly flow to exist without coalescence and formation of Taylor bubbles. This expression is represented by Equation 2.12. In addition to that, for vertical two-phase flow in large-diameter pipes, Taylor bubbles (which are the main feature of slug flow regimes) are not stable. Kataoka and Ishii (1987) determined that there is a maximum pipe diameter size, calculated with Equation 2.13, for slug flow to exist under these conditions.

$$d_{min} = 19.01 \left[\frac{(\rho_l - \rho_g)\sigma_L}{\rho_l^2 g} \right]^{1/2} \quad 2.12$$

$$d^* = d \left[\frac{g(\rho_l - \rho_g)}{\sigma} \right]^{1/2} \quad 2.13$$

where σ is the surface tension between gas and liquid phases, ρ_g and ρ_l are the gas and liquid densities, g is the gravitational acceleration, and d is the pipe diameter.

Some papers have reported that Taylor bubbles should not be stable for $d^* > 30$, while other studies for $d^* > 40$ (Kataoka & Ishii, 1987; Shen et al., 2015; Schlegel et al., 2012). Figure 2.5 and Figure 2.6 show plots of pressure versus pipe diameter that illustrate when different flow regimes can occur depending on these two parameters. In these figures, there are two main regions separated by the colored curves (red and blue). The region above the solid curves represent the large diameter region ($d^* > 30$), which Taylor bubbles are not stable and slug flow cannot exist. On the other hand, slug flow can exist in any diameter and pressure below the dashed curves ($d^* < 18$). Taylor bubbles may not be stable in “transition zone” where $18 < d^* < 40$. In addition to that, Figure 2.5 and Figure 2.6 also show a representation of the regions where bubbly flow can be encountered. The black curves present the minimum diameter necessary for bubble existence from Equation 2.12. Flow regimes that can be present in each region are illustrated by the figures.

Curves in these figures were derived from Equation 2.12 and Equation 2.13, in which fluid properties were calculated at 60 °F; 30° API oil and gas with 96.5% methane system were considered for the calculations.

**Typical range of pipe diameters
for lab experiments**

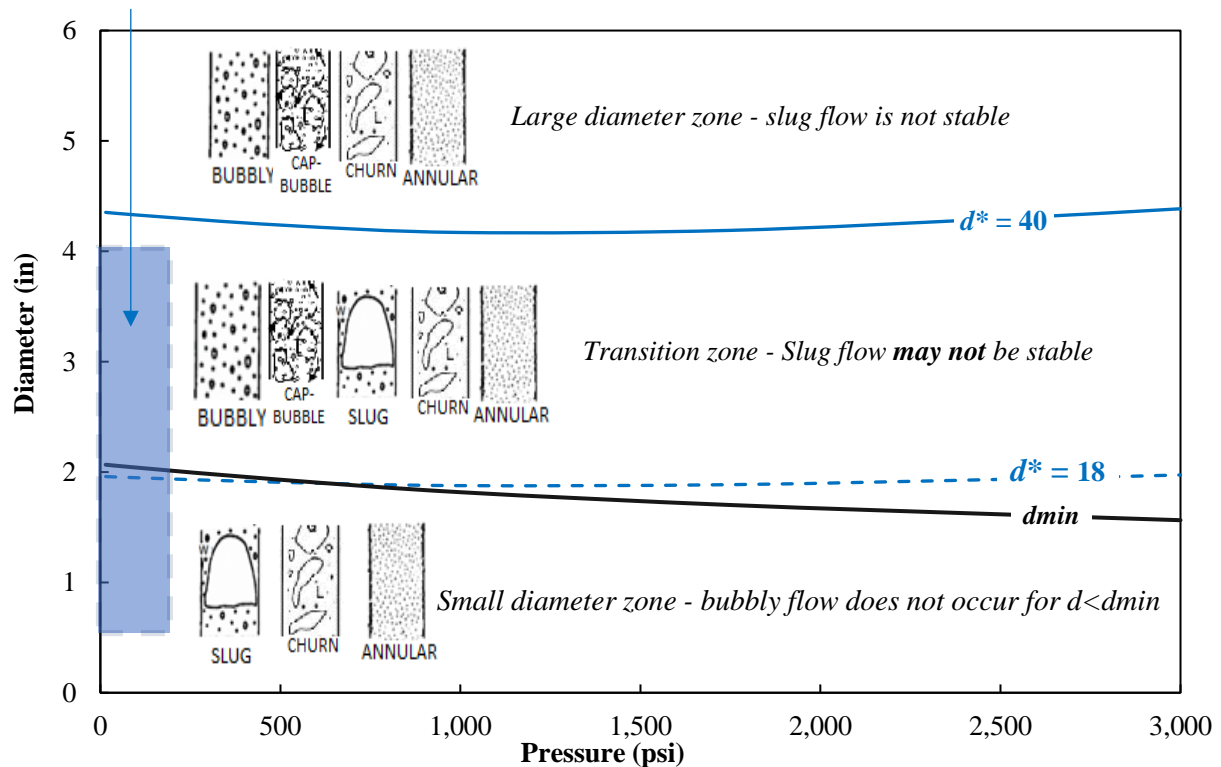


Figure 2.5. Minimum diameter for bubbly existence for water and air. Large diameter transition zone for Taylor bubbles existence.

Typical range of pipe diameters
for lab experiments

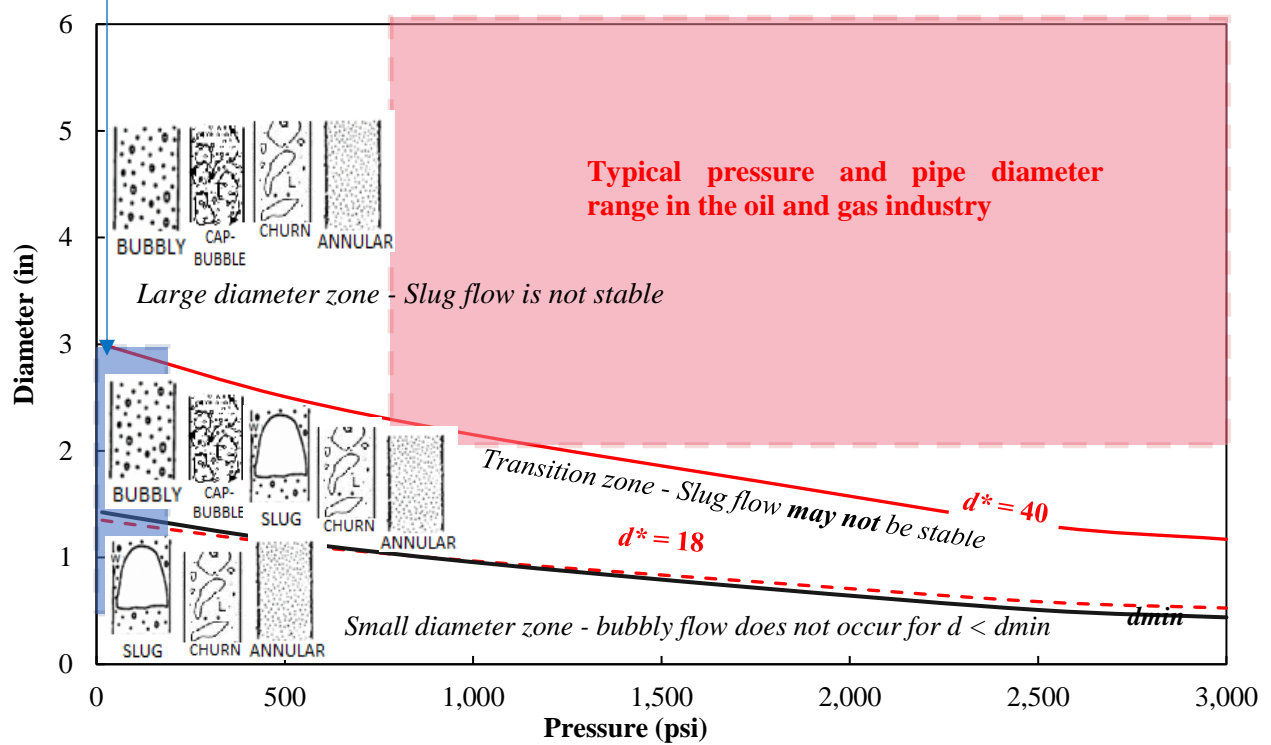


Figure 2.6. Minimum diameter for bubbly existence for oil and natural gas. Large diameter transition zone for Taylor bubbles existence.

According to Kataoka and Ishii (1987) as proposed in Equation 2.13, Figure 2.5 shows that, for air-water two-phase flow in pipes near atmospheric conditions, Taylor bubbles are not stable in pipe diameters larger than 4 inches. However, for oil and natural gas, Taylor bubbles should be stable only for pipe diameters smaller than three inches, as shown in Figure 2.6. The differences in pipe diameter for Taylor bubble stability are mainly caused by the differences in surface tension between air-water and oil-natural gas systems. The surface tension of oil and gas decreases significantly as pressure increases, while the surface tension for air-water systems is not as affected as in oil-natural gas systems.

It is important to mention that the application of flow regime models for slug flows for pipe diameters between 1 and 4 inches is widely used in empirical and mechanistic models in the oil

and gas industry. Moreover, as seen in the shaded area of Figure 2.5, most experimental data available in the literature are only for conditions that slug flow is stable, according to the Taylor bubbles stability concept given by Equation 2.13. While looking at the shaded area in Figure 2.6, we see that Taylor bubbles are not stable in most of the pipe diameters and pressure conditions in the field for the oil and gas industry. Therefore, it is not a surprise that there is still a significant debate in the literature about the stability of slug flow (or Taylor bubbles) for larger-diameter and high-pressure two-phase flow in pipes.

Figure 2.5 and Figure 2.6 imply that current models may deliver erroneous results, as they possibly are modeling churn flow using a mechanistic model for slug flow regime. Omebere-Iyari and Azzopardi (2007) showed that in most of the empirical models and for most of the important closure parameters for modeling two-phase flow in vertical pipes, the experimental scenarios consider flow rates and pipe diameters smaller than those found in the field. Omebere-Iyari and Azzopardi (2007) conducted a series of experimental studies with a mixture of naphtha and nitrogen in a 170 feet long pipe with approximately 7.2 inches pipe and concluded that the flow regimes prediction from previously published works poorly predicted the flow regimes in this large diameter pipe, which reinforces the Taylor bubbles existence condition mentioned before. Furthermore, the study conducted at Louisiana State University by Teles et al. (2018), observed that determining the pressure drop for certain flow regimes when actually there is another flow behavior, can significantly impact the pressure drop calculation.

Bendiksen et al. (1991) formulated a comprehensive model named OLGA, which is widely used nowadays in multiphase modeling in the oil and gas industry. This mechanistic model consists of the basic conservation of mass, energy, and momentum principles to predict pressure drop, liquid holdup and flow regimes in pipes. Its simulations results were compared with field data and

experimental data from SINTEF Two-Phase Flow Laboratory in Norway. OLGA flow model has two classes of flow regimes, they are named distributed, which includes bubbly and slug flow, and separated which includes stratified and annular-mist flow regimes. It can be noted that the model formulated by Bendiksen et al. (1991) does not include churn flow regime, what may lead to inaccurate results of pressure gradient when churn flow is present. In addition to that, OLGA commercial software has shown a discontinuity of holdup trend for certain flow conditions, and this model has not been extensively validated for downward flow in pipes.

2.7. Drift-Flux Models for Two-Phase Flow in Pipes

A simpler, reliable and fast computing model has been obtained by the development of drift-flux models (Zuber & Findlay, 1965; Shi et al., 2005; Hasan, Kabir, & Sayarpour, 2010). Zuber & Findlay (1965) idealized a model that depends mainly on two parameters: the distribution coefficient (C_o) and the drift velocity (V_d). The equation below represents the drift-flux equation and how the liquid holdup can be correlated to it.

$$V_G = C_o(V_{sg} + V_{sl}) + V_d \quad 2.14$$

$$H_L = 1 - \frac{V_{sg}}{V_G} \quad 2.15$$

where V_G is the real gas velocity, V_{sl} and V_{sg} are the liquid and gas phases superficial velocities.

Throughout the years, many modifications and new correlations for the liquid holdup based on the drift-flux approach have been developed. Some of them assume a constant drift-flux distribution coefficient and equations to determine drift-velocity based on fluid properties, as the work presented by Shipley (1982). Hibiki and Ishii (2003) developed correlations for drift-flux parameters based on flow regimes. Their work presented correlations for bubbly, slug, and annular

flow regimes. Several studies (Choi, 2013; Bhagwat & Ghajar, 2014; Tang et al., 2019; Hasan et al., 2010), have been focused on improving drift-flux models and better estimating its parameters. However, there are still some limitations when these models are applied in high velocities and high gas contents (i.e. annular flow), deviated pipes, and viscous fluids (low to medium viscosity).

Bhagwat and Ghajar (2014) proposed a set of correlations to predict drift-flux parameters which are flow regime independent. Their model presented reasonable results for several types of fluids and flow regimes. Inclinations varied from downward to upward vertical flow, most of the data being either for fully vertical or horizontal flow. Differently from other drift-flux models, Bhagwat and Ghajar (2014) correlations performed well for high gas fraction scenarios (i.e. annular) used in their validation data-set. However, the study from Tang et al. (2019) evaluated the performance of Bhagwat and Ghajar (2014) model and concluded that it did not perform well for downward flow and stated that further improvements are still needed.

Tornisiello (2020) developed a simplified transient two-phase flow model adopting Bhagwat and Ghajar (2014) correlations to obtain drift-flux parameters and determine liquid holdup. This model was validated with data for full ranges of pipe inclinations (from downward to upward vertical flow) and resulted in better performance than the commercial software OLGA to predict liquid holdup and pressure gradient when compared with experimental data. On the other hand, her model shows discontinuities in the distribution coefficient (C_o) and the drift velocity (v_d) correlations from Bhagwat and Ghajar (2014). The models proposed by Tornisiello (2020) requires some improvements in the drift-flux correlations that could be addressed through the direct estimations of drift-flux parameters using the data-driven approach suggested in this work.

2.8. Future of Multiphase Flow Modeling

An interesting study by Shippen (2012) describes an evaluation of multiphase flow models and the main challenges that this area of study will be facing in the future to better predict the pressure gradient in wells. These authors mention several times that although mechanistic models should be theoretically more accurate than empirical models, these models still depend on many empirical closure relationships, and this also makes mechanistic models empirical in nature. Figure 2.7 shows the evolution of models regarding fluid phases and pipe inclinations. Shippen (2012) summarized well the challenges to further improve multiphase flow modeling. These challenges are listed below:

- Characterization of three-phase (oil-water-gas) flow modeling.
- Consideration of more complex fluids.
- More accurate and generalized closure relationships
- Eliminate discontinuities in the models
- Improvements on the integration of multiphase flow models with reservoir and facilities.

Although Shippen (2012) presented a reasonable summary, as shown above, their representation does not account for important aspects such as pipe diameter. The effect of pipe diameter has been discussed more recently in the literature (Waltrich et al., 2017), but there is still a lack of studies on this subject.

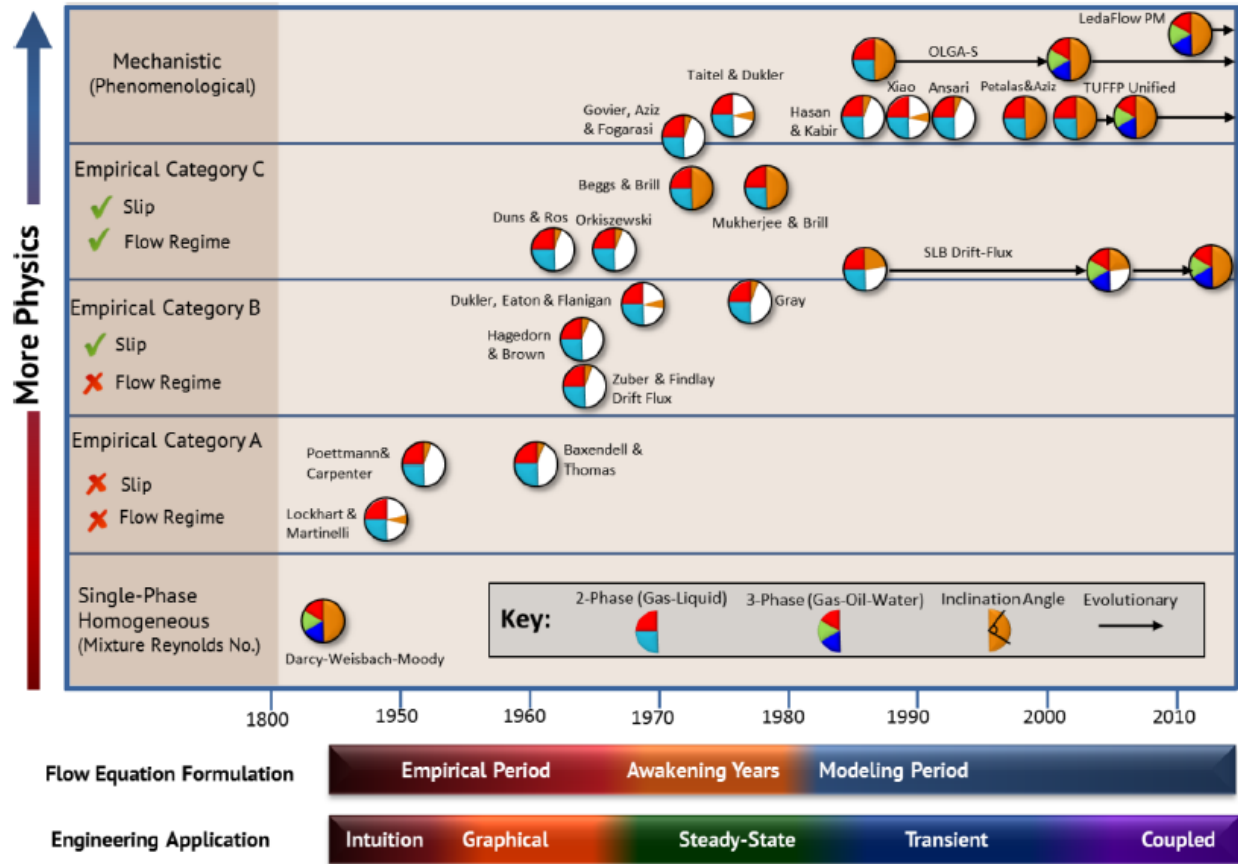


Figure 2.7. Evolution of flow models Shippen (2012).

Trying to overcome some of the multiphase flow challenges and to eliminate the need for flow regime determination when calculating pressure gradient, Nagoo (2014) performed an extensive study on both experimental and field observations from several industrial applications and showed that single-phase flow mechanics can be generalized to multiphase flow. His work claims that there is a relationship between pressure and velocity in single-phase flow, which can also be found in multiphase flow. The author developed an extensive single and two-phase database called ANNA, which he uses to perform wellbore flow modeling under several conditions.

Over the years, several new ideas were introduced to improve modeling, for instance, Waltrich et al. (2014) proposed to perform remote experiments through a virtual environment with

access to several research facilities around the world. Their idea is to generate data for a wide range of conditions that could cover scenarios very similar to the ones found in the oil and gas industry since these facilities have the capacity to operate under different flow conditions. The idea of remote real-time experiments also consists of using existing data to determinate well performance. Their work proposes a promising idea that if implemented with a self-tuning and data-driven approach could enhance the accuracy and range of applicability of multiphase flow models.

In the past decades, the implementation of self-tuning and data-driven models have increased in the oil and gas industry. Several studies were carried out aiming to improve multiphase flow models in wells. For instance, Osman (2004) used Artificial Neural Networks (ANN) to implement a model that can predict flow regimes and liquid holdup for horizontal flow. His model has a reduced number of input parameters and is able to provide better results for a given data-set than empirical correlations developed for those conditions. Alizadehdakhel et al. (2009) performed a series of experiments in a 0.78-in (2-cm) ID pipe in vertical and horizontal flow. The latter authors used dimensionless numbers derived from their data-set in an ANN model to determine the pressure gradient. Their model results showed a reasonable agreement with their experimental data.

Hernandez et al. (2019) proposed an indirect method to determine flow regimes. They created a data-driven model capable to indicate the best equations to predict flow regimes. However, their paper states that the prediction capability of their method for cases near or inside transition zones is limited. Similarly, Mohammadi et al (2019) proposed a methodology using genetic algorithms to select the set of closure relationships for a given set of data to improve accuracy for pressure gradient predictions.

Kanin et al. (2019) performed an interesting work on the application of machine learning algorithms to predict the pressure gradient. They developed an algorithm containing three models. The first model predicts liquid holdup. The second predict flow regimes using the calculated liquid from the first model holdup as one of the inputs of the second model. The third determines pressure gradient based on both flow regime and liquid holdup from the two previous models. Kanin et al. (2019) trained their models with experimental data and applied it to field cases. As a result, the data-driven model provided slightly better results than empirical and mechanistic models commonly used in the oil and gas industry.

The current ability to determine the pressure gradient in pipes has limitations. Many of the models mentioned above have flow regimes as one of the inputs. As it has been mentioned throughout this literature review, flow regime determination is subjective and can lead to errors. The ability of data-driven models to train data independently of the flow regime can potentially improve the prediction of the pressure gradient.

3. Evaluation of Multiphase Flow Models

An extensive study of several commonly used multiphase flow models was carried out at Louisiana State University under award M17PX00030 funded by United States Bureau of Ocean Energy Management (BOEM).

The main goal was to evaluate the performance of mechanistic and empirical models at different flow conditions, which most of the current models have deficiencies, such as large diameters, high pressure, and high flow rates. The LSU model proposed for large diameters and high velocities herein called Teles and Waltrich (2018) consists of a model that can determine pressure drop in large diameter pipes and also considers the presence of churn flow regime. The Appendix shows an overview of Teles and Waltrich (2018) model algorithm. The models below were evaluated in this study:

- Teles and Waltrich (2018)
- Beggs and Brill (1973)
- Duns and Ros (1963)
- Mukherjee and Brill (1985)
- Hagedorn and Brown (1965)
- Gray (1974)
- Ansari et al. (1994)
- OLGA (2000)

The simulations results from these models are compared to field data found in the literature from (Asheim, 1986; Aziz & Govier, 1972; Espanol et al., 1969; Fancher & Brown, 1963; Reinicke et al., 1987), data provided by Petrobras, and to the dataset of the experiments carried out

at Louisiana State University's Petroleum Engineering Research Technology and Transfer Laboratory (PERTT Lab) for a previous research project also funded by US BOEM (Waltrich et al., 2019). Table 3.1 summarizes the source and main characteristics of the field and experimental data used to evaluate the performance of the models previously mentioned.

Table 3.1. Source and main characteristics of the database.

Source	Pipe ID (in)	Liquid flow rate (STB/d)	Gas-Liquid-Ratio (GLR) (SCF/STB)	Fluids	Pressure (psi)
Fancher and Brown (1963)	2	75 – 936	525 – 7,283	Natural gas and oil	Up to 616
Reinicke et al. (1987)	3.98	7.5 – 493	7,734 – 1,403,645	Natural gas and water	Up to 8,880
Asheim (1986)	≈ 4, 6.2	Up to 27,700	≈ 325	Natural gas and oil	Up to 2,616
PERTT Lab	4, 8, 12	Up to 29,200	Up to 887	Air and water	≈ 14.7
Petrobras	3.74, 4.5	Up to 3,665	Up to 5,720	Natural gas, oil and water	Up to 7,595

3.1. Summary of Models Evaluation Results

The study presented in this chapter reinforces the need for a more accurate way to predict the pressure drop in wells. The simulation results from different empirical and mechanistic models showed that all these models do not provide accurate results when they are applied in conditions beyond their limitations, such as large pipe diameters, higher velocities, and inclination. Below are the main conclusions from the models for the field and laboratory data included in this study:

As shown in Figure 3.1 and Figure 3.2, for the field data of high GLR, Teles and Waltrich (2018) model showed a better performance than the other empirical and mechanistic models such as OLGA (2000), Gray (1974), Beggs and Brill (1973), Mukherjee and Brill (1985), Duns and Ros (1963), and Hagedorn and Brown (1965). The average absolute error for Teles and

Waltrich (2018) model was about 5% while for the other flow regime dependent models it was up to 25%.

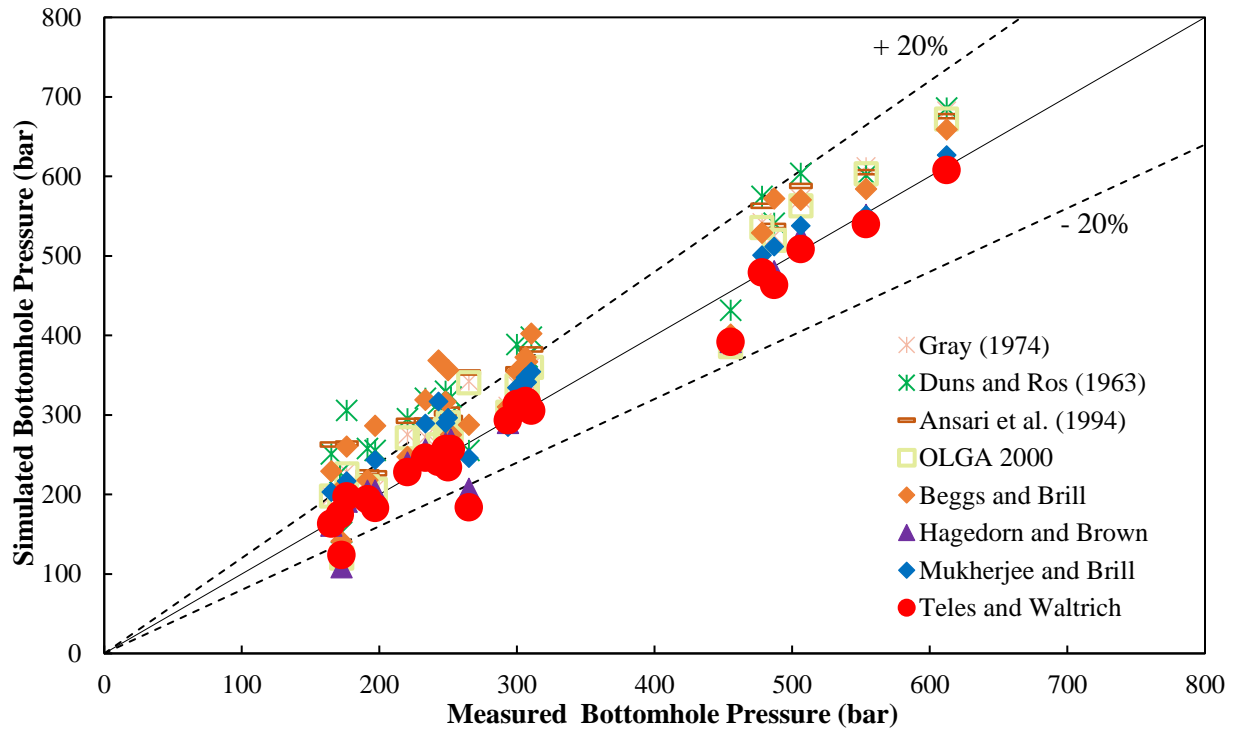


Figure 3.1. Comparison of field bottomhole pressure and simulated bottomhole pressure for Reinicke et al. (1987) Field Data.

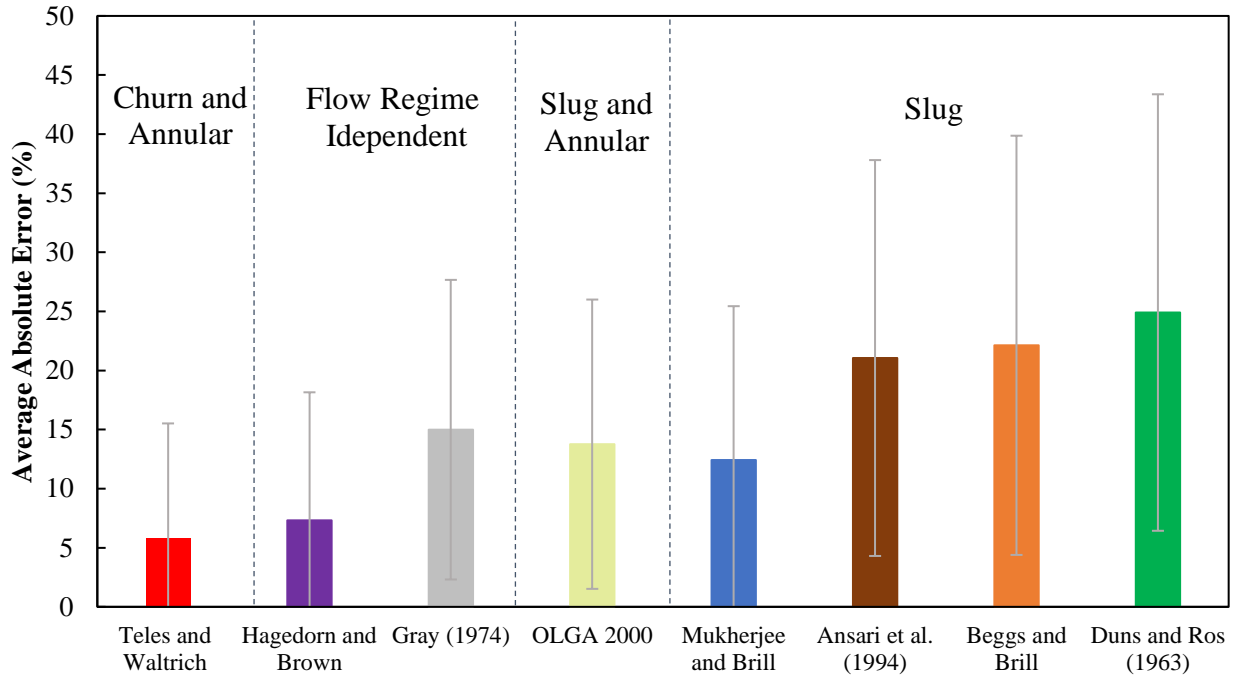


Figure 3.2. Average absolute error and standard deviation of the errors for Reinicke et al. (1987) Field Data. Error bars represent the standard deviation.

With Reinicke et al. (1987) data set, it was concluded that considering slug flow when there is churn flow on the pipe segment leads to significant errors. Therefore, churn flow needs to be modeled separately, and improvements in the flow regimes determination are needed to obtain more accurate results. Hagedorn and Brown (1965), as a flow regime independent model, presented low errors. However, this model was not accurate when evaluating the other field and experimental data.

Figure 3.3 and Figure 3.4 summarize the experimental results from PERTT Lab. For these cases, Teles and Waltrich (2018) model was not as accurate as Mukherjee and Brill (1985), Beggs and Brill (1973), Duns and Ros (1963). The average absolute error of pressure gradient was around 35%. As for the other models, Teles and Waltrich (2018) also showed higher errors for pressured gradient prediction in scenarios with a slip ratio greater than one unit. This can also be observed

in the pressure gradient versus gas superficial velocity plots when the simulated pressure starts to deviate from the measured pressure for higher gas superficial velocities.

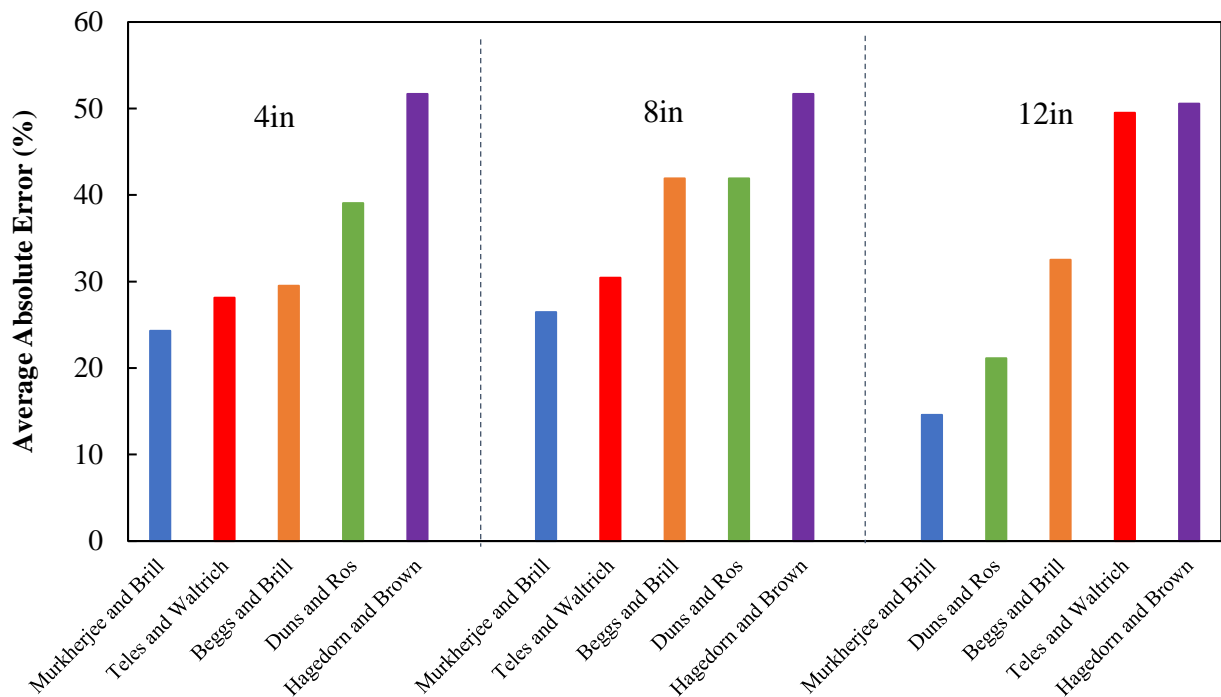


Figure 3.3. Average Absolute Error of pressure gradient in % for Flow Models for the LSU/PERTT Lab experimental data reported by Waltrich et al. (2017).

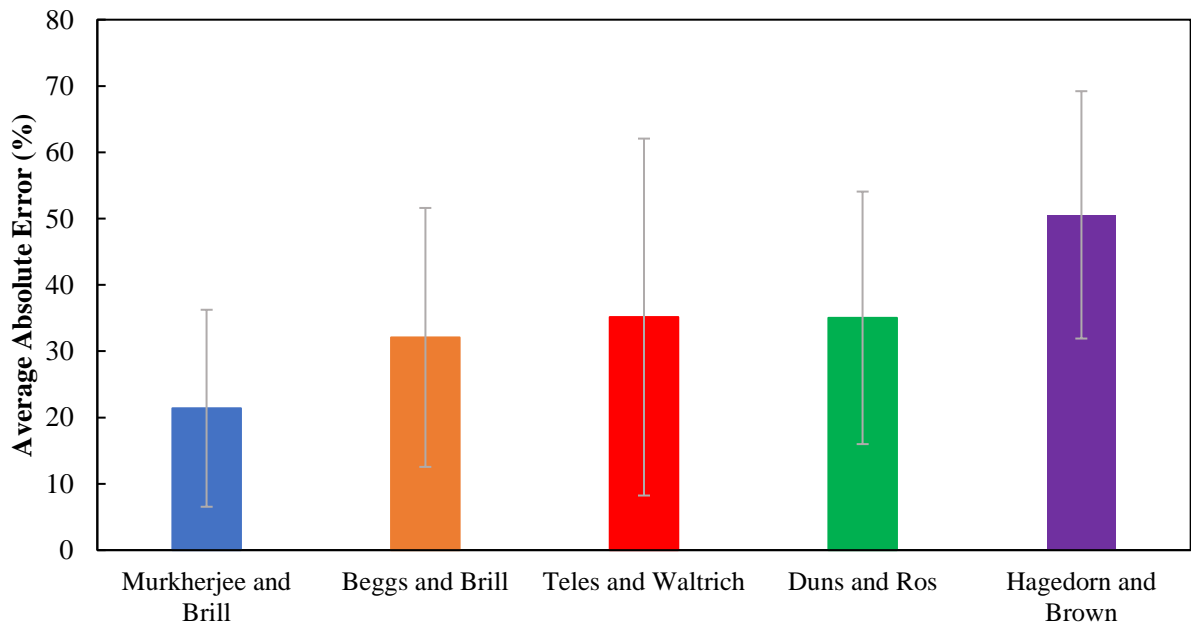


Figure 3.4. Overall average absolute error of pressure gradient in % for Flow Models for the LSU/PERTT Lab experimental data reported by Waltrich et al. (2017). Error bars represent the standard deviation.

The hybrid model from Teles and Waltrich (2018) showed reasonable results for the investigations of Petrobras data set with an average absolute error of 10%, as shown in Figure 3.5 and Figure 3.6. It was observed that the presented model has a better performance when used for calculating the pressure gradient for high GLR cases, as for well C, for which conditions churn flow would be present. The evaluation carried out evidenced that empirical models might provide erroneously results when the flow conditions are out of the applicability range (i.e. GLR and water cut), as shown in Beggs and Brill (1973) and Duns and Ros (1963) results for well C in Petrobras data.

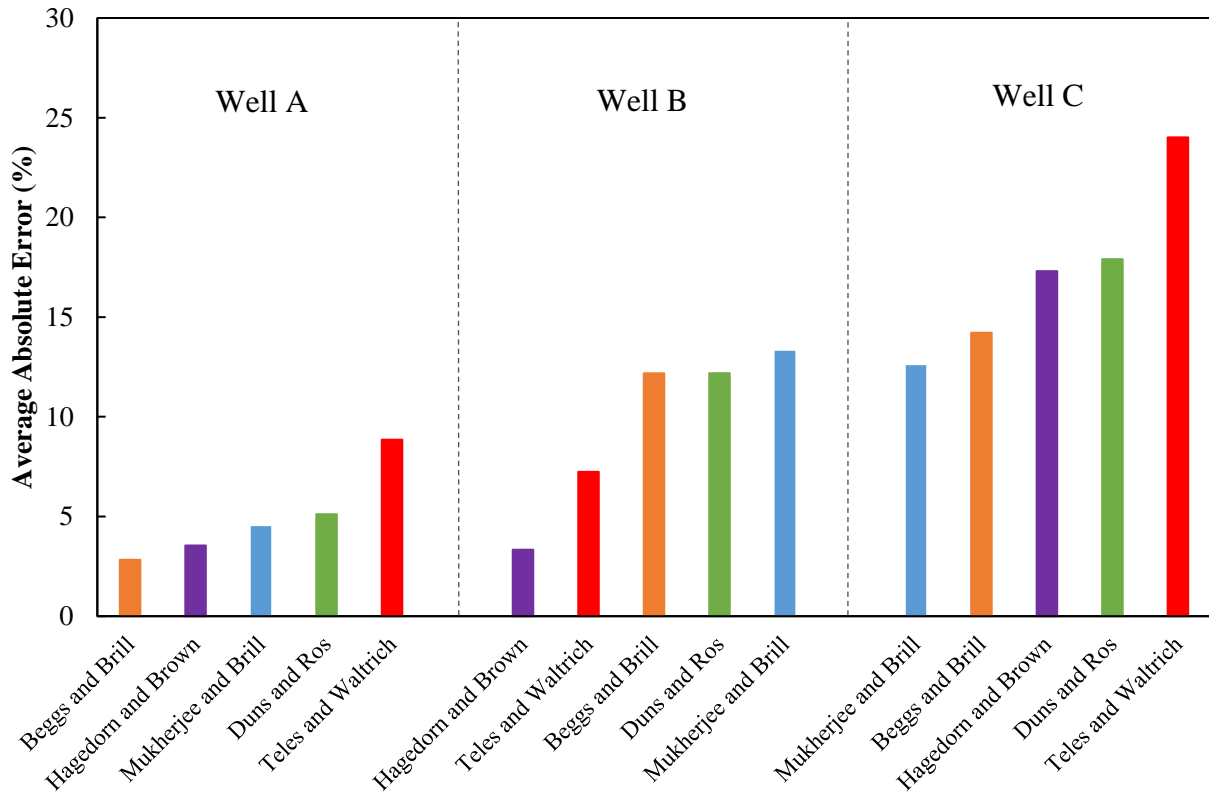


Figure 3.5. Average absolute error of the simulated bottomhole pressure of the three different wells for Petrobras data.

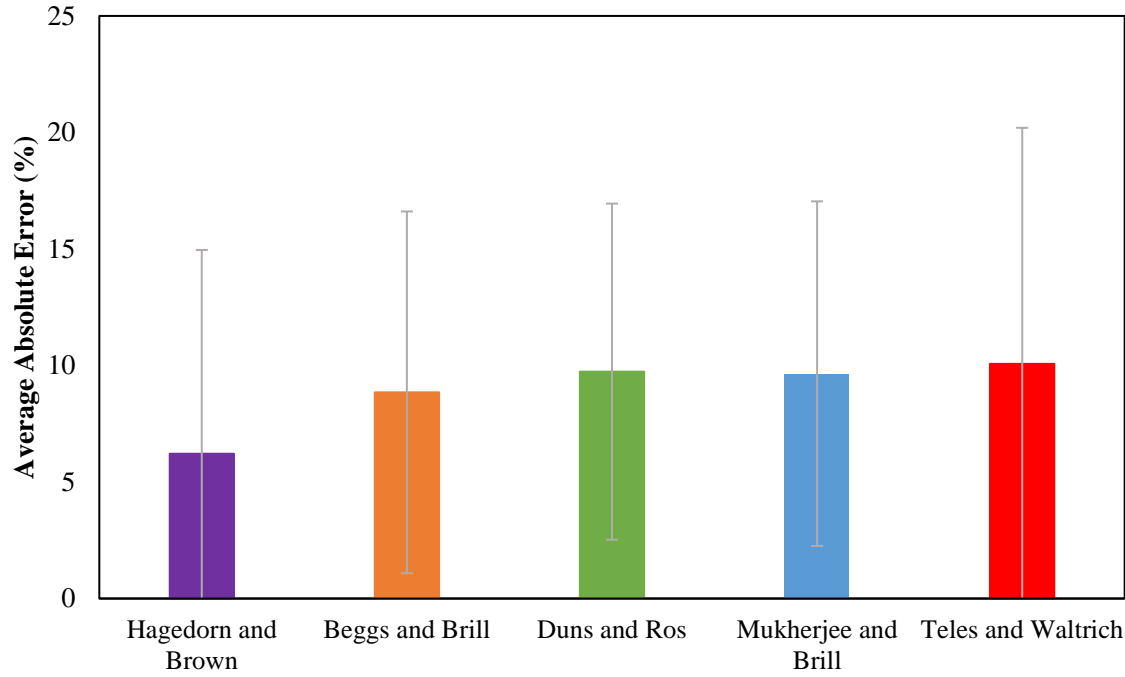


Figure 3.6. Overall average absolute error of the simulated bottomhole pressure for Petrobras data. Error bars represent the standard deviation.

Hagedorn and Brown (1965) correlations showed good results for most of the vertical wells with smaller diameters and lower liquid velocities scenarios. However, this model has limitations regarding some other parameters and pipe inclination and yielded higher errors for PERTT lab, Asheim (1986) datasets, and well 5 for Petrobras dataset. The comparison results are shown in Figure 3.7 for Asheim (1986) field data.

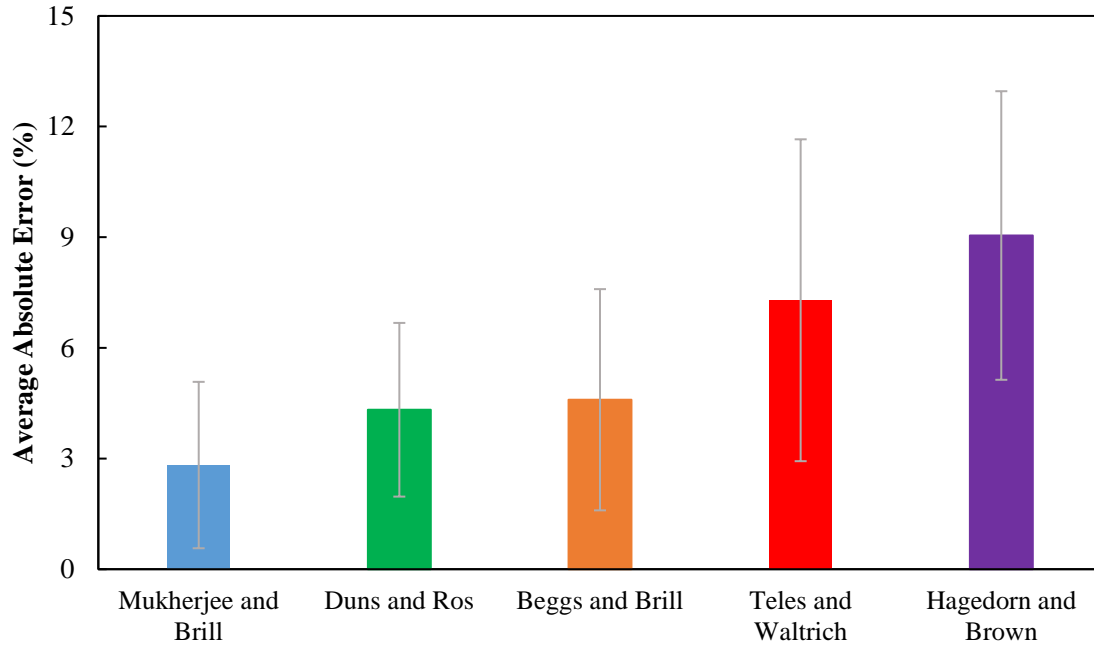


Figure 3.7. Average absolute error of the simulated bottomhole pressure for Asheim (1986) field data. Error bars represent the standard deviation.

Overall, Teles and Waltrich (2018) model showed a reasonable match to the field data of Fancher and Brown (1986) as shown in Figure 3.8. It was observed that for a liquid rate of 144 BBL/D, when the GLR increases Beggs and Brill (1973) and Hagedorn and Brown (1965) deviate from the field data trend. This is probably due to the fact that the first does not consider churn flow and the latter is flow regime independent, which leads to higher errors when predicting the pressure gradient in either churn or annular flow conditions. Mukherjee and Brill (1985) shows a deviation from the field data for most of the cases, while Duns and Ros (1963) model provides a good fit mainly for the slug flow conditions.

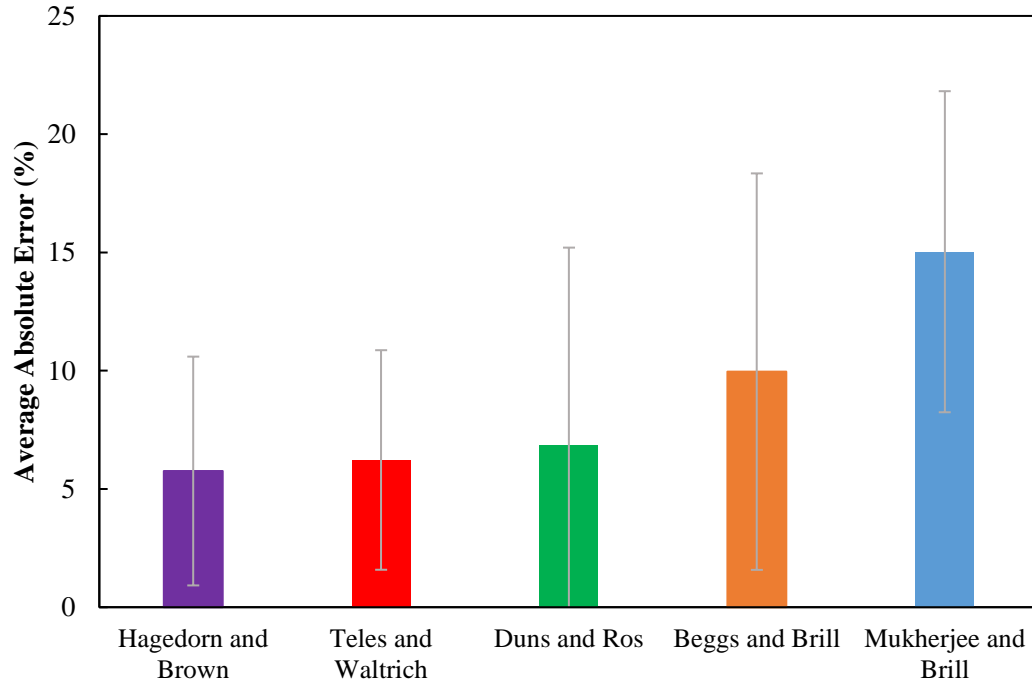


Figure 3.8. Average absolute error of the simulated bottomhole pressure for Fancher and Brown (1963) field data. Error bars represent the standard deviation.

3.2. Possible Causes of the Models Inaccuracies

The model evaluations from this chapter show that flow regime consideration is one of the main sources of errors for mechanistic and empirical models. The field and laboratory data from Table 3.1 contains several scenarios that predicted to have slug flow when according to the Kataoka and Ishii (1987) concept is considered either a large diameter or is located in the transition zone ($18 < d^* < 30$). For instance, for the Reinicke et al. (1987) data set the models having the highest errors were those that predicted to have mostly slug flow along the wells. On the other hand, Teles and Waltrich (2018) model indicated to have churn and had the lowest errors. Similar results were encountered in Fancher and Brown (1973) evaluation, the highest errors were for having large diameter pipes and high gas content cases.

Studies have revealed the differences in flow regimes between large and small diameter pipes. It has been noted the non-existence of Taylor bubbles in conditions where flow models

predict slug flow (Hibiki & Ishii, 2003; Zabaras et al. 2013; Roullier et al., 2018). This makes the applicability of flow regime maps for large pipe diameter questionable. For instance, Roullier et al. (2018) pointed out that OLGA commercial software has shown a discontinuity holdup trend in ranges of $18 < d^* < 30$, possibly because it is in the transition zone between small and large diameter regions.

A new flow regime map for large diameter pipes and a flow regime called cap-bubble were implemented in the two-phase flow model by Capovilla (2018). This flow regime consists of large bubbles that do not occupy the entire pipe diameter, having flow recirculation and increased turbulence. In Capovilla (2018) work, flows in large pipe diameter believed to behave slug flow were modeled either as churn or cap-bubble. It was observed a decreased error in the cases that the new flow regime map predicted cap-bubble and modeled it as such. Cavalcante (2020) has also noted that flow regimes change with fluid properties and geometrical parameters, and certain conditions will not allow the existence of slug flow. He points out the lack of studies of the large diameter effect and the non-existence of slug flow in annuli.

As can be seen, the Taylor bubble stability criteria should be considered in multiphase flow in pipes. The reason that slug flow can occur only in smaller pipes is related to the gravitational and buoyancy forces involving Taylor bubbles. For small pipe diameters, the Taylor bubbles can be sustained by the pipe walls, while for large pipe diameters the force balance cannot be sustained and the bubbles break.

Besides flow regime maps related errors, empirical models such as Hagedorn and Brown (1965) showed higher errors when applied to conditions beyond the range in which it was derived. For instance, as seen in Asheim (1986) field data, this model presented the highest average absolute error among the models. As seen on the results for each of the field and laboratory data

evaluated, models had different performances. It supports the fact that no model provides a reliable prediction of pressure gradient for a wide range of conditions.

3.3. Possible Solutions for Models Shortcomings

In order to overcome the limitations in two-phase flow modeling, it is suggested to implement the large diameter concept and the consideration of churn and cap-bubble flows in the formulation of the established models. As it was shown, evidence for improvement is needed for both flow regime dependent and independent models. However, expanding the modeling capabilities for other flow regimes and flow conditions will not overcome all limitations of empirical or mechanistic (semi-empirical) models by itself.

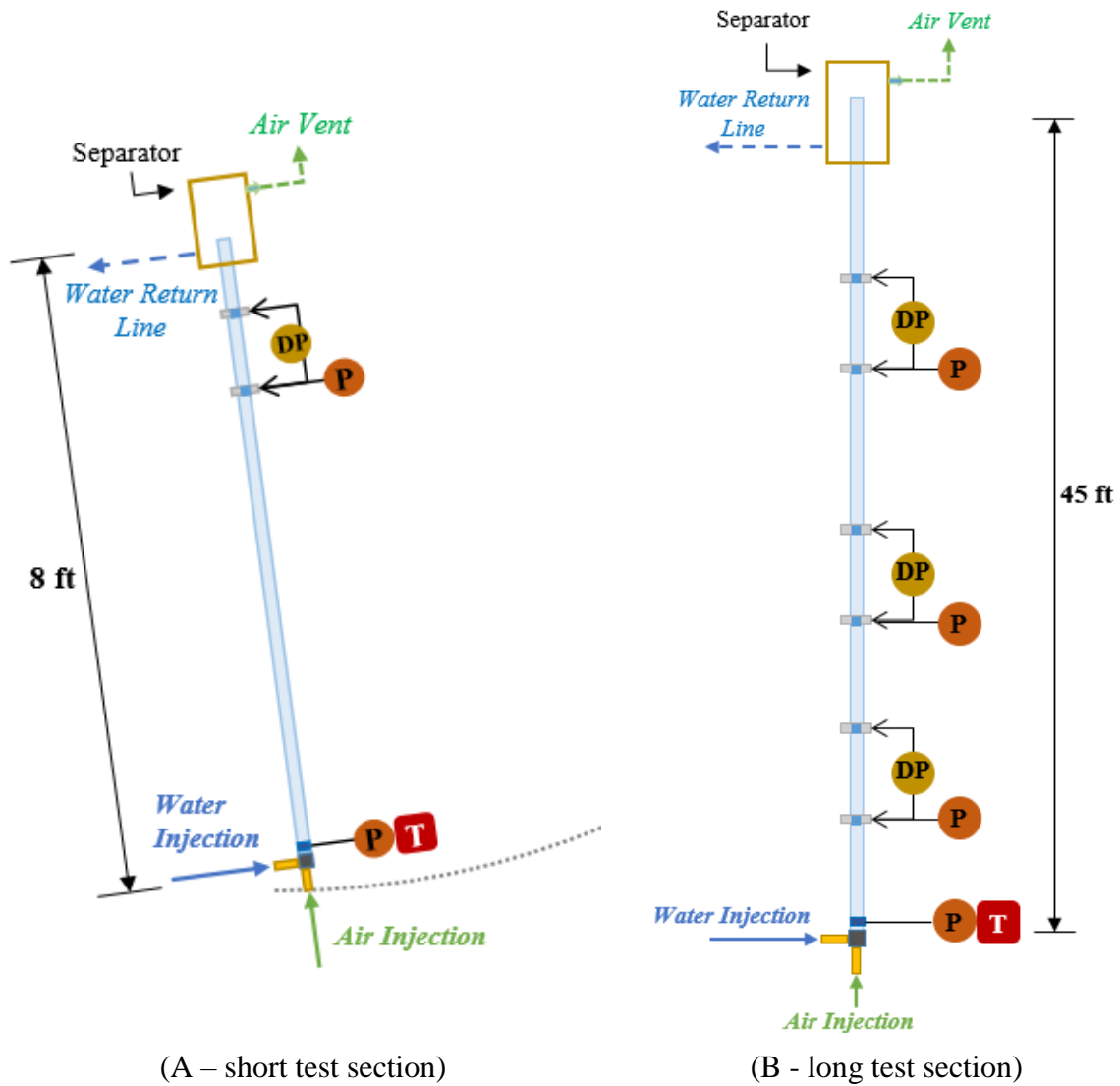
On the other hand, data-driven approaches can significantly enhance two-phase flow modeling, since it will not depend on flow regimes determination prior to determine the pressure gradient. The next chapter describes in more detail the methodology proposed in this work to overcome the limitations existent in the currently established models.

4. Fully Automated Flow Loop for Two-Phase in Pipes

4.1. Introduction

The main objective of designing and building a fully automated flow loop is to have a facility capable of remotely and continuously performing multiphase flow experiments for different pipe inclinations, from 0° (horizontal) to 90° (vertical) with the horizontal direction. Initially, water and air were used for this purpose, but later on more complex fluids could be used.

The flow loop is located at Louisiana State University. This facility includes measurement devices for differential pressure and liquid/gas flow rates for pipe inclinations. The automated multiphase flow loop has two parts: a short test section and a long test section, as shown in Figure 4.1. The short test section includes an 8-ft long transparent PVC 1.049-in ID pipe, which can be positioned at different inclinations. As many authors in the literature argue that the entrance effect can impact two-phase flow in short pipes, a longer test section is also included. The long test section includes a 45-ft 1.049-in ID pipe, positioned only in the vertical direction. This test section was built primarily to evaluate the effect of length for the short test section.



(A – short test section) (B - long test section)
 Figure 4.1. Inclination short test section (A) and long test section (B) illustration.

4.2. Test Sections and Instrumentation

A centrifugal pump (Grundfos, model: 96799044-P3-1736) is used to pump water from a 50 gallons tank to the flow sections. Compressed air at 150 psi is fed and continually stored in a tank to supply air to the flow sections. Water volumetric rate and air mass rate are measured upstream of the flow injection at actual conditions using a Rosemount Micro Motion Coriolis flow meter (CMFS010M) for lower air flow rates and an Omega Gas Turbine flow meter (FTBG-101)

for higher gas flow rates, and an Omega Turbine Water (FTB2005) volumetric flow meter. Table 4.1 summarizes the flow measurement devices installed.

Table 4.1. Flow Measurement Devices Specification.

Manufacturer	Model	Fluid	Flow Range
Rosemount	CMFS010M	Air	Up to 4.2 g/s
Omega	FTBG-101	Air	0.13 to 1.6 ACFM
Omega	FTB2005	Water	1 to 25 LPM

As the Omega air flow meter measures volumetric rates, pressure and temperature are measured downstream to the flow meter to determine actual flow conditions to obtain the mass flow rates. First, the gas density is calculated using Equation 4.1.

$$\rho_g = \frac{P}{ZRT} \quad 4.1$$

Then, having the air density and the air volumetric rate, the air mass flow rate downstream to the flow meter can be determined by the expression below:

$$\dot{m} = \rho_g q_g \quad 4.2$$

where P is the pressure, R is the specific gas constant for air, T is the air temperature, and q_g is the air volumetric flow rate.

Gas and liquid superficial velocities for the experimental work conducted for this thesis are calculated at the locations of pressure gradient measurement (e.g., specifically at Differential Pressure Transmitter 1 for the short test section and at Differential Pressure Transmitter 4 for the long test section-see Figure 4.2 and Figure 4.5).

Air density is calculated by Equation 4.1 having the pressure at pressure gradient measurement locations previously mentioned. Temperature is measured by Thermocouple 1 and

Thermocouple 2 at the inlet of the flow sections. Gas compressibility factor for air at the pressure and temperature conditions of the experiments conducted in this study is assumed as a unit. Having air density (ρ_g) and mass flow rate (\dot{m}) provided by the flow meter, the actual flow rate q_g is calculated with Equation 4.2. With the water volumetric flow rate, q_l , and pipe cross sectional area, A , the gas and liquid superficial velocities are determined by the Equations 2.3 and 2.4.

4.2.1. Short Test Section

As inclination plays a significant effect on multiphase flow behavior and consequently on the liquid holdup and pressure gradient, the short test section was designed to perform experiments with different inclinations. Figure 4.2 illustrates this flow section in the vertical position, which is supported by a series of stainless-steel unit struts and connected to a hinge to allow for a change of inclination using a hoist crane. Figure 4.3 and Figure 4.4 show the short test section in the horizontal position. Accurate inclination measurement is achieved using the hoisting system along with a dual-axis inclinometer attached to the short test section.

In the outlet of the short test section there is a 5 gallons capacity tank that was modified to be used as a separator for this flow loop. As shown in Figure 4.2, the tank has an air vent outlet and hoses connected as water return lines that are directly connected into the water tank supply to allow cyclic flow during experiments. This separator was built aiming an open-ended pipe in the outlet of the flow section, avoiding flow restriction at the test section outlet. Pressure and temperature next to the fluid injection point and near the flow regimes visualization towards the end of the pipe are recorded to monitor the operating conditions during the experiments. Flow regimes are visualized using a high-speed camera (120 frames per second). The short test section

can accommodate experiments with gas superficial velocities from 0.2 to 38 ft/s, and liquid superficial velocities from 0.44 to 2.2 ft/s.

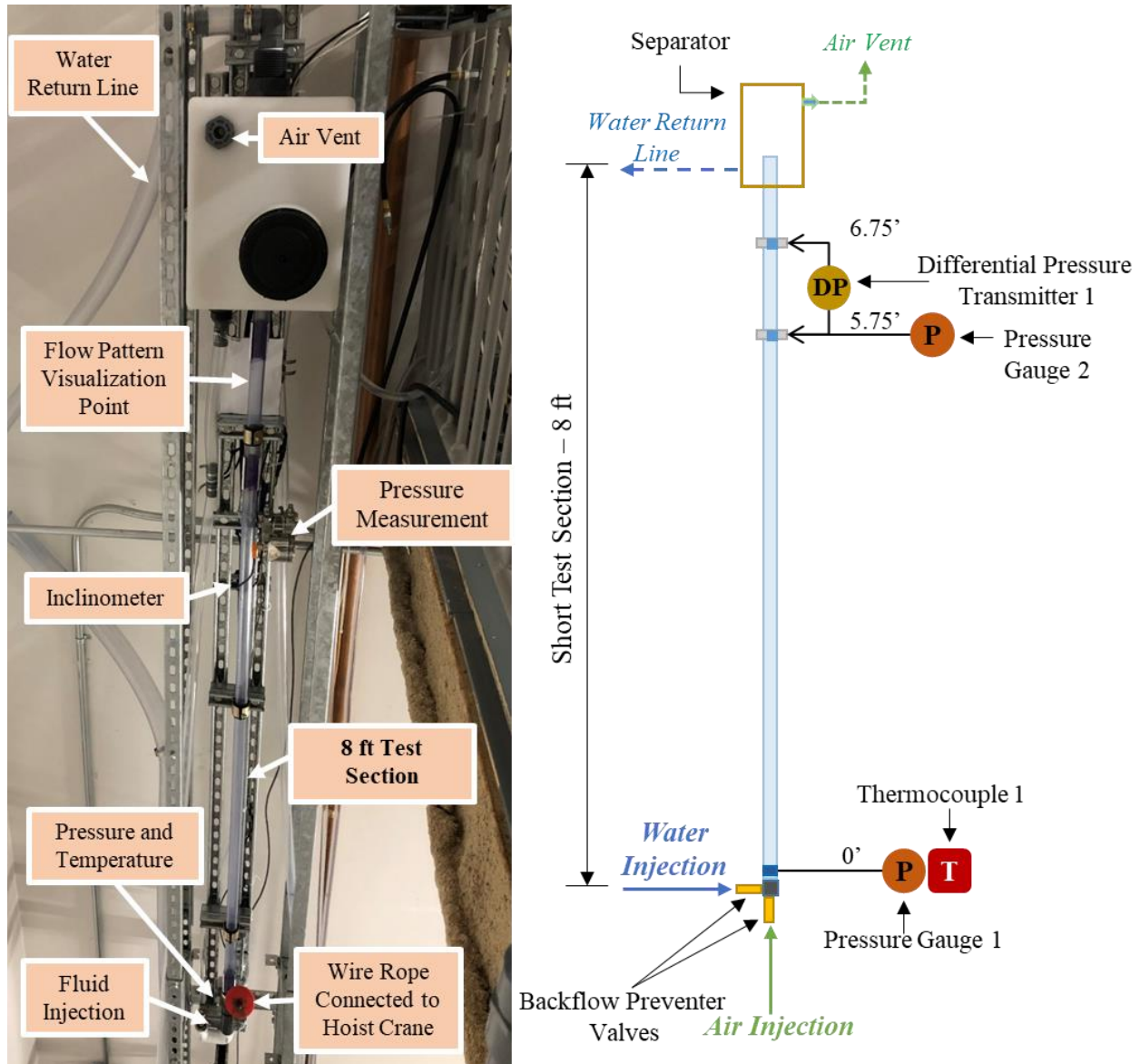


Figure 4.2. Short test section in the vertical position.

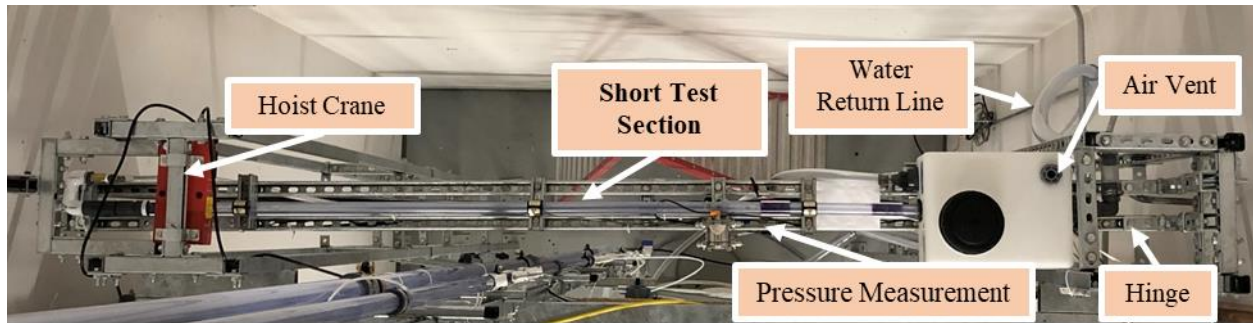


Figure 4.3. Short test section in the horizontal position.

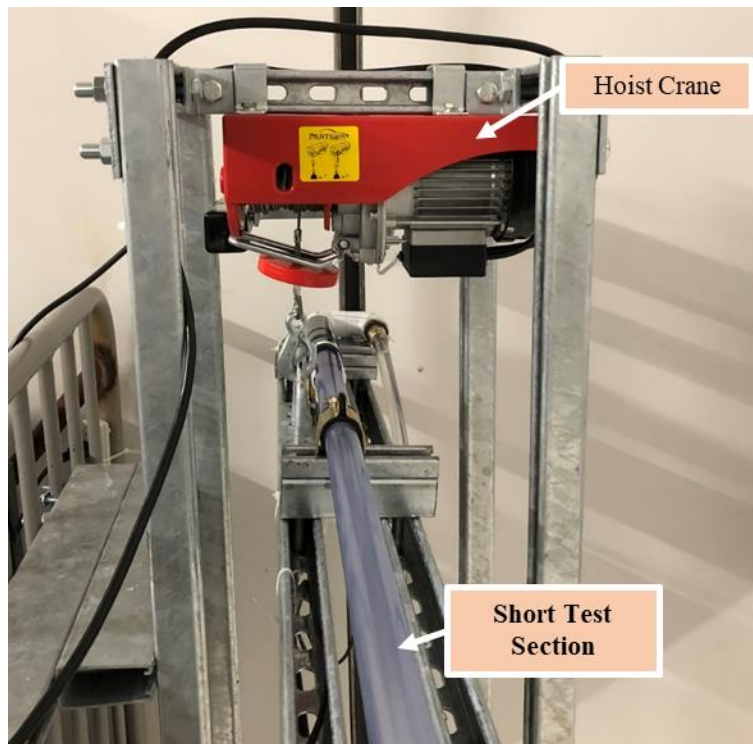


Figure 4.4. Hoist system for the short test section.

4.2.2. Long Test Section

As previously mentioned, the main objective of having a long test section is to investigate if the length of the short test section would have a significant effect on the measurement of pressure and flow regimes. As shown in Figure 4.5, the long test section has a similar separator at the outlet (to prevent flow restrictions at the outlet), which also has an air vent and a water return line to return water to the water supply tank.

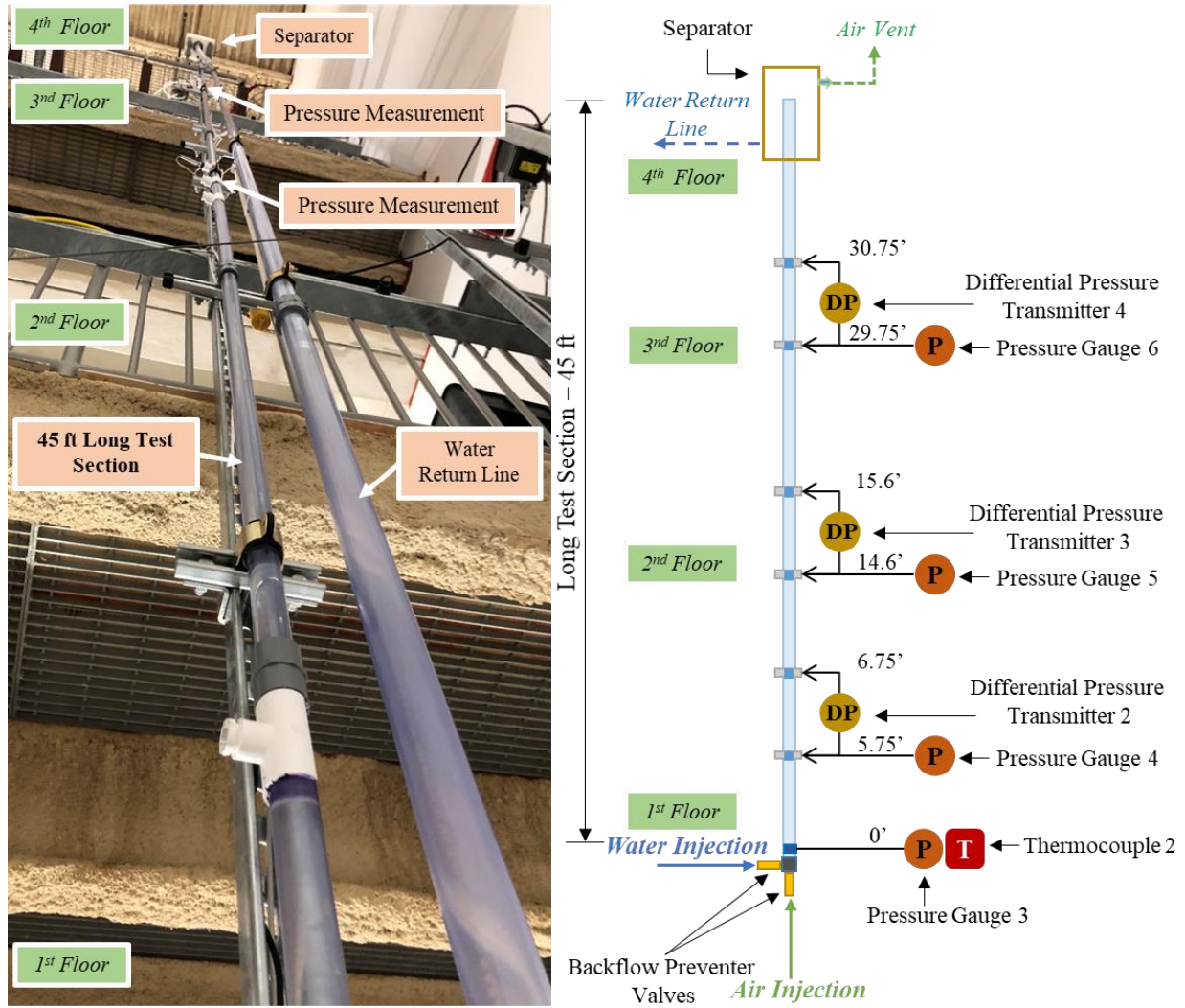


Figure 4.5. Long test section description.

4.3. Pressure and Temperature Measurements

Figure 4.2 and Figure 4.3 show a detailed illustration of the short flow section and long flow section with the specific locations of each pressure and temperature measurement devices and valves. Heights are shown in units of feet. Dark yellow circles named “DP” represent the locations where the differential pressure transmitters are installed. Such transmitters measure the difference in pressure between two pressure taps (1 foot apart from each other) in a location for short flow section and four locations along the pipe for long flow section. The resulting pressure gradient in (psi/ft) at the “DP” locations in the flow sections are calculated by Equation 4.3, where

the pressure drop ΔP in inches of water is provided by the differential pressure transmitters and ΔL is the distance between the two pressure taps (1 foot). The constant in Equation 4.3 is the conversion factor from inches of water to psi. In addition to the pressure differential measurements, both flow sections have pressure gauges placed at several locations represented by the orange circles named “P”. The gauges provide absolute pressure measurements that are used to determine the fluid and flow properties.

$$\frac{dP}{dL} = 0.0360912 \frac{\Delta P}{\Delta L} \quad 4.3$$

Table 4.2 provides the models, manufactures and pressure ranges of each of the measurement devices included in the test sections.

Table 4.2. Pressure measurement instrumentation.

Description	Model	Measurement	Manufacturer	Range
Pressure Transmitter 1	628 Series	Absolute	Dwyer	0 to 30 psig
Pressure Transmitter 2	A4	Absolute	Ashcroft	0 to 15 psig
Pressure Transmitter 3	GC51	Absolute	Ashcroft	0 to 100 psig
Pressure Transmitter 4	628 Series	Absolute	Dwyer	0 to 30 psig
Pressure Transmitter 5	GC51	Absolute	Omega	0 to 100 psig
Pressure Transmitter 6	5DEP3	Absolute	Ashcroft	0 to 15 psig
Pressure Transmitter 1	PX3005	Differential	Omega	-25 to 25 inH ₂ O
Pressure Transmitter 2	PX3005	Differential	Omega	-25 to 25 inH ₂ O
Pressure Transmitter 3	3051C	Differential	Rosemount	0 to 25 inH ₂ O
Pressure Transmitter 4	3051C	Differential	Rosemount	0 to 25 inH ₂ O

Each flow section has a temperature measurement at the locations of Thermocouple 1 and Thermocouple 2 represented by the red squared named “T”. Temperature measurements were obtained using thermocouples (Type T) connected to a National Instruments Module (NI 9210). Furthermore, both flow sections have two backflow preventer valves connected to the water and the air injection points. These valves are used to avoid that water flows into the air injection line or vice-versa during experiments. Facilitating the measurement of the liquid holdup is another application of the backflow preventer valves. By quickly stopping the air and water flows into the flow section downstream of the injection point, these valves do not allow backflow, holding the liquid phase inside the pipe. Therefore, the height of the liquid column can be determined either based on the pressure reading from the bottom pressure gauge or manually using a measuring tape. In the experiments performed in this work, the values for liquid holdup were determined by manually measuring the liquid column heights.

4.3.1. Calibration of the Equipment

An example of the calibration results for one of the pressure transducers is shown on Figure 4.6. The black dots represent the values for measured pressure in inches of water and their respective current signal. The dashed line is the trend line among the measured points, which represents the calibration curve. To obtain reliable measurements, calibrations parameters for pressure and flowrate measurements were input in the data acquisition and control software. The methodology used to calibrate the pressure measurement devices consisted of using a Dwyer Flex U-Tube filled with liquid (specific gravity 0.8) applied pressure and reading the different pressure readings in inches of water for the four differential transmitters listed in Table 4.2. For the pressure gauges, a deadweight machine was used to calibrate the pressure measurement devices having higher pressure ranges.

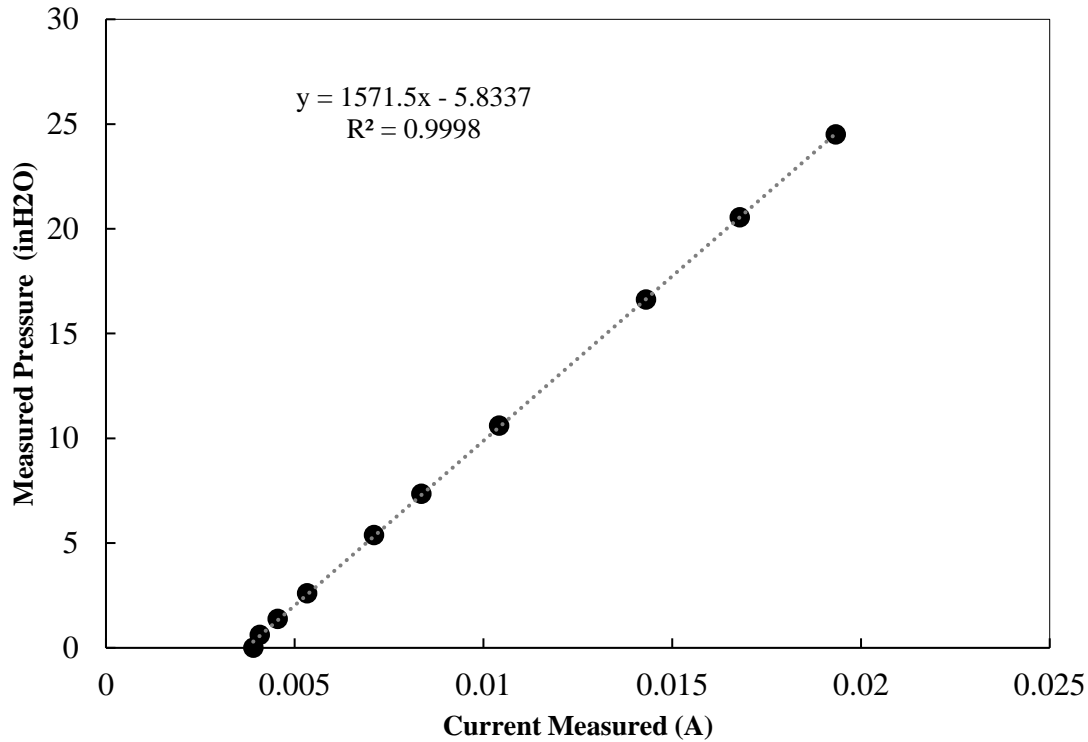


Figure 4.6. Example of a calibration curve representation for a pressure measurement device.

The water turbine flow meter was calibrated using a small water container and recording the filling time in order to calculate the volumetric flowrate using the equation below. For the air mass and volumetric flow rates, the calibration curve was provided by the manufacture, although air rotameters were used to validate these readings.

$$q_l = \frac{V}{t} \quad 4.4$$

where V is the volume of water filled in the container and t is the filling time.

4.3.2. Uncertainty Calculations

Quantifying the uncertainty of the measurements and considering the limitations of the precision in measurement devices is an important step in an experimental study. Therefore, after calibration of procedures have been finished, uncertainty calculations were performed for the pressure measurements. The uncertainty calculation followed the procedure described in

ISO (1998) and summarized by Waltrich (2012). The calculations based on the average (\bar{q}) and standard deviation (DP) of the measurements.

$$\bar{q} = \frac{1}{n} \sum_{i=1}^n q_i \quad 4.5$$

$$DP = \sqrt{\frac{\sum (q_i - \bar{q})^2}{n - 1}} \quad 4.6$$

q_i is each measurement reading and n is the total number of measurements.

The expanded uncertainty (U) is calculated by the equations below:

$$U = k \sqrt{u_o^2 - u_s^2} \quad 4.7$$

Where k is the Student coefficient, for this work it was equal to 2 for 95% probability for all calculations, u_o is the standard uncertainty from the measurements, u_s is the uncertainty from the measurement device, accuracy provided by the manufacturer.

u_o is the standard uncertainty for time-independent variables, obtained by the equation below:

$$u_o = \frac{DP}{\sqrt{n}} \quad 4.8$$

The uncertainty associated with the calibration process (u_{cal}) is calculated by:

$$u_{cal} = \sqrt{u_o^2 - u_a^2} \quad 4.9$$

Lastly, the uncertainty related to the curve fit from the calibration curves u_a is given by:

$$u_a = \sqrt{\frac{\sum (x_o - x_{fit})^2}{N - (1 + PD)}} \quad 4.10$$

x_o is the measured value for every calibration point, x_{fit} is the point in the curve fit associated with x_o , N is the total number of points for the calibration procedure, PD is the polynomial degree of the calibration curve fit.

4.4. Flow Regime Visualizations

To identify the flow regimes during each experimental run, a high-speed camera was used to record the flow between the pressure differential taps, in slow motion (recording 120 frames per second). Figure 4.7 and Figure 4.8 show a snapshot of different flow regimes obtained for vertical (90°) and inclined (45°) upward flow using the short test section.

The first picture in Figure 4.7 shows a visualization of a Taylor Bubble, the main feature of slug flow. The second shows a chaotic movement of both gas and liquid phase, which is the main characteristic of churn flow. Lastly, the third observation shows annular flow, having a gas core flowing in the middle of the pipe, and the liquid film on the wall.

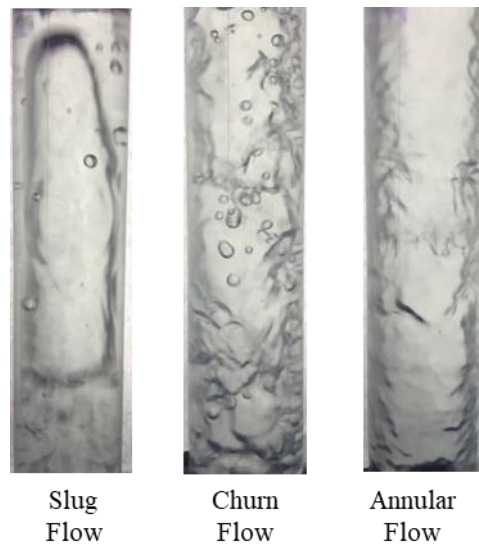


Figure 4.7. Snapshot of video recorded during experimental runs for Slug, Churn, and Annular for flow in a vertical pipe (90°).

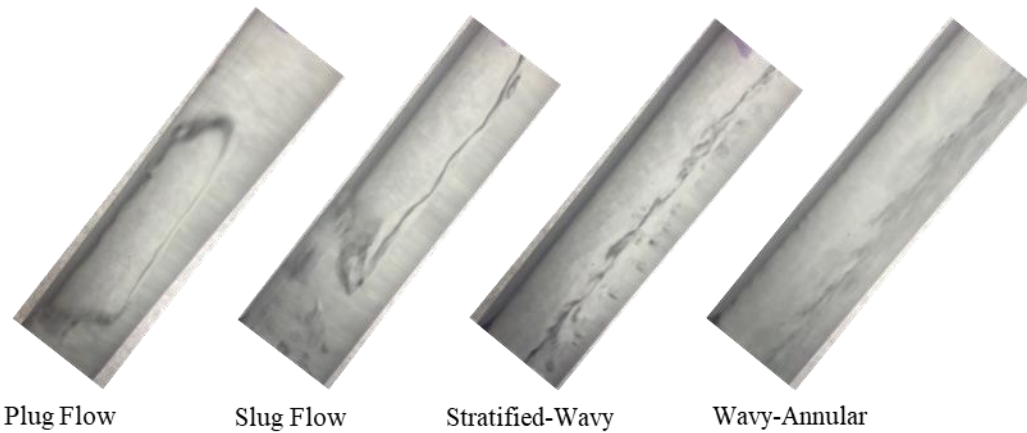


Figure 4.8. Snapshot of video recorded during experimental runs for Plug, Slug, Stratified-wavy, Wavy-annular for flow in an inclined pipe (45°).

4.5. Control and Data Acquisition System

The control system was developed in LabVIEW environment (LabVIEW 2017). This system allows the user to open and close valves, to control the hoist crane and change inclinations, set pump speed. It can acquire voltage signals for inclinations, flow rates, pressure, and temperature measurements. This data acquisition and control system can be remotely controlled and perform experiments. Figure 4.9 shows a snapshot of the control and data acquisition panel in LabVIEW.

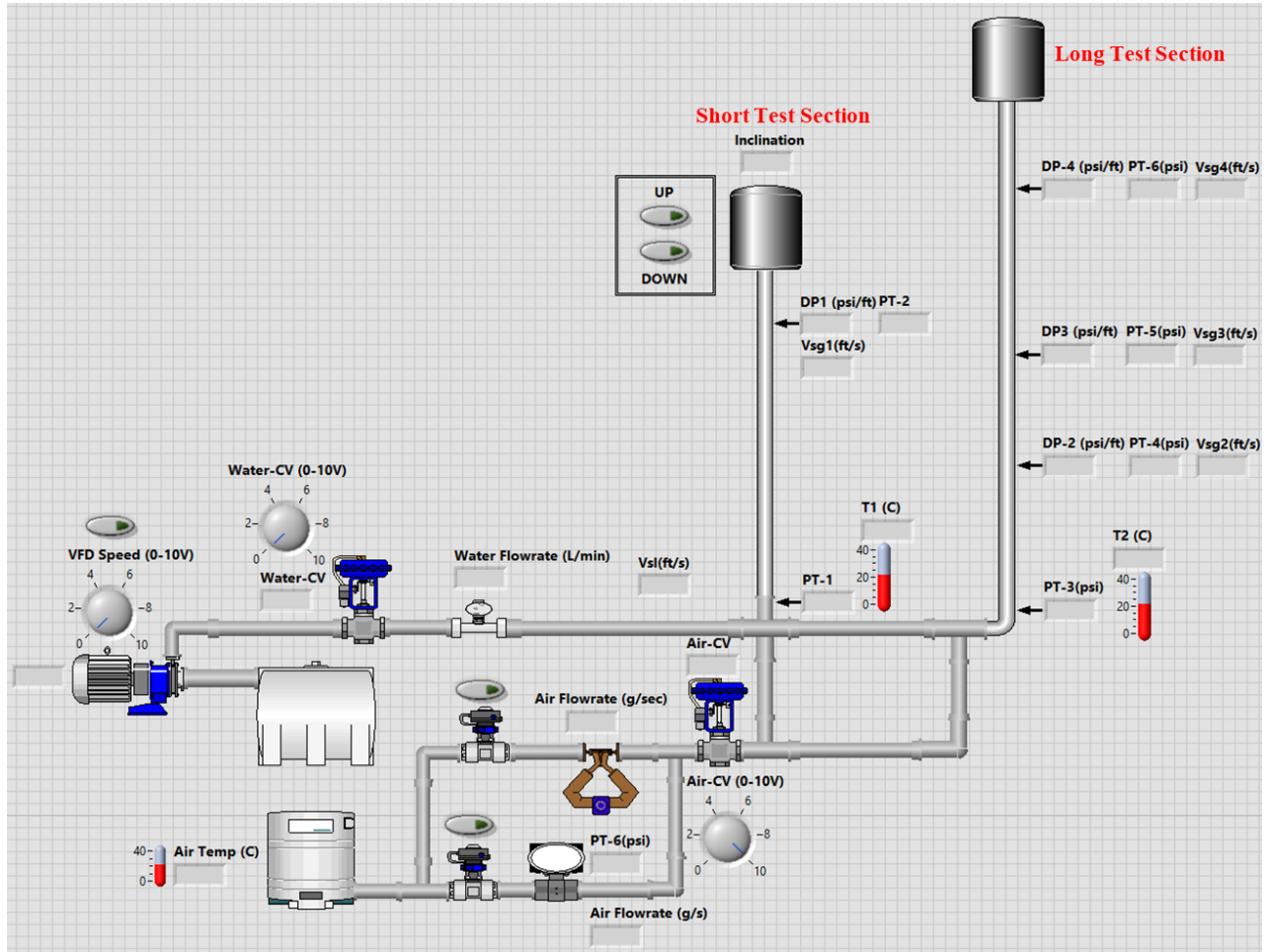


Figure 4.9. Snapshot of the control and data acquisition panel in LabVIEW 2017.

4.6. Direct Experimental Simulation and Data-Driven Approach

The concept of data-driven modeling for multiphase flow in pipes consists of either generating new data or using existing data to estimate the pressure gradient in gas-liquid two-phase flow in a given pipe section. The complete pipe system is discretized in several sections as shown in Figure 4.10. This figure presents an illustration of a well divided in “ n ” segments from the top to the bottomhole node. Each section has its inclination, gas and liquid velocities, and fluid properties.

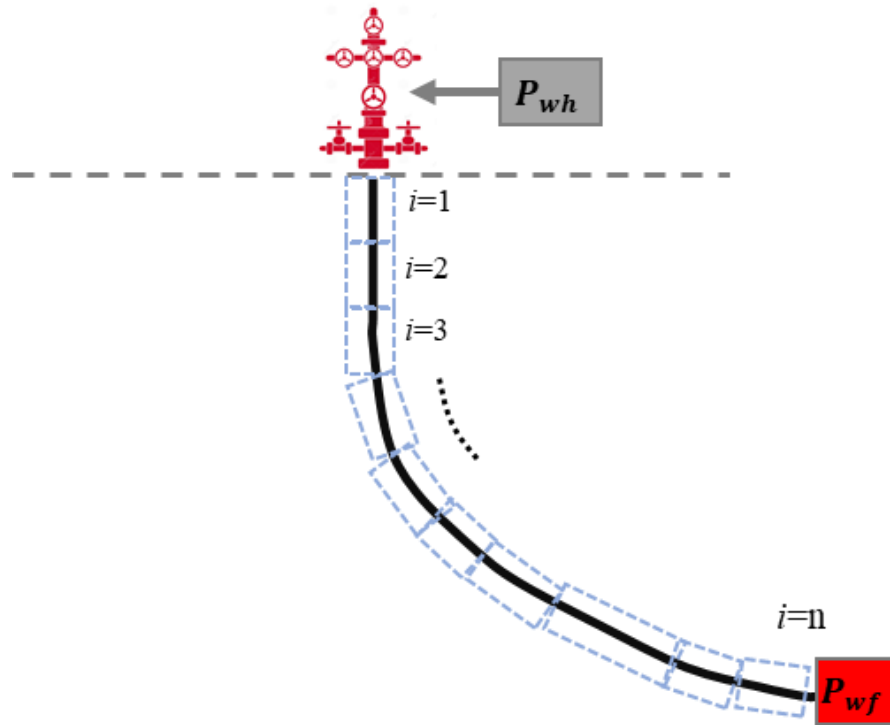


Figure 4.10. Pipe segmentation illustration.

Once data is available for the same or similar flowing conditions, it is possible to calculate the pressure gradient to each desired pipe segment. Figure 4.11 shows a workflow of the main steps, which in the data-driven method would be applied (light blue box) to determine the bottomhole pressure (P_{wf}), assuming that the wellhead pressure (P_{wh}) is given.

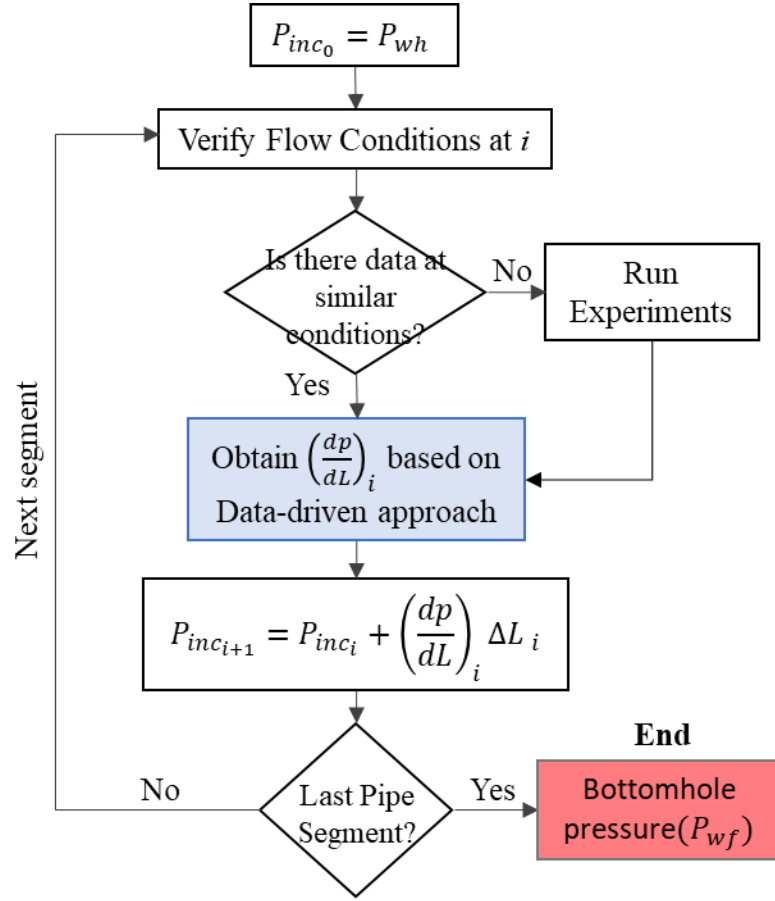


Figure 4.11. Workflow for direct experimental simulation based on a data-driven approach.

As can be seen in the figure above, pressure gradient is calculated in each pipe increment (ΔL_i) until the bottomhole pressure is obtained. There are two-ways in which the determination of pressure gradient can be accomplished and they are described in the flowcharts illustrated in Figure 4.12.

First, through the use of dimensionless numbers, such as the liquid, diameter, and velocities numbers (see Equations 2.1 – 2.4), said to account for the forces that govern multiphase flow (buoyancy, inertia, viscous, and surface tension) (Soo, 1990). These dimensionless numbers can be determined for each piece of the pipe discretization and used to directly determine pressure

gradient for their respective inclinations and flow conditions using data regression methods and machine learning algorithm trained with a data-set containing flow similar flow conditions.

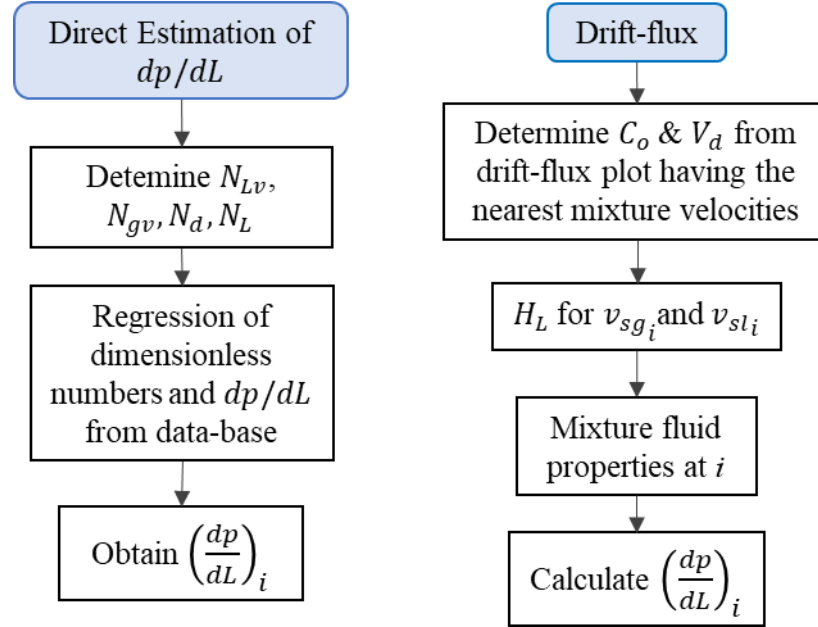


Figure 4.12. Flowcharts of drift-flux and direct estimations of dp/dL approaches.

The second approach is based on drift-flux concepts. The drift-flux distribution coefficient C_o and the drift velocity V_d are estimated for each inclination and flow condition based on a drift-flux plot (as shown in Figure 4.13). In this methodology, drift-flux parameters are derived from the slope and intercept of the straight line through the nearest points of the mixture velocity ($V_{sl} + V_{sg}$) of each pipe segment. The drift-flux coefficients allow the calculation of liquid holdup (H_L), which will be utilized to determine mixture fluid properties. Then, pressure gradient can be calculated.

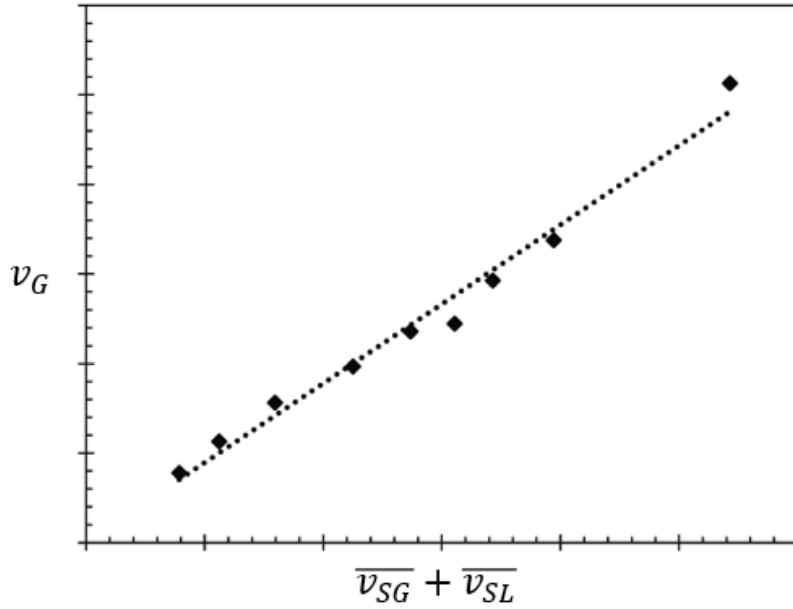


Figure 4.13. Drift-flux plot illustration.

This methodology presents a reliable way to accurately predict drift-flux parameters and liquid holdup. Distribution parameters and drift-velocities derived from this data-driven approach can also be used to improve transient models requiring steady-state liquid holdup. Some of these models have presented limitations, such as the work from Tornisiello (2020), likely to be caused when empirically derived correlations to predict C_o and V_d are used in a range of conditions that are beyond those which they were created.

This work will focus on the steps illustrated in Figure 4.12 for both data-driven approaches. Several experimental runs in vertical and inclined positions were performed on the short test section of the fully automated flow loop described in section 4.2.1. The data generated in the experiments will be used to obtain pressure gradient in both drift-flux and direct estimation of pressure gradient methods. The flow parameters will be obtained through regression of the nearest dimensionless number points for each case.

An extension of this approach aims to have existing multiphase flow data from different facilities around the world and be able to generate data to ensure a more accurate estimation of the pressure gradient in the field. The concept of direct experimental simulation along with the idea of Waltrich et al., (2014) of remotely running experiments and acquire important two-phase flow parameters have the potential of overcoming several multiphase flow challenges. The list below shows some of the facilities that today together have the potential of generating an extensive database for a wide range of conditions:

- Petroleum Engineering Research and Technology Transfer Laboratory (PERTT Lab) at Louisiana State University;
- The Tulsa University Fluid Flow Projects (TUFFP) at Tulsa University;
- TowerLab at Texas A&M University;
- SINTEF Multiphase Flow Laboratory in Norway;

5. Results and Discussion

This chapter presents the results and discussion of the experimental work performed for this thesis. The first section shows a summary of the experimental test matrix. Section 5.2 provides the results and discussion for the entrance effect evaluation, in which the experimental data for both short and long test sections were compared to each other. The experimental data is then used to evaluate the performance of empirical and mechanistic flow regime maps from the literature. Finally, the results from the data-driven model proposed in this study are compared to the experimental data and to other models often used in the oil and gas industry. As it is shown later in this chapter, the proposed data-driven model shows improvement when compared to the other models.

5.1. Experimental Test Matrix

Table 5.1 summaries the range of the two-phase flow conditions of the experiments carried in this thesis project. It includes pipe inclinations (measured from the horizontal), liquid and gas superficial velocities, pressure, and temperature of the tests using the short and long flow sections described in the previous chapter.

Table 5.1. Summary of the flow conditions of the experiments carried in this study.

Inclinations	Fluids	V_{sg} (ft/s)	V_{sl} (ft/s)	Pressure (psia)	Temperature (°F)
45° and 90°	Air–Water	0.2 to 38	0.44 to 2.2	≈15.7	72

Both data-driven techniques to obtain the drift-flux parameters and to directly measure the pressure gradient proposed in this thesis were compared to existing multiphase flow models. The next sections describe the entrance effect investigation, the flow regime map validation, the

models' performance evaluation and comparisons for upward vertical (90°) and inclined (45°) flow of air and water.

5.2. Entrance Effect Evaluation

As in multiphase flow in pipes in field applications, the pipe length is much longer than those in small scale experimental lab facilities, it is crucial to ensure that reliable evaluations of pressure gradient and other two-phase flow parameters are obtained in short test sections.

The first analysis of the experiments performed in this study was to determine whether the short test section is long enough to avoid the test section entrance effects. Five test runs with very similar flow conditions were performed for the short ($L/D = 72$) and long ($L/D = 346$) test sections. Because axial flow development and entrance effect of flow in pipes cannot be captured only by flow regime visualizations, pressure gradient at those locations were also recorded together with average liquid holdup in the entire pipe section.

Figure 5.1 summarizes the results of the experimental tests performed for entrance effects evaluation. The error bars in the latter figure represent the uncertainty of each pressure gradient measurement calculated using the method described in section 4.3.2.

As shown in Figure 5.1, the measurement for each of the cases was within the accuracy range of each other for both short and long test sections. Cases 1 and 5 resulted in high values of standard uncertainty on the long flow section measurements, mainly caused by the uncertainty component due to the calibration of the pressure transmitter, and also having an impact of the natural flow oscillations for those two-phase flow conditions (likely in churn flow regime). Visual observation of the flow regimes for the five cases in each flow section agreed for the same flow condition.

Therefore, the results of this analysis show that for an approximately 5 times longer pipe length, for similar local liquid and gas superficial velocities, the flow regimes and pressure gradient obtained for both sections agree, supporting the assumption that the short test section is not highly sensitive to the entrance effects.

The short pipe section length follows the recommended design methods for two-phase flow in pipes from Govier and Aziz (2008), which suggests that the distance required for flow stabilization of two-phase turbulent flow can be determined by Equation 5.1 from Knudsen and Katz (1958), described below for Newtonian fluids (two-phase Reynold's number above 2,100).

$$\frac{X_E}{D} \geq 50 \quad 5.1$$

where X_E is the pipe length and D is the diameter.

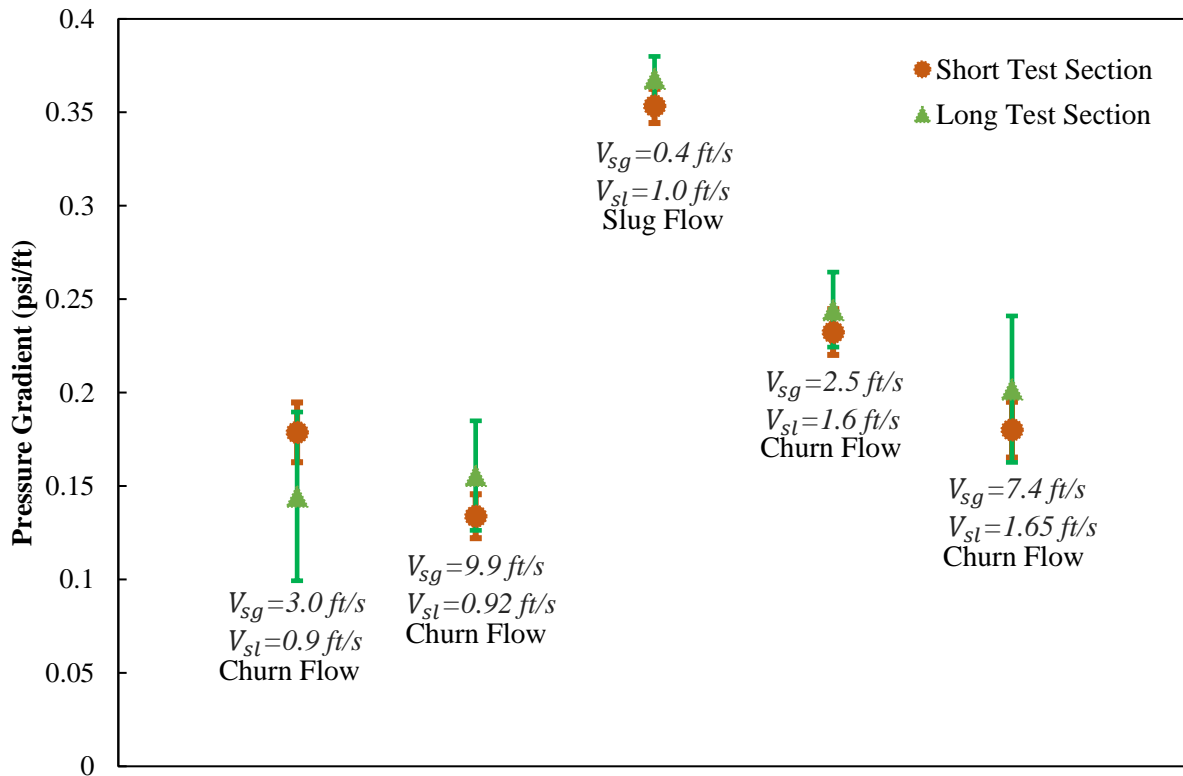


Figure 5.1. Entrance effect analysis for flow regime and pressure gradient at different liquid and gas superficial velocities.

For inclined pipes, the asymmetry caused by the gravitational force should be considered to determine the flow stabilization along the pipe length. However, no description of the impact of angle on the entrance effect in liquid-gas two-phase flow was found on the literature, other than Govier and Aziz (2008), who mentioned that for horizontal flow the impact of flow development is similar to the vertical, and the entrance effect for the two-phase in inclined and horizontal flow would be slightly less affected due to the reduction on the buoyancy effect.

Therefore, for this study, it was assumed that the short test section has no significant impact of entrance effects.

5.3. Flow Regime Validation

The high-speed camera allowed us to identify the flow regimes for each experimental run through visual observation. In addition to that, the liquid holdup was determined for most of the tests to quantitatively support the flow regime observation. In this section, the outcomes of the observations are compared and validated with empirical and mechanistic flow regime maps existing in the literature.

Figure 5.2 illustrates the validation of the results for upward vertical flow with the mechanistic flow regime map from Taitel et al (1980) and Aziz et al. (1972). As can be noted in Figure 5.2, only slug, churn, and annular flows were observed. For the pipe diameter (1.049-inch ID) used in this study, bubbly flow was not expected to be observed in any gas or liquid velocities.

The inexistence of bubbly flow is supported by the minimum diameter criteria to have bubbly flow proposed by Taitel et al (1980), which is represented by Equation 2.12. Based on their criteria for air-water flow and near atmospheric pressure, bubbles would be able to freely move in the liquid phase only when the pipe inner diameter is larger than 2 inches.

Moreover, according to the dimensionless diameter criteria proposed by Kataoka and Ishii (1987) presented by Equation 2.13, the flow condition of the pipe diameter is classified as small diameter flow, which means that Taylor bubbles are stable and slug flow can exist. For lower superficial gas velocities, slug flow was present as shown in Figure 5.2.

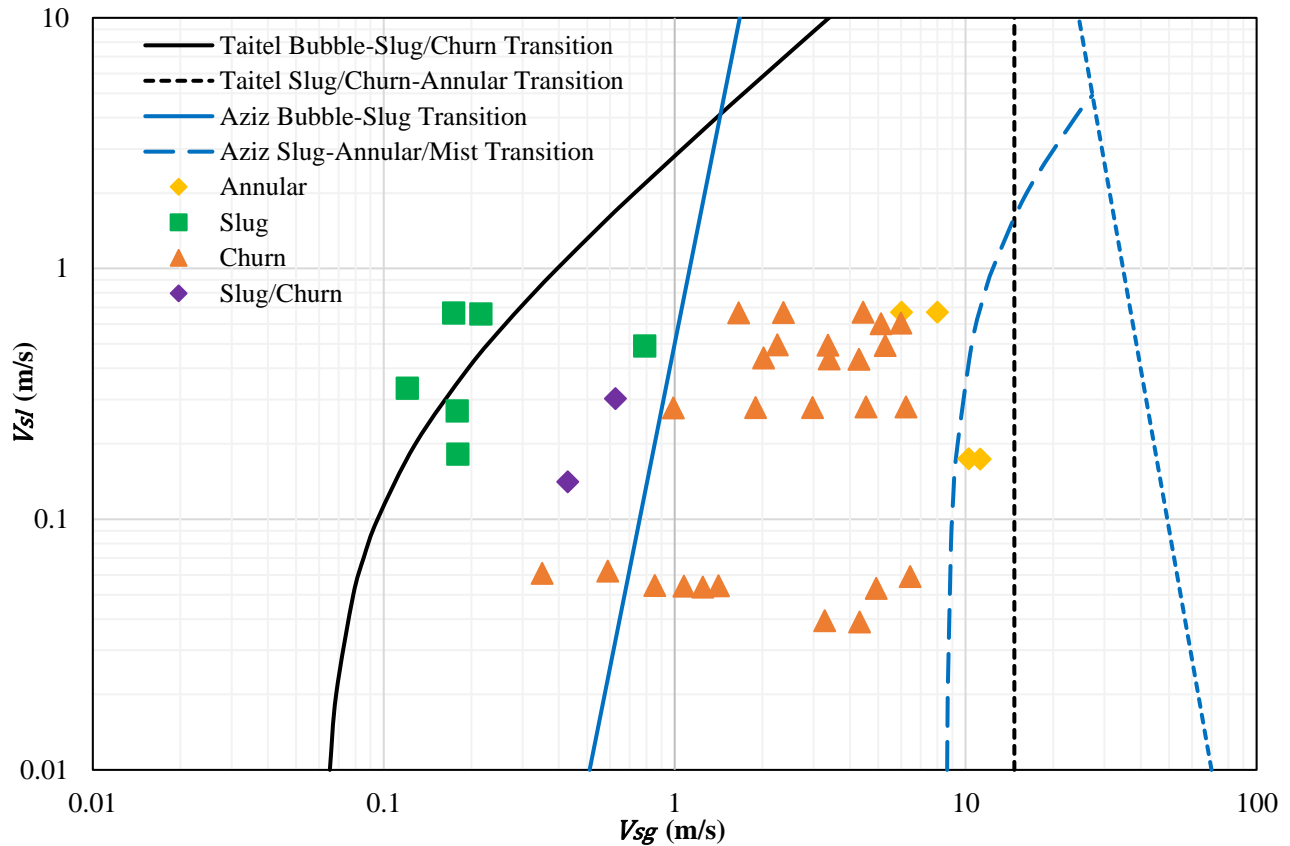


Figure 5.2. Validation of experimental flow regimes observation with Taitel et al. (1980) Aziz et al. (1972) vertical flow regime map.

Two-phase flow regime observations for vertical pipe indicate that most of the flow regimes of the experimental runs in this study are in churn flow regime, as shown in Figure 5.2 and Figure 5.3.

For the Taitel et al. (1980) flow regime map (Figure 5.2), the observed churn flows are encountered mainly on the slug/churn region. For Aziz et al. (1972) flow regime map (Figure 5.2), most of churn flow observations are in the slug and transition zone regions. The validation of the

churn flow observation can be supported by the comparison with Duns and Ros (1963) empirical flow regime map, as shown in Figure 5.3. When the flow observations from this work are compared with those from the flow regime map, of Duns and Ros (1963), similarities are seen on the slug and plug flow region, and churn and slug flow region.

Duns and Ros (1963) original flow regime map called slug flow a two-phase flow observation that can be compared to churn flow regime. Churn flow is still not well understood and many studies have considered it as a transition zone between slug and annular flow, or entrance-developing regime for slug flow (Taitel et al., 1980). More recently, the study of Waltrich et al. (2013) supported the existence of this churn flow regime for long vertical pipes.

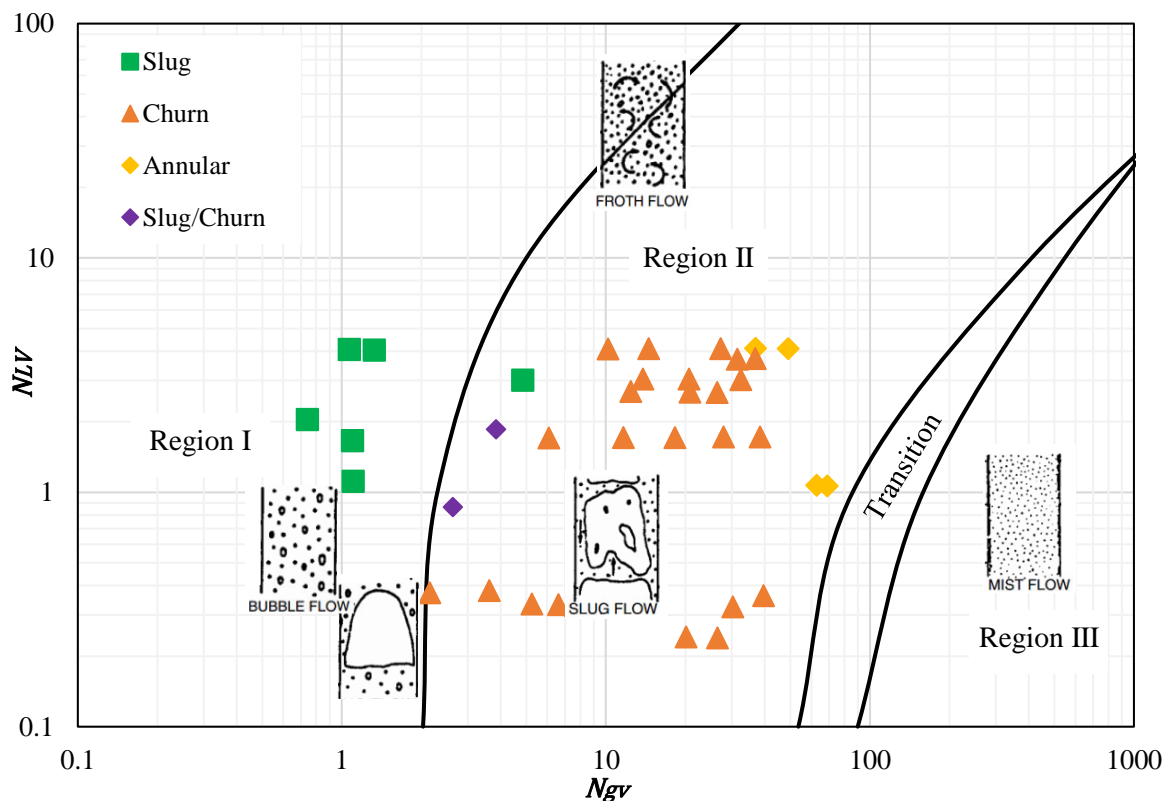


Figure 5.3. Validation of experimental flow regimes observation with Duns and Ros (1963) empirical vertical flow regime map.

The presence of churn flow can be reinforced by the transition criteria of Brauner and Barnea (1986), which is said to occur when the void fraction reaches a maximum liquid holdup value of 0.48 (Shoham, 2006). This agrees with the flow observations of this study, since all flow regimes identified as churn flow in this study had a measured liquid holdup of at least 0.42.

Overall, the flow regime observations for upward vertical flow presented a reasonable match when compared to Taitel et al. (1980), Aziz et al. (1972), and Duns and Ros (1963) flow regime maps, considering it is acceptable to have churn flow on the slug flow region as discussed previously. However, for higher gas superficial velocities, some discrepancies were observed for annular flow, as shown in Figure 5.2 and Figure 5.3.

Figure 5.4 shows the comparison of the flow observations for this work for upward flow in the short test section having an inclination of 45° with the horizontal. For this purpose, the flow regime map of Barnea et al. (1985) is used, which is an extended version of the mechanistic model of Taitel et al. (1980) that considers the effect of pipe inclination. It can be noted in Figure 5.4 that most of the flow observations are stratified wavy and annular flow. All annular flow observations are on the left of the intermittent annular transition, as for the annular flow cases for the vertical. The results do not have a good agreement with the flow regime map, however, it is close to the transition zone. Dispersed bubbles were not observed as well, mainly due to the small diameter of this flow section, as shown in Figure 2.5.

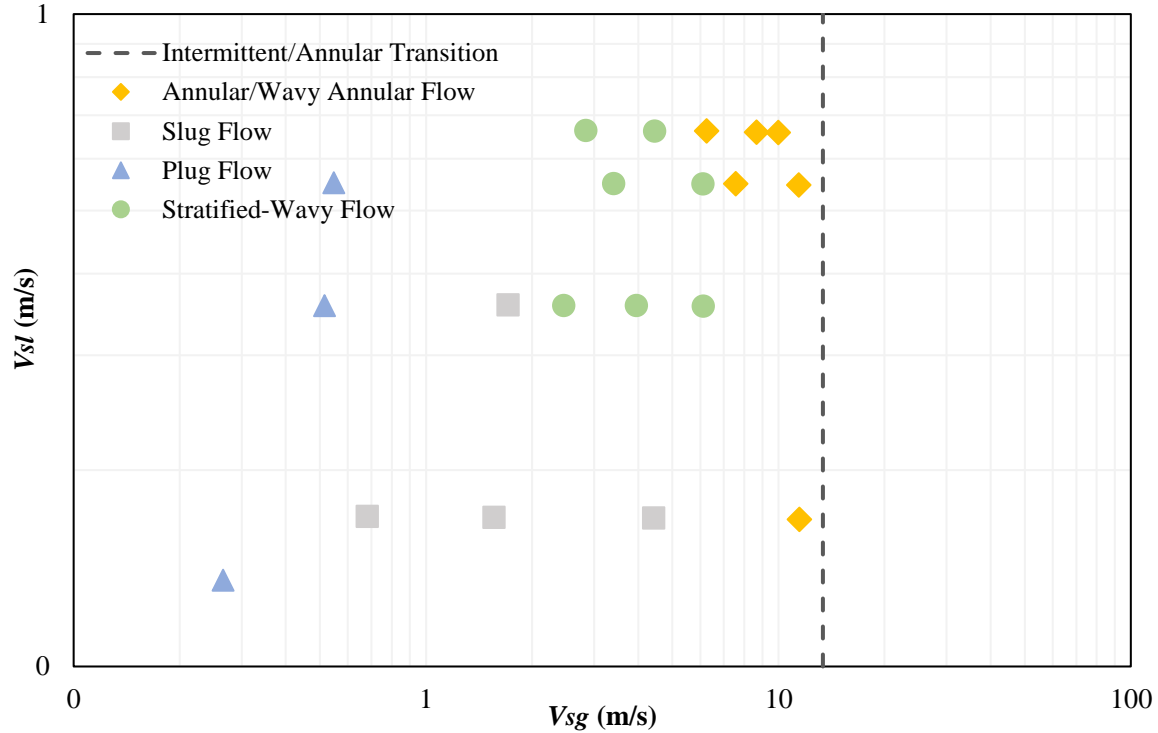


Figure 5.4. Validation of experimental flow regime observation at 45° with Barnea et al. (1985) empirical flow regime map for inclined pipes. This is a modification of Taitel et al. (1980) to account for pipe inclination.

From these experimental observations, it can be concluded that both vertical and inclined upward two-phase flow experimental observations have a reasonable agreement with the flow regime maps from Taitel et al. (1980), Aziz et al. (1972), Duns and Ros (1963).

5.4. Data-Driven Approach Applied to Liquid Holdup Followed by Pressure Gradient Predictions

Steady-state superficial gas and liquid velocities, and liquid holdup measurements were utilized to determine the classical drift-flux parameters proposed by Zuber and Findlay (1965), for vertical and inclined pipes. The results of this data-driven method were compared to the models results from Beggs and Brill (1973), Hagedorn and Brown (1965), Duns and Ros (1963), and Bhagwat and Ghajar (2014) correlation.

5.4.1. Results for Application of Drift-flux Concepts

The results of gas velocity as a function of the mixture velocity for upward vertical (90°) and inclined (45°) flows are shown in Figure 5.5. Twelve experimental tests for vertical and fifteen for inclined flow represented by the black circles were utilized as training data for the data-driven approach. These tests have the same experimental conditions of the testing cases that will be described in subsection 5.4.1.1. Table 5.2 shows the details of all training data in the data-driven approach.

As shown in Figure 5.5, three straight lines for each pipe inclination were plotted for Region I (low mixture velocities: 1 – 4ft/s), Region II (medium mixture velocities: 4 – 20ft/s), and Region III (high mixture velocities: 20 – 40ft/s). The variations of drift-flux velocity (V_d) and distribution coefficient (C_o) in the three regions shows that the two parameters are variant with respect to liquid and gas superficial velocities and are affected by the fluid dynamics in both inclinations. This observation supports the fact that the drift-flux parameters are flow regime dependent. Besides the lines for the three derived regions from the training data, the classic drift-flux straight line fit was plotted and is represented by the black and red lines. The drift-flux parameters derived from these six new lines define the drift-flux parameters for low, medium and high mixture velocities for vertical (90°) upward and inclined (45°) flow in this study.

Table 5.3 shows the obtained distribution coefficient (slope) and drift velocity (intercept) of the straight-line fit of all training experimental data points in Figure 5.5. The coefficient of determination (R squared) for each line from Figure 5.5 is shown in Table 5.3 as well.

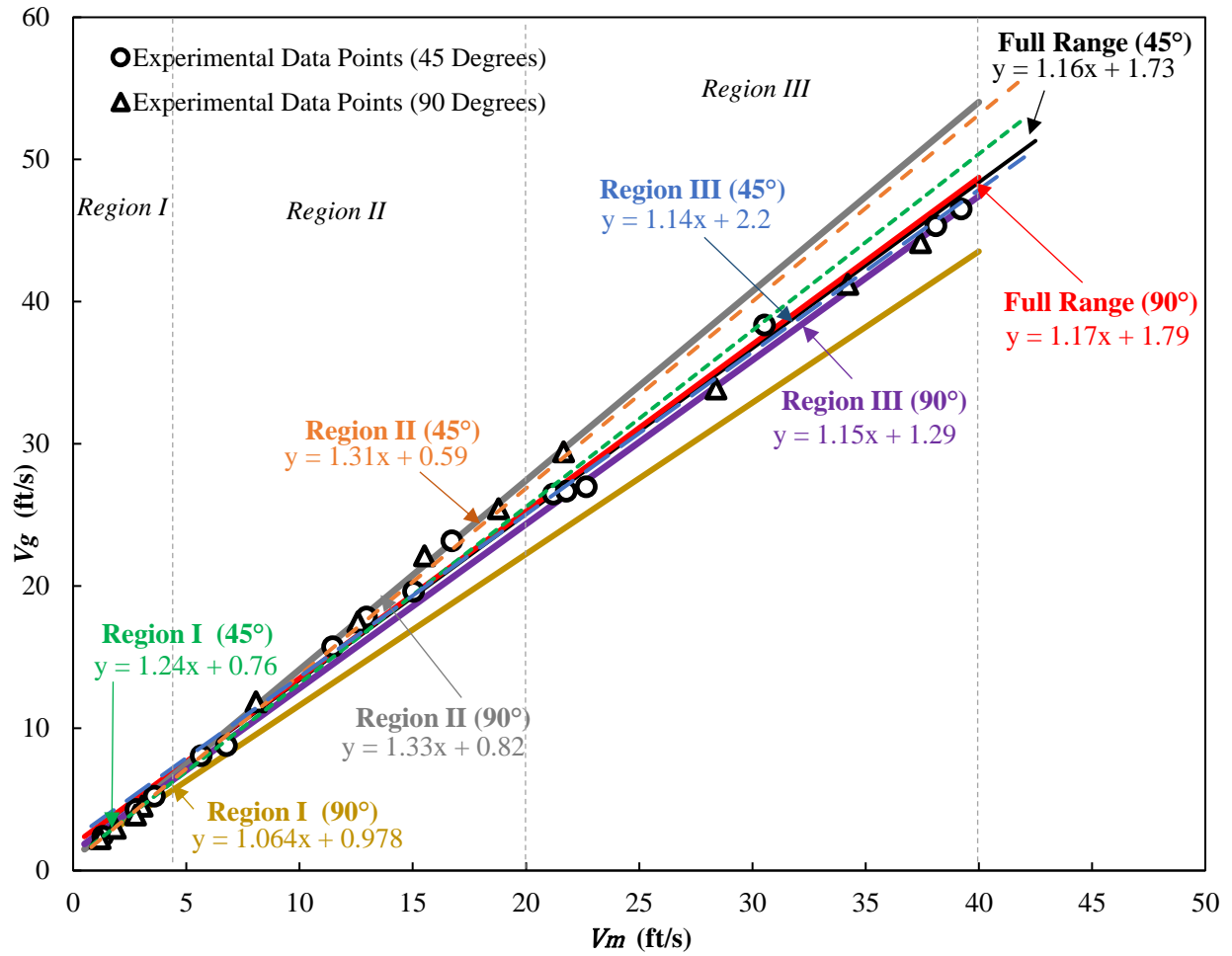


Figure 5.5. Drift-flux plot for experimental runs on short flow section for vertical (90°) and inclined (45°) two-phase flow, Region I (1 – 4ft/s), Region II (4 – 20ft/s), Region III (20 – 40ft/s), All Ranges (1 – 40ft/s).

Table 5.2. Training data for upward vertical (90°) and inclined (45°) flow performed in the short test section.

<i>Inclination</i>	<i>V_{sl}(ft/s)</i>	<i>V_{sg}(ft/s)</i>	$\frac{dP}{dL}$ (psi/ft)	<i>H_L</i>	<i>Flow Regime</i>
90°	0.46	1.407	0.189	0.528	Slug/Churn
	0.56	36.8	0.103	0.165	Annular
	0.57	33.6	0.107	0.183	Annular
	0.59	0.59	0.298	0.735	Slug
	0.99	2.05	0.224	0.547	Slug/Churn
	1.42	14.0	0.161	0.363	Churn
	1.43	11.13	0.171	0.363	Churn
	1.44	6.63	0.185	0.441	Churn
	1.97	16.8	0.254	0.339	Churn
	1.98	19.67	0.267	0.332	Churn /Annular
	2.18	0.57	0.384	0.853	Slug
	2.19	26.2	0.269	0.226	Annular
45°	0.44	0.87	0.157	0.636	Plug
	0.55	2.23	0.092	0.481	Slug
	0.55	5.10	0.066	0.366	Slug
	0.55	14.48	0.073	0.261	Slug
	0.55	37.6	0.080	0.171	Annular
	1.8	1.8	0.180	0.657	Plug
	1.8	11.2	0.130	0.373	Slug
	1.8	19.9	0.151	0.250	Stratified-wavy
	1.8	24.8	0.216	0.266	Stratified-wavy
	1.8	37.4	0.218	0.195	Stratified-wavy
	2.17	9.3	0.179	0.409	Plug
	2.17	14.6	0.174	0.371	Wavy-annular
	2.17	20.5	0.196	0.24	Wavy-annular
	2.16	28.4	0.228	0.26	Annular
	2.15	32.7	0.204	0.219	Annular

Table 5.3. Drift-flux parameters obtained for vertical (90°) and inclined (45°) two-phase flow.

<i>Inclination</i>	<i>Region</i>	<i>V_m (ft/s)</i>	<i>C_o</i>	<i>V_d (ft/s)</i>	<i>R²</i>
90°	Full range	1 to 40	1.17	1.79	0.9914
	I	1 to 4	1.06	0.97	0.9997
	II	4 to 20	1.33	0.82	0.9981
	III	20 to 40	1.15	1.29	0.9937
45°	Full range	1 to 40	1.16	1.73	0.9941
	I	1 to 4	1.24	0.76	0.9999
	II	4 to 20	1.31	0.59	0.9953
	III	20 to 40	1.14	2.20	0.9936

For both Regions I and III, the distribution coefficients obtained are within the range of 1.0 – 1.2 typically reported in the literature. When observing the C_o for Region II, which according to flow regimes observations is where most of the churn flow tests were encountered, the value of the distribution parameter agrees with that reported by Sharaf et al. (2016). The latter authors gathered data from the literature on several studies for churn flow and identified that this parameter can be as high as 1.3 for churn flow at low liquid superficial velocities, as also reported by Gouvier and Short (1958). For higher liquid mixture velocities (Region III), the obtained C_o also agrees with the literature (Bhagwat and Ghajar, 2014; Shi, 2004), approaching to a unit.

As shown in Table 5.3, the distribution coefficients (C_o) for inclined flow only had a relatively small change when compared to those from the vertical flow. As reported in the paper from Bhagwat and Ghajar (2014), the distribution coefficients are not impacted by flow inclination, instead, it depends mostly on the flow patterns. It can be confirmed looking at the

results of the high-velocity Region III, which both contain a higher fraction of gas (characteristic of annular flow), resulting in the distribution coefficient closer to 1 due to the uniformity of the velocity profile in the gas core. In contrast, the drift velocity (V_d) is the result of the interaction of the gravity, buoyancy, surface tension and inertia, and therefore, it is affected by the change of inclination.

The results of drift velocity in Region III (higher velocities – heterogeneous flow) in Table 5.3 for inclined flow are higher than those for vertical flow. This agrees with the results observed by Gokcal et al. (2009) which saw that the drift velocity increases with the inclination angle until a maximum value at around 40° from horizontal and then decreases until it reaches the lowest value for the vertical flow. A similar study with a qualitative explanation was done by Bonnecaze et al. (1971), which concluded that the drift velocity is proportional to the distance of a gas bubble to a given point at the pipe cross-section flow, and as the inclination changes that distance increases until a maximum value and then decreases until to a minimum. The same trend was not observed for Regions I and II, which drift-velocities were slightly higher for vertical flow.

Liquid Holdup Results Table 5.4 provides the experimental measurements for each of the vertical and inclined testing cases evaluated. These testing cases are not included in the drift-flux plots previously described. They have the same flow conditions and include velocities and flow regimes within training data.

Table 5.4. Testing cases for vertical (90°) and inclined (45°) upward flow.

<i>Case #</i>	<i>Inclination</i>	$V_{sl}(ft/s)$	$V_{sg}(ft/s)$	$\frac{dP}{dL} (psi/ft)$	H_L	<i>Flow Regime</i>
1	90°	1.3	0.92	0.311	0.73	Slug
2		1.3	2.01	0.224	0.57	Churn
3		1.3	6.65	0.161	0.41	Churn
4		1.3	13.9	0.185	0.33	Churn
5		1.3	20.0	0.193	0.32	Annular
6		1.3	28.9	0.165	0.24	Annular
7	45°	1.17	1.68	0.164	0.6	Plug
8		1.17	6.77	0.109	0.36	Slug
9		1.17	9.22	0.115	0.34	Stratified-wavy
10		1.17	14.12	0.10	0.33	Stratified-wavy
11		1.17	21.2	0.139	0.24	Stratified-wavy

For each testing case, the drift-flux parameters from Region I, II or III from Table 5.4 were used to determine the liquid holdup, depending on the mixture velocity. Figure 5.6 and Figure 5.7 show the percentage error of the calculated liquid holdup of each testing data for all models evaluated. Hagedorn and Brown (1965) was included only for the vertical flow cases since this model is not expected to perform well for deviated pipes. Therefore, Beggs and Brill (1973) empirical model for inclined pipes was employed for performance comparison only for the inclined flow testing cases.

As shown in Figure 5.6 and Figure 5.7 for most of the vertical and inclined testing cases, the methodology proposed in this work to estimate liquid holdup based on exiting dataset provides better results than commonly used empirical models of Duns and Ros (1963), Beggs and

Brill (1973), Hagedorn and Brown (1965), and the drift-flux correlation of Bhagwat and Ghajar (2014). Figure 5.6 indicates that Bhagwat and Ghajar (2014), Duns and Ros (1963), Hagedorn and Brown (1965), Beggs and Brill (1973) models under predicted liquid holdup for all cases.

In Figure 5.6 and Figure 5.7, we can notice that the overall liquid holdup errors are increasing with gas superficial velocities. For the drift-flux models, including this work; classic drift-flux method; and Bhagwat and Ghajar (2014), the main reason of having higher errors at higher velocities is the fact that as gas superficial velocity increases, liquid and gas phase distribution will become more heterogeneous, and drift-flux models are not recommended for these scenarios. On the other hand, Beggs and Brill (1973) and Duns and Ros (1965), predicted slug flow regime for the majority of the cases that were identified as either churn or plug flow during experiments. As a result, their correlations provided lower values of liquid holdup and led to relatively errors (up to -50%) when compared to the measured ones. The opposite behavior happens with Hagedorn and Brown (1965) model in Figure 5.6. For their results, liquid holdup errors become smaller for higher velocities. These discrepancies are possible due to the nature of their correlations, which correlate pseudo liquid-holdup instead of measured ones. According to Mukherjee and Brill (1999) not attempt had been made to know whether this assumption can affect a wide range of flow conditions. For friction dominated conditions, liquid holdup errors are not going to have a major impact on the pressure gradient calculation, and this will be further explained in the next section.

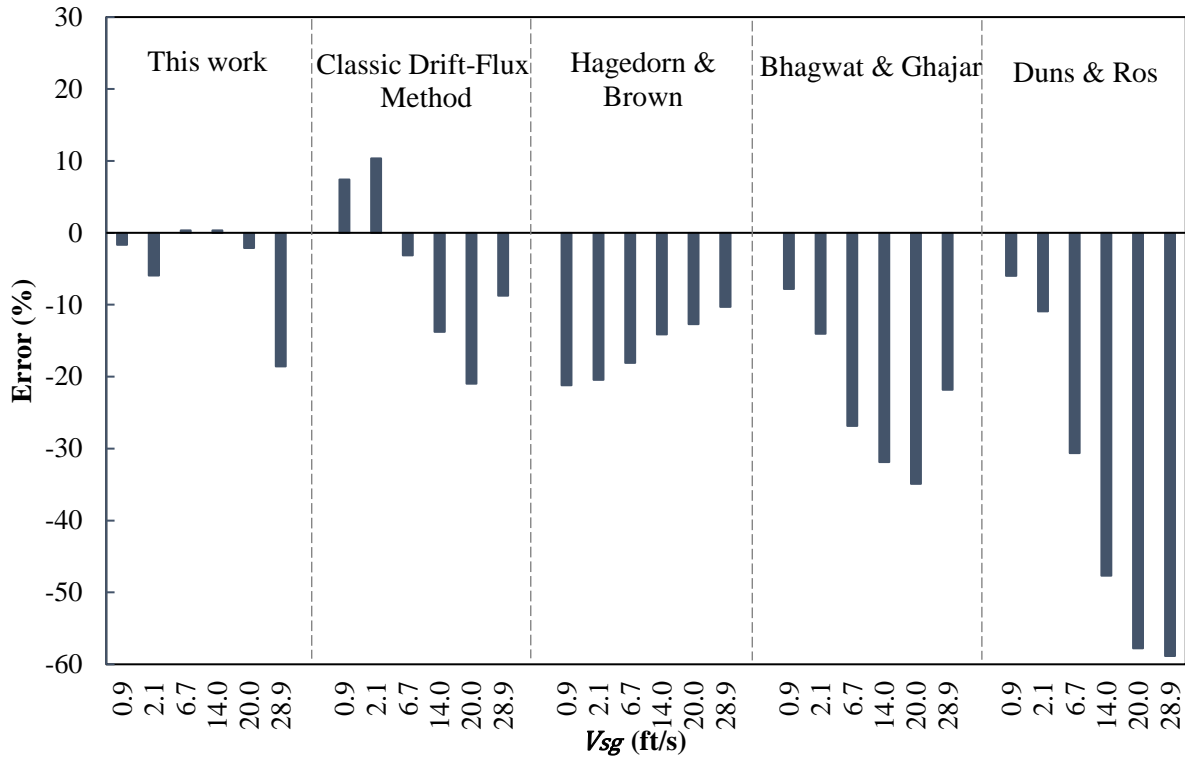


Figure 5.6. Liquid holdup errors for each model in upward vertical (90°) flow having constant liquid superficial velocity ($v_{sl}=1.3\text{ft/s}$).

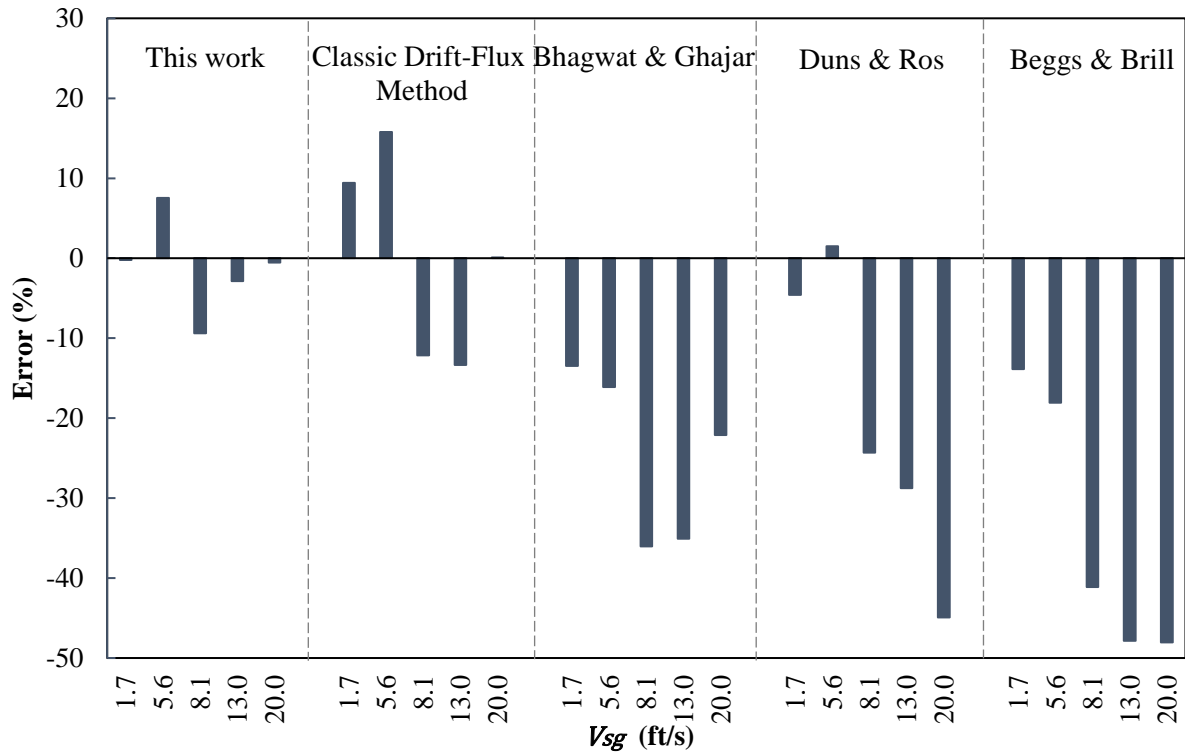


Figure 5.7. Liquid holdup errors for each model in upward inclined (45°) flow having constant liquid superficial velocity ($v_{sl}=1.17\text{ ft/s}$).

Figure 5.8 summarizes the evaluation of the overall performance for all models investigated. The empirical models of Duns and Ros (1963) and Beggs and Brill (1973) resulted in larger errors. Both models were derived from a series of experiments containing air-water and also having a pipe diameter similar to this study. Although Hagedorn and Brown (1965) did not experimentally measure liquid holdup, they developed a correlation to obtain the pseudo liquid holdup to match their measured pressure gradient. When comparing the average absolute errors in Figure 5.8, the approach proposed in this study shows an improvement of approximately 11% compared to Hagedorn and Brown (1965) model, approximately 30% compared to Duns and Ros (1963) model, and an improvement of approximately 28% compared to Beggs and Brill (1975) model. Looking at the standard deviations represented by the error bars, it can be observed the all models have a wide variation of errors, which is mainly resulted from the errors for higher gas superficial velocities observed in Figure 5.7.

The results comparison from the classical drift-flux model with this approach implies that assuming that the drift-flux parameters (C_o and V_d) are invariant with velocities changes can significantly impact the prediction of the liquid holdup. For all cases, except for the vertical flow $V_{sg} = 28.9$ ft/s (Case 6), the classical drift-flux approach resulted in an average absolute error of at least 2 times higher than this work. Bhagwat and Ghajar (2014) presents higher errors when compared to the results of this work. Although their work includes the range of conditions tested in this study, the approach proposed here showed an average improvement of approximately 20% on the estimation of the liquid holdup for both vertical (90°) and inclined (45°) cases. For the inclined flow cases, the empirical model from Beggs and Brill (1973) model, which accounts for inclination effects, resulted in the highest errors as seen in Figure 5.7 and Figure 5.8.

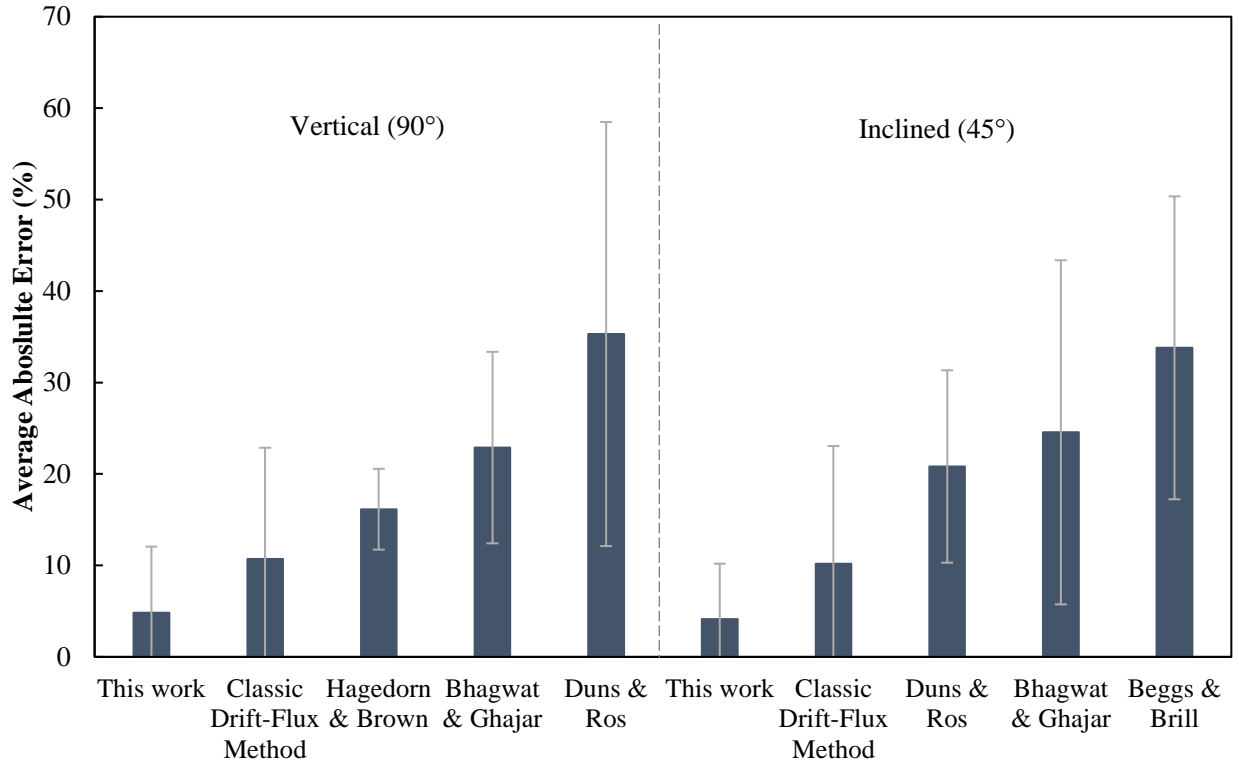


Figure 5.8. Average absolute error of the liquid holdup for vertical (90°) and $v_{sl}=1.3$ ft/s; inclined (45°) and $v_{sl}=1.17$ ft/s. Error bars represent the standard deviation of liquid holdup calculation of all cases for each model and pipe inclination.

5.4.1.1. Pressure Gradient Results

Figure 5.9, Figure 5.10, and Figure 5.11 provide the results of the pressure gradient prediction for the cases in Table 5.4. The liquid holdup previously obtained were used to determine the mixture fluid properties and the pressure gradient components for each case. Figure 5.9 shows that the approach proposed in this work does not provide improved results for high gas velocities for the pressure gradient. However, the same conclusion is not observed for the liquid holdup predictions. For the cases with high gas velocity (Cases 5 and 11), this method led to relatively low errors for the liquid holdup.

This discrepancies of errors between liquid holdup and pressure gradient, and the overall trend of errors as gas superficial velocity increases, can be explained by the fact that, for high gas

velocities, the liquid holdup does not have a major impact on the pressure gradient, since the gravitational component of total pressure gradient becomes significantly smaller than the friction component as velocity increases. Therefore, in high gas content (or gas superficial velocity), the total pressure gradient is frictional dominated, mainly dependent on the velocities. This is more evident when the results for 45° inclined flow tests are analyzed. In inclined pipes, the gravitational component is lower due to the lower hydrostatic force. For instance, the test having the highest gas superficial velocity for inclined flow ($V_{sg} = 20\text{ft/s}$) has liquid holdup prediction with small errors for this work, but the results of pressure gradient have the highest errors

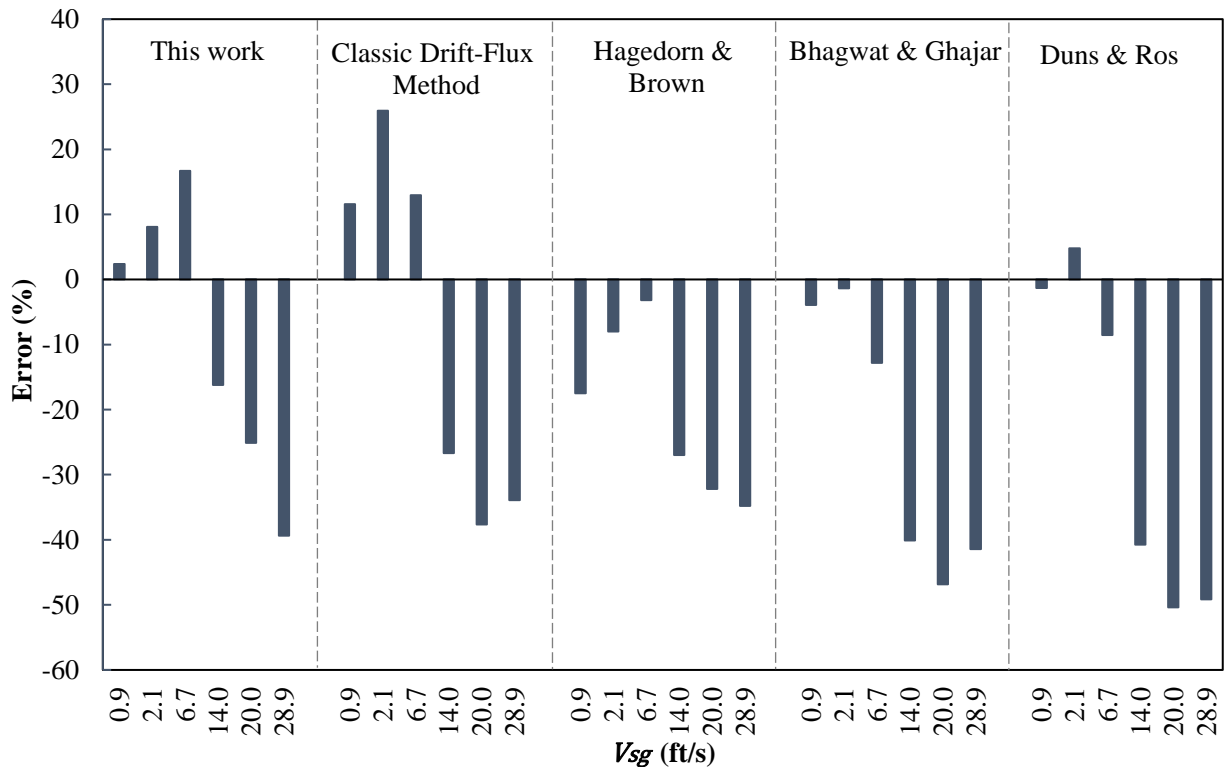


Figure 5.9. Pressure gradient errors in each model for upward vertical (90°) flow having constant liquid superficial velocity ($v_{sl}=1.3\text{ft/s}$).

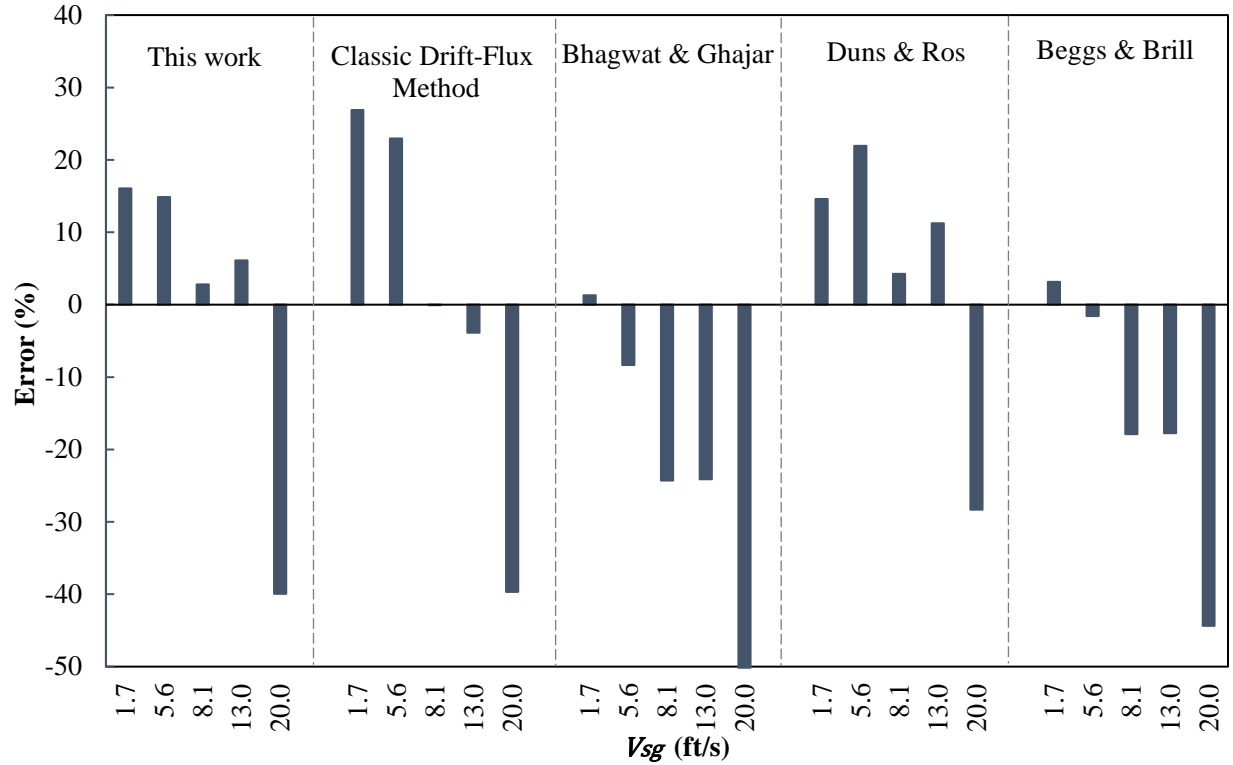


Figure 5.10. Pressure gradient errors in for each model for upward inclined (45°) flow having constant liquid superficial velocity ($v_{sl}=1.17$ ft/s).

To explain the results for the churn flow scenarios (Cases 2, 3, 4), we can use the definition of the mixture density below,

$$\rho_m = \rho_g(1 - H_L) + \rho_L H_L \quad 5.2$$

where ρ_m is the mixture density, ρ_g is the density of the gas phase, ρ_L is the density of the liquid phase, and H_L is the liquid holdup.

The relatively high errors for the pressure gradient for Duns and Ros (1963), Bhagwat and Ghajar (2014), and Hagedorn and Brown (1965) are a consequence of the under prediction of liquid holdup from Figure 5.6. The gravitational component for churn flow has a significant impact on the estimation of the total pressure gradient (see Figure 2.4). As shown in Equation 5.2, the mixture density is proportional to the liquid holdup. High errors from Duns as Ros (1963) are

mostly due to the mismatch with the flow regime prediction. It predicted to have slug flow in all cases, which led to poor liquid holdup determination and consequently erroneous pressure gradient. Therefore, large errors in the estimation of liquid holdup will have a significant impact on the total pressure gradient.

As can be seen in Figure 5.11, an estimation of the pressure gradient using the liquid holdup with the data-driven approach for drift-flux parameters determination resulted in a relatively lower average absolute error than the other models. Overall, the average absolute error for this approach was impacted by the high errors of Cases 6 and 11 (highest velocities). It is important to mention that the applicability of the drift-flux concept in a non-homogenous flow regime such as in annular flow is not typically recommended. In addition to that, these results show that the classical drift-flux method assuming that the distribution coefficient and drift velocities are flow regime independent and lead to higher errors on the liquid holdup prediction and pressure gradient. The work from Turney et al. (2018) also observed the effects caused by the drift-flux curve shift due to the change of two-phase flow regimes. The error bars in Figure 5.11 represent the standard deviation of the errors for cases evaluated with different models. As for the liquid holdup evaluation, they are indicating that all models resulted in a wide range of pressure gradient values.

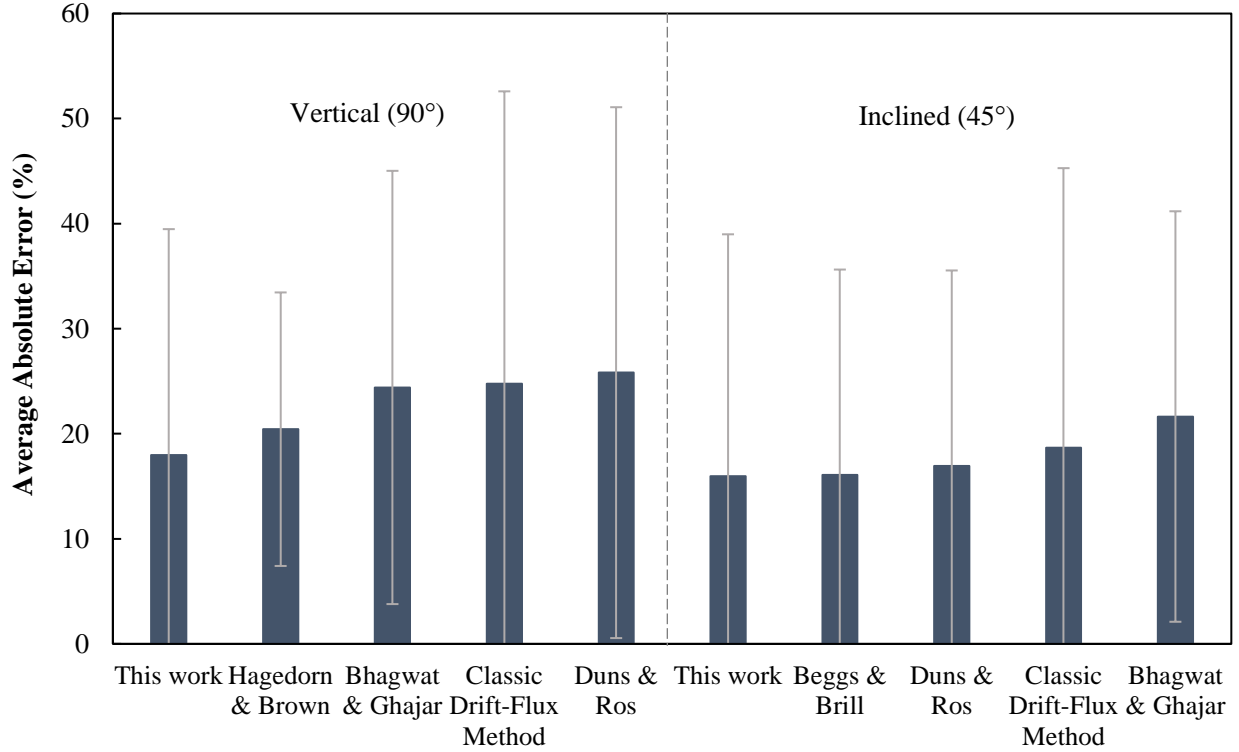


Figure 5.11. Average absolute error of the pressure gradient for vertical (90°) and $v_{sl}=1.3$ ft/s; inclined (45°) and $v_{sl}=1.17$ ft/s. Error bars represent the standard deviation of pressure gradient calculation of all cases for each model and pipe inclination.

5.4.2. Summary of Results

Figure 5.12 and Figure 5.13 show the main results obtained for all experiments and cases evaluated in Section 5.4. Figure 5.12 shows the measured liquid holdup as a function of the calculated liquid holdup for each model, for both vertical and inclined cases.

The approach introduced in this work provided excellent results for liquid holdup calculations, having all (except one) points within $\pm 10\%$ error. However, for the pressure gradient determination based on the liquid holdup predicted with the drift-flux approach, it presented errors higher than 20% for a couple of scenarios, particularly for high gas velocities. This trend was observed for the models of Bhawat and Ghajar (2014), Beggs and Brill (1973), Duns and Ros (1965), which showed even higher errors for a significant number of cases.

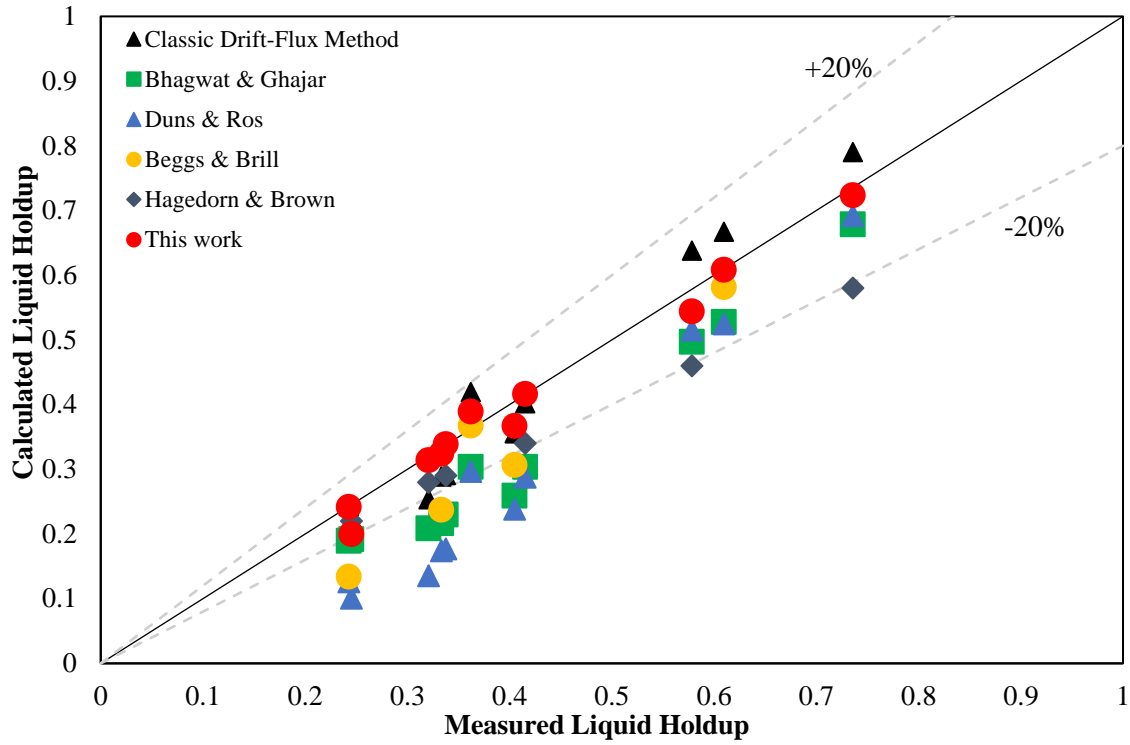


Figure 5.12. Results summary for liquid holdup calculation of all cases for all models in vertical (90°) and inclined (45°) two-phase flow. Dashed lines represent the $\pm 20\%$ error region.

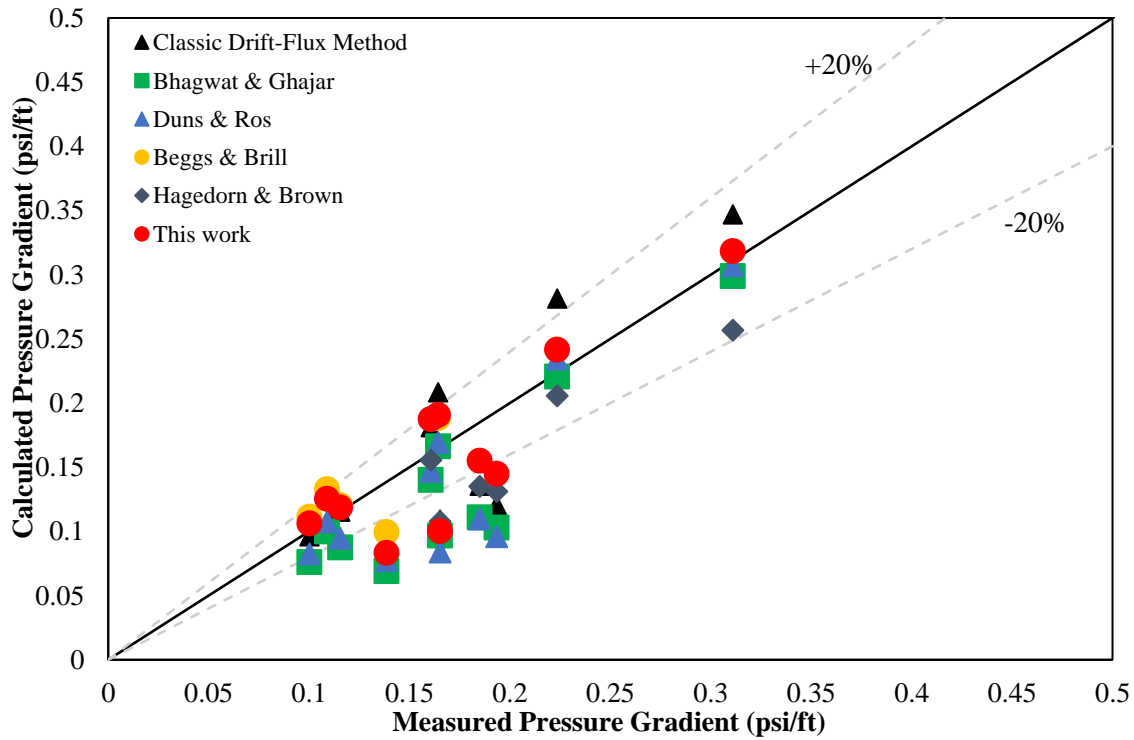


Figure 5.13. Results summary for pressure gradient calculation of all cases for all models in vertical (90°) and inclined (45°) two-phase flow. Dashed lines represent the $\pm 20\%$ error region.

From the results of the proposed data-driven drift-flux approach and other existing methods, it is clear that all models have limitations due to the nature of the drift-flux concept not being recommended for non-homogeneous flow, for instance. The models comparison from Section 5.4 reinforces that most of the multiphase flow models have limitations when being used on the conditions different to which these were developed from.

The drift-flux approach has shown to be an improved method for liquid holdup determination, however, it might not be feasible to determine the pressure gradient for a wide range of flow velocities. An application of the improved method to determine drift-flux parameters can be implemented in transient models, such as the one proposed by Tornisiello (2020), which she uses Bhagwat and Ghajar (2014) correlations to determine drift velocity and distribution coefficient. As it was seen, the results presented in this thesis have shown relatively high errors of liquid holdup prediction with Bhagwat and Ghajar (2014) correlations. Figure 5.14 illustrates the flowchart of the model algorithm by Tornisiello (2020), in which the red box shows the step that the data-driven approach would be implemented. Thus, the improved method proposed in this work can calculate steady-state liquid holdup needed to determine transient pressure change in wells.

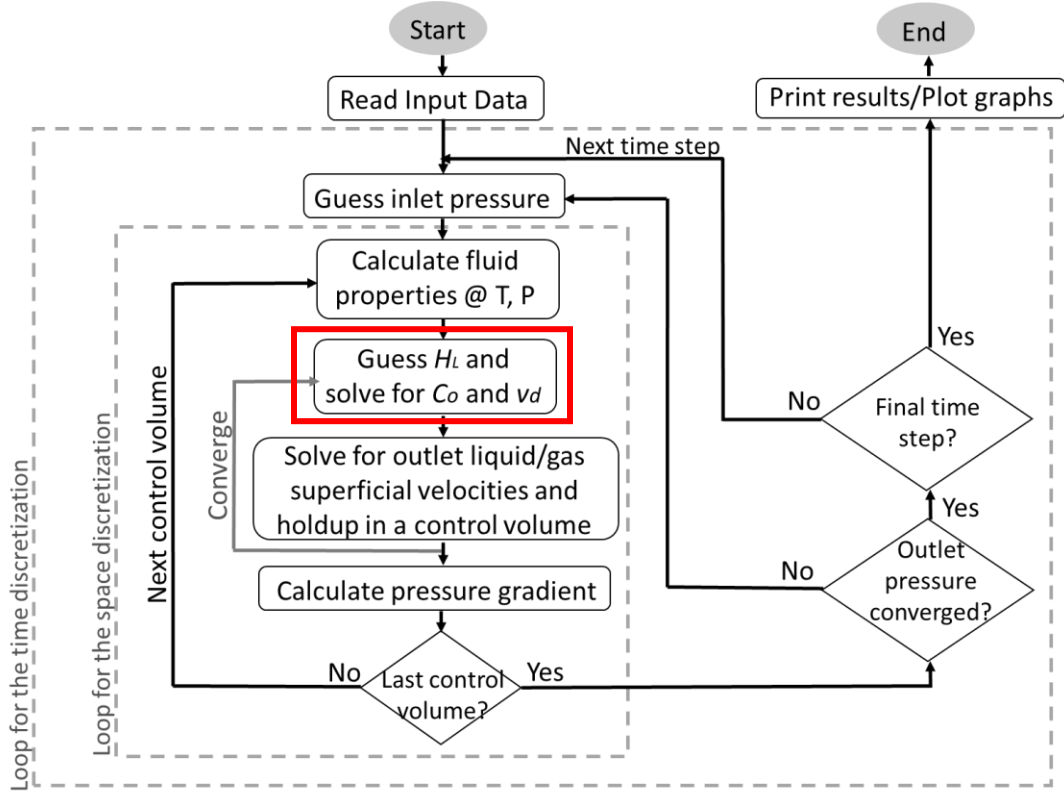


Figure 5.14. Flowchart for simplified transient multiphase flow model algorithm from Tornisiello (2020). Red box represents the step in which the data-driven approach can be implemented.

5.5. Data-Driven Approach for Direct Calculation of Pressure Gradient

Figure 5.15., Figure 5.16, and Figure 5.17. represent the pressure gradient results based on the liquid and gas velocities numbers from Equation 2.8 and Equation 2.9. As can be seen for both vertical and inclined pipes, the pressure gradient is larger for low gas velocities numbers. As the gas velocity numbers increase, the pressure gradient decreases until a minimum value. Then, it starts to increase again (as shown in Figure 2.4) as velocity keeps increasing. Figure 5.15 also shows the effect of the liquid velocity numbers on the pressure gradient. The higher the liquid number, the higher the pressure gradient, due to the increase in the gravitational component of the total pressure gradient, as a consequence of higher liquid holdup and friction.

Comparing the results from vertical ($N_{Lv}=1.72, N_{Lv}=4.4$) and inclined ($N_{Lv}=1.04, N_{Lv}=3.37, N_{Lv}=4.04$) experimental data points in Figure 5.15., it can be seen the effect of inclination. The pressure gradient results from inclined upward flow in are lower than those for vertical upward flow due to the lower gravitation component when the pipe is inclined. However, after the minimum pressure gradient point, as the gas velocity numbers increase, the pressure gradient will become less impacted by the change in inclination.

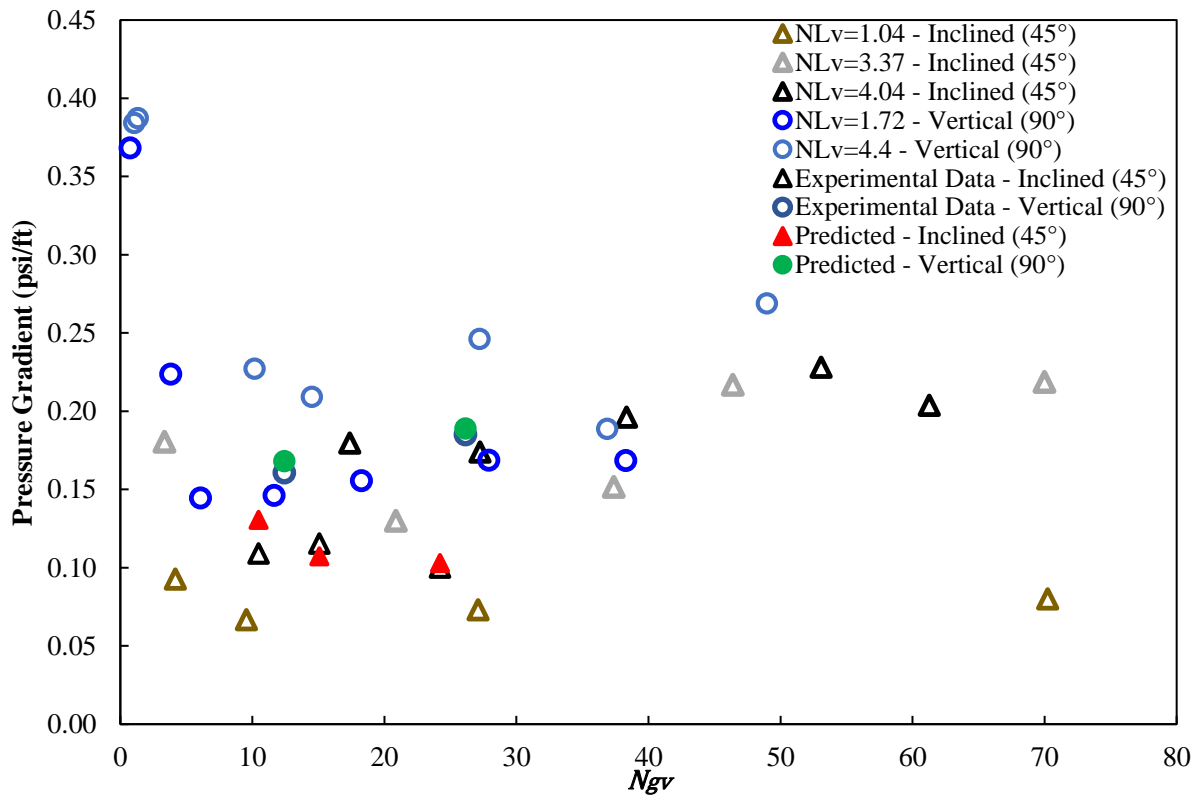


Figure 5.15. Pressure gradient versus N_{gv} for constant N_{Lv} in vertical (90°) and inclined (45°) two-phase flow.

The predicted data in Figure 5.15 for vertical (90°) and inclined (45°) pipes are the pressure gradient in (psi/ft) results for the cases listed in Table 5.5 for the direct estimation based on the regression function of the closest experimental data points in terms of gas (N_{gv}) and liquid (N_{Lv}) velocity numbers (methodology described in Figure 4.12). As pipe diameter and fluids are the

same for all testing cases, diameter ($N_d = 9.83$) and viscosity ($N_d = 0.0022$) numbers from Equation 2.10 and Equation 2.11 are not included in this evaluation:

Table 5.5. Testing cases for direct estimation of pressure gradient at vertical (90°) and inclined (45°) flow at different gas and liquid superficial velocities.

Case #	Inclination	V_{sl} (ft/s)	V_{sg} (ft/s)	Flow Regime
1	90°	1.3	6.65	Churn
2		1.3	13.9	Churn
3	45°	1.17	5.6	Slug
4		1.17	8.0	Stratified-wavy
5		1.17	13.0	Stratified-wavy

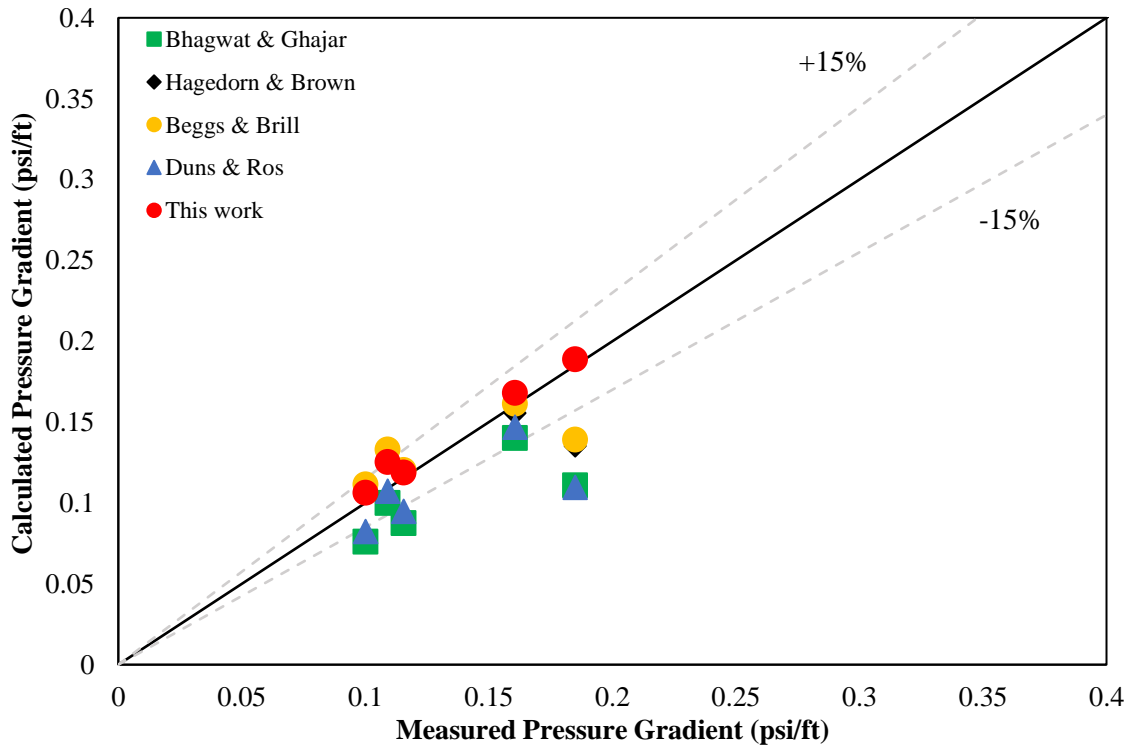


Figure 5.16. Results summary for direct estimation of pressure gradient for all cases and other models in vertical (90°) and inclined (45°) two-phase flow. Dashed lines represent the $\pm 15\%$ error region.

The data-driven method results were compared with empirical models of Beggs and Brill (1973), Duns and Ros (1963), Hagedorn and Brown (1965). As in Section 5.4, Bhagwat and

Ghajar (2014) was included in this comparison. As can be seen in Figure 5.16, the results from the data-driven approach for the direct estimation of pressure gradient have a reasonable agreement with the experimental data being within the $\pm 15\%$ errors, while the other models, such as Hagedorn and Brown (1965) and Duns and Ros (1963) have errors as large as 32%. Figure 5.17 shows the average absolute error of the pressure gradient for all results of the five cases from Table 5.5. In Figure 5.17, we notice that the data-driven approach has the lowest overall average absolute errors among the models, while Bhagwat and Ghajar (2014) resulted in the largest. However, the standard deviation for all models indicates that Bhagwat and Ghajar (2014) results are not spread as the other models, while Duns and Ros (1963) and Hagedorn and Brown (1965) presented a wide range errors when all cases are compared. The reasons for the errors of Beggs and Brill (1973), Duns and Ros (1963), and Hagedorn and Brown (1965), were discussed in the previous Section 5.4, in which the errors are mostly associated with poor flow regime prediction, homogeneous flow assumption, and effect of inclination on the performance of their models. A similar data-driven methodology was adopted by Alizadehdakhel et al. (2009), which applied Artificial Neural Networks to predict the pressure gradient in vertical and horizontal pipes. Their results presented a reasonable agreement with experimental data for a 2-inches ID pipe system with using air-water for pressure gradients above 0.1 psi/ft, but, high errors ($>40\%$) for lower pressure gradient values, possibly in the horizontal and friction dominated flow.

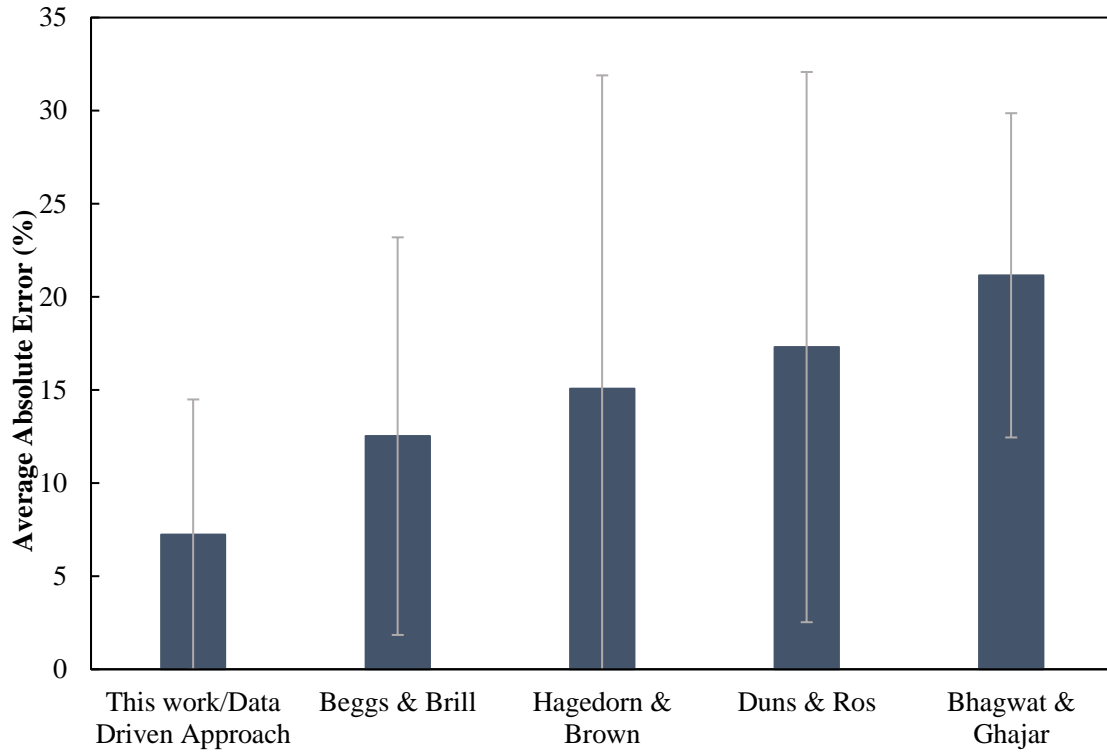


Figure 5.17. Average absolute error of pressure gradient for the Data-Driven Approach, Beggs and Brill (1973), Duns and Ros (1965), Bhagwat and Ghajar (2014), Hagedorn and Brown (1965). Error bars represent the standard deviation of pressure gradient calculation of all cases for each model.

The above results show that the direct determination of pressure gradient using this data-driven approach is expected to have significant improvements as the more data in different conditions are added to the model, such that a wide range of governing forces considered in the liquid, gas, diameter, and viscosity dimensionless numbers along with pipe inclination can be used for training and then prediction of pressure gradient in an extended range of scenarios.

6. Conclusions and Recommendations for Future Work

The models evaluation presented in this work reinforces the need for a more accurate method to predict the liquid holdup and pressure gradient for multiphase flow in pipes. Simulation results from different empirical and mechanistic models showed errors higher than 50% for liquid holdup and pressure gradient for several different flowing conditions, such as different gas and liquid velocities, and pipe inclinations.

The data-driven approach applied to the drift-flux concepts to determine liquid holdup followed by pressure gradient prediction provided a reasonable agreement with the experimental data. However, this approach is not recommended for high-velocity scenarios, since the drift-flux concept is not suitable for non-homogeneous flow, which is usually the case for annular flow regime occurring at high gas velocities. Overall, the method proposed in this work resulted in an improvement of liquid holdup prediction of at least 15% when compared with the results of other models for inclined and vertical flow. Therefore, the data-driven approach to determine drift-coefficients can be implemented in the simplified transient models having steady-state liquid holdup calculation to determine transient pressure change in pipes, such as the one proposed by Tornisiello (2020). The improved drift-flux model from Bhagwat and Ghajar (2014) shows higher than 50% for in high gas velocity flows and inclined pipe (45° with the horizontal direction).

The objective of evaluating the concept of direct determination of pressure gradient using a data-driven method was achieved. It was evident that using dimensionless numbers that account for the dynamics of two-phase flow as input for data-driven prediction has the potential of providing better results than currently used two-phase flow models. In this method, the prior determination of the flow regime, which has been the reason for inaccuracies, is not needed. The

proposed methodology resulted in lower errors for pressure gradient prediction when compared to Beggs and Brill (1973), Hagedorn and Brown (1965), Duns and Ros (1963), and Bhagwat and Ghajar (2014).

A fully-automated experimental flow loop was built and it has the capability to safely perform two-phase flow tests in different inclinations. Having an integrated database containing field and experimental data from different facilities will enable the gathering and generation of training data that will significantly improve the data-driven approach for direct estimation of the pressure gradient. The application of advanced analytic techniques, such as machine learning is a powerful tool that can be applied to large data-set having multiple driving forces numbers and can be used to improve the methodology proposed in this work.

Based on the results and conclusions of this thesis, suggestions and recommendations for future work are the following:

- Perform experiments in different inclinations, gather field and experimental data available in the literature to extend the evaluation and validate the approach proposed in this work.
- Implement a Machine-Learning algorithm (i.e ANN) to directly predict the pressure gradient, not needing prior determination of liquid holdup and flow regime. Apply this algorithm in a large amount of training data and test it for several two-phase flow conditions, including hydrocarbon fluids, different inclinations, and large pipe diameter scenarios.
- Modify the short test section and have a more accurate method to measure liquid holdup, also capable of measuring liquid fraction in horizontal flow.

- Built a test section having different inclinations in order to demonstrate the applicability of the data-driven method for direct estimation of the pressure gradient in several pipe segments, aiming to determine bottomhole pressure (inlet).

Appendix. Teles and Waltrich (2018) Model Description

A hybrid wellbore multiphase flow model has been developed at LSU to predict pressure gradient for all flow regimes in large-diameter pipes. This model consists of the combination of the model proposed by Pagan et al. (2017) for churn and annular flow for large pipe diameters, with the empirical correlation of Duns and Ros (1963) for bubbly and slug flow. In addition, the hybrid model, herein referred as Teles and Waltrich (2018) model, also accounts for the concept of large and small diameter proposed by Kataoka and Ishii (1987). The purpose was to implement the concept of large and small diameter in order to identify whether slug flow occurs or not.

The main objective of Teles and Waltrich (2018) model is to accurately predict pressure gradient for oil and gas flow along large diameter pipes with high gas-liquid-ratios, as most of the models used to determine pressure drop along wells were originally developed and validated for air and water two-phase flow in pipe diameters smaller than 8 inches.

The flow chart shown in Figure A illustrates how the algorithm of the proposed model works for the calculation of pressure in each section of the well. This algorithm is deployed for each length increment from a known pressure (for instance, from the wellhead) to the bottom of the well. In the previous report from LSU to BOEM (Waltrich et al., 2017 - Award M15PC00007), the main conclusion of that experimental study was that any wellbore flow correlation tested would provide errors lower than 10% for superficial velocity ratios lower than the unit ($V_{sg}/V_{sl} < 1$). Thus, for ratios lower than the unit, the model of Duns and Ros (1963) is selected to calculate the pressure gradient in the wellbore for small diameters and any flow regime.

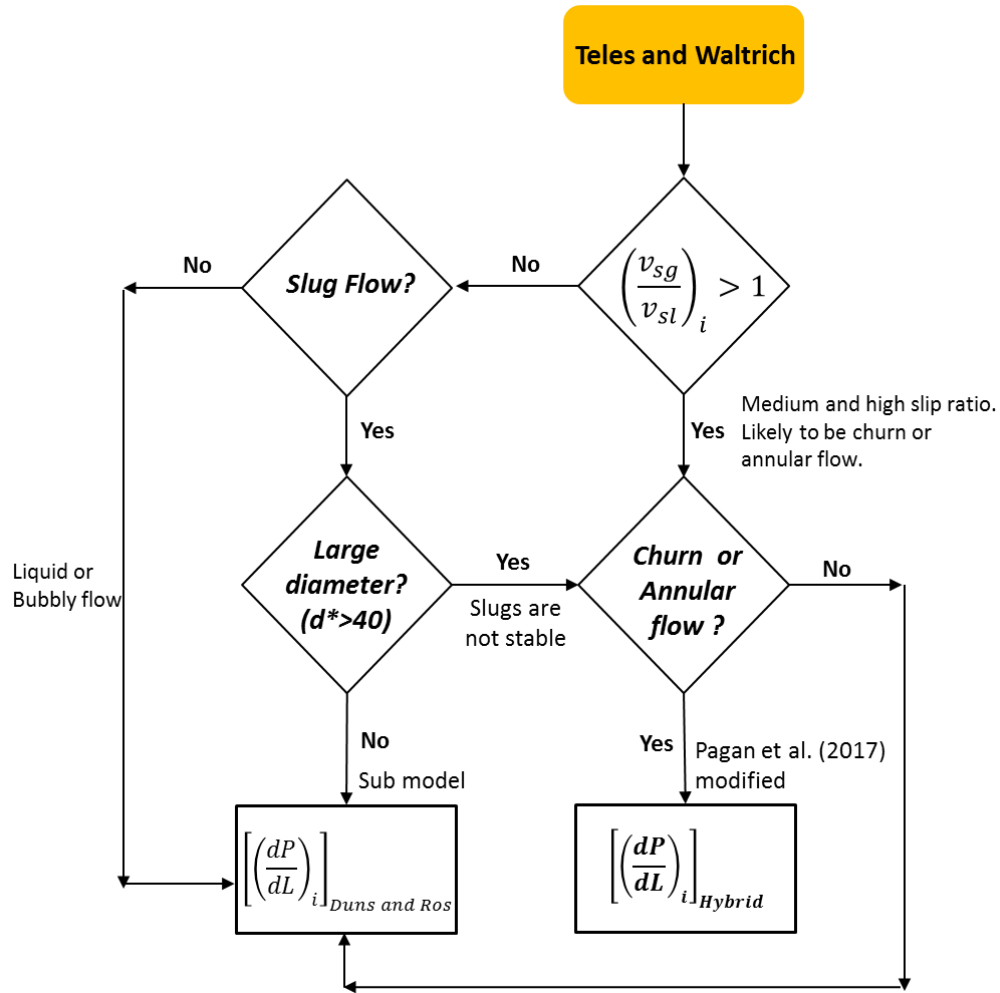


Figure A. Teles and Waltrich model workflow. The model uses Pagan et al. (2017) approach for churn and annular flow. The chosen sub model for bubbly and slug flow in this study is Duns and Ros (1963).

References

- Alizadehdakhel, A., Rahimi, M., Sanjari, J., & Alsairafi, A. A. (2009). CFD and Artificial Neural Network Modeling of Two-Phase Flow Pressure Drop. *International Communications in Heat and Mass Transfer*, 36(8), 850-856. <https://doi-org.libezp.lib.lsu.edu/10.1016/j.icheatmasstransfer.2009.05.005>
- Al-Naser, M., Elshafei, M., & Al-Sarkhi, A. (2015). Two-Phase Flow Regimes Identification Using Artificial Neural Network with Nonlinear Normalization. In *Proceedings of the 2nd International Conference on Fluid Flow, Heat and Mass Transfer*.
- Al-Naser, M., Elshafei, M., & Al-Sarkhi, A. (2016). Artificial Neural Network Application for Multiphase Flow Patterns Detection: A new approach. *Journal of Petroleum Science and Engineering*, 145, 548-564.
- Ansari, A. M., Sylvester, N. D., Sarica, C. Shoham, O., & Brill, J. P. (1994). A Comprehensive Mechanistic Model for Upward Two-Phase Flow in Wellbores. *SPE Production and Facilities*, 9 (02): 143-152. SPE-20630-PA. <http://dx.doi.org/10.2118/20630-PA>
- Asheim, H. (1986). MONA, An Accurate Two-Phase Well Flow Model Based on Phase Slippage. *SPE Production Engineering*, 1(03), 221-230. doi:10.2118/12989-PA
- Aziz, K., & Govier, G. W. (1972). Pressure Drop In Wells Producing Oil And Gas. *Journal of Canadian Petroleum Technology*, 11(03). doi:10.2118/72-03-04
- Barnea, D. (1986). Transition from Annular Flow and From Dispersed Bubble Flow-Unified Models for the Whole Range of Pipe Inclinations. *International Journal of Multiphase Flow*, 12(5), 733-744. [https://doi-org.libezp.lib.lsu.edu/10.1016/0301-9322\(86\)90048-0](https://doi-org.libezp.lib.lsu.edu/10.1016/0301-9322(86)90048-0)
- Barnea, D., Shoham, O., Taitel, Y., & Dukler, A. E. (1985). Gas-Liquid Flow in Inclined Tubes: Flow Pattern Transitions for Upward Flow. *Chemical Engineering Science*, 40(1), 131-136. [https://doi-org.libezp.lib.lsu.edu/10.1016/0009-2509\(85\)85053-3](https://doi-org.libezp.lib.lsu.edu/10.1016/0009-2509(85)85053-3)
- Beggs, D. H., & Brill, J. P. (1973). A Study of Two-Phase Flow in Inclined Pipes. *Journal of Petroleum Technology*, 25(05), 607-617. doi:10.2118/4007-PA
- Bendiksen, K. H., Maines, D., Moe, R., & Nuland, S. (1991). The Dynamic Two-Fluid Model OLGA: Theory and application. *SPE Production Engineering*, 6(02), 171-180. doi:10.2118/19451-PA

- Bhagwat, S. M., & Ghajar, A. J. (2014). A Flow Pattern Independent Drift Flux Model Based Void Fraction Correlation for a Wide Range of Gas–Liquid Two Phase Flow. *International Journal of Multiphase Flow*, 59, 186-205.
- Bonnecaze, R. H., Erskine Jr, W., & Greskovich, E. J. (1971). Holdup and Pressure Drop for Two-Phase Slug Flow in Inclined Pipelines. *AIChE Journal*, 17(5), 1109-1113.
- Brauner, N., & Barnea, D. (1986). Slug/Churn Transition in Upward Gas-Liquid Flow. *Chemical Engineering Science*, 41(1), 159-163. [https://doi-org.libezp.lib.lsu.edu/10.1016/0009-2509\(86\)85209-5](https://doi-org.libezp.lib.lsu.edu/10.1016/0009-2509(86)85209-5)
- Brill, J. P., & Arirachakaran, S. J. (1992). State of the Art in Multiphase Flow. *Journal of Petroleum Technology*, 44(05), 538-541. doi:10.2118/23835-PA
- Cavalcante, P. S. (2020). The Dynamics of Drilling Fluid Rheology, Wellbore Flow, and Formation Pressure in Well Control. Texas A&M University.
- Chierici, G. L., Ciucci, G. M., & Sclocchi, G. (1974). Two-Phase Vertical Flow in Oil Wells- Prediction of Pressure Drop. *Journal of Petroleum Technology*, 26(08), 927-938. doi:10.2118/4316-PA
- Choi, J., Pereyra, E., Sarica, C., Lee, H., Jang, I. S., & Kang, J. (2013). Development of a Fast Transient Simulator for Gas–Liquid Two-Phase Flow in Pipes. *Journal of Petroleum Science and Engineering*, 102, 27-35. doi: <https://doi.org/10.1016/j.petrol.2013.01.006>
- Duns, H., Jr., & Ros, N. C. J. (1963). Vertical Flow of Gas and Liquid Mixtures in Wells. In *6th World Petroleum Congress*. World Petroleum Congress.
- Espanol, J. H., Holmes, C. S., & Brown, K. E. (1969). A Comparison of Existing Multiphase Flow Methods for the Calculation of Pressure Drop in Vertical Wells. In *Fall Meeting of the Society of Petroleum Engineers of AIME*. Society of Petroleum Engineers. doi:10.2118/2553-MS
- Fancher Jr, G. H., & Brown, K. E. (1962). Prediction of Pressure Gradients for Multiphase Flow in Tubing. In *Fall Meeting of the Society of Petroleum Engineers of AIME*. Society of Petroleum Engineers. doi:10.2118/440-PA
- Gokcal, B., Al-Sarkhi, A. S., & Sarica, C. (2009). Effects of High Oil Viscosity on Drift Velocity for Horizontal and Upward Inclined Pipes. *SPE Projects, Facilities & Construction*, 4(02), 32-40. doi:10.2118/115342-PA
- Govier, G. W., & Aziz, K. (2008). *The Flow of Complex Mixtures in Pipes*. Society of Petroleum Engineers.

- Govier, G. W., & Short, W. L. (1958). The Upward Vertical Flow of Air-Water Mixtures: II. Effect of tubing diameter on flow-pattern, holdup and pressure drop. *The Canadian Journal of Chemical Engineering*, 36(5), 195-202. doi:10.1002/cjce.5450360501
- Gray, H. E. (1974). Vertical Flow Correlation in Gas Wells. User's Manual for API B, 14.
- Griffith, P., & Wallis, G. B. (1961). Two-Phase Slug Flow. *Journal of Heat Transfer*, 83(3), 307–318. <https://doi.org/10.1115/1.3682268>
- Guet, S., & Ooms, G. (2005). Fluid Mechanical Aspects of the Gas-Lift Technique. *Annual Review of Fluid Mechanics*, 38(1), 225-249. doi:10.1146/annurev.fluid.38.061505.093942
- Hagedorn, A. R., & Brown, K. E. (1965). Experimental Study of Pressure Gradients Occurring During Continuous Two-Phase Flow in Small-Diameter Vertical Conduits. *Journal of Petroleum Technology*, 17(04), 475-484. doi:10.2118/940-PA
- Hasan, A. R., Kabir, C. S., & Sayarpour, M. (2007). A Basic Approach to Wellbore Two-Phase Flow Modeling. In *SPE Annual Technical Conference and Exhibition*. Society of Petroleum Engineers. doi:10.2118/109868-MS
- Hasan, A. R., Kabir, C. S., & Sayarpour, M. (2010). Simplified Two-Phase Flow Modeling in Wellbores. *Journal of Petroleum Science and Engineering*, 72(1-2), 42-49. <https://doi.org/10.1016/j.petrol.2010.02.007>
- Hibiki, T., & Ishii, M. (2003). One-Dimensional Drift-flux Model for Two-phase Flow in a Large Diameter Pipe. *International Journal of Heat and Mass Transfer*, 46(10), 1773-1790. doi: 10.1016/j.ijmultiphaseflow.2011.11.004
- Hibiki, T., Ishii, M., & Xiao, Z. (2001). Axial Interfacial Area Transport of Vertical Bubbly Flows. *International Journal of Heat and Mass Transfer*, 44(10), 1869-1888. [https://doi.org/10.1016/S0017-9310\(00\)00232-5](https://doi.org/10.1016/S0017-9310(00)00232-5)
- ISO/IEC Guide 98, Guide to the Expression of Uncertainty in Measurement, (1998). Geneva, Switzerland: Iso.
- Jayanti, S., & Hewitt, G. F. (1992). Prediction of the Slug-to-Churn Flow Transition in Vertical Two-Phase Flow. *International Journal of Multiphase Flow*, 18(6), 847-860. [https://doi.org/10.1016/0301-9322\(92\)90063-M](https://doi.org/10.1016/0301-9322(92)90063-M)
- Jayanti, S., & Brauner, N. (1994). Churn flow. *Multiphase Science and Technology*, 8(1-4). doi:10.1615/MultScienTechn.v8.i1-4.90

- Kataoka, I., & Ishii, M. (1987). Drift Flux Model for Large Diameter Pipe and New Correlation for Pool Void Fraction. *International Journal of Heat and Mass Transfer*, 30(9), 1927-1939. [https://doi.org.libezp.lib.lsu.edu/10.1016/0017-9310\(87\)90251-1](https://doi.org.libezp.lib.lsu.edu/10.1016/0017-9310(87)90251-1)
- Knudsen, J. G., & D. L. Katz. (1958). *Fluid Dynamics and Heat Transfer*, McGraw-Hill.
- Mukherjee, H., & Brill, J. P. (1999). Multiphase Flow in Wells. *Society of Petroleum Engineers of AIME*.
- Mohammadi, S., Papa, M., Pereyra, E., & Sarica, C. (2019). Genetic Algorithm to Select a Set of Closure Relationships in Multiphase Flow Models. *Journal of Petroleum Science and Engineering*, 181, 106224. <https://doi.org/10.1016/j.petrol.2019.106224>
- Mukherjee, H., & Brill, J. P. (1985). Pressure Drop Correlations for Inclined Two-Phase Flow. *Journal of Energy Resources Technology*, 107(4), 549-554. doi:10.1115/1.3231233
- Musaab M. A., & Mohammed A. A. (2014). A Comprehensive Study on the Current Pressure Drop Calculation in Multiphase Vertical Wells; Current Trends and Future Prospective. *Journal of Applied Sciences*, 14: 3162-3171. doi: 10.3923/jas.2014.3162.3171
- Nagoo, A. S. (2014). *Pipe Fractional Flow Theory: Principles and Applications* (Doctoral dissertation). The University of Texas at Austin.
- OLGA Dynamic Multiphase Flow Simulator. (2000). Schlumberger.
- Omebere-Iyari, N. K., Azzopardi, B. J., & Ladam, Y. (2007). Two-Phase Flow Patterns in Large Diameter Vertical Pipes at High Pressures. *AIChE Journal*, 53(10), 2493-2504. <https://doi.org/10.1002/aic.11288>
- Orkiszewski, J. (1967). Predicting Two-Phase Pressure Drops in Vertical Pipe. *Journal of Petroleum Technology*, 19(06), 829-838. doi:10.2118/1546-PA
- Osman, E. S. A. (2004). Artificial Neural Network Models for Identifying Flow Regimes and Predicting Liquid Holdup in Horizontal Multiphase Flow. *SPE Production & Facilities*, 19(01), 33-40. doi:10.2118/86910-PA
- Pagan, E., Williams, W. C., Kam, S., & Waltrich, P. J. (2017). A Simplified Model for Churn and Annular Flow Regimes in Small-and Large-Diameter Pipes. *Chemical Engineering Science*, 162, 309-321. <https://doi.org/10.1016/j.ces.2016.12.059>
- Qi, D., Zou, H., Ding, Y., Luo, W., & Yang, J. (2018). Engineering Simulation Tests on Multiphase Flow in Middle-and High-Yield Slanted Wellbores. *Energies*, 11(10), 2591.

- Rao, B. (1998). Multiphase Flow Models Range of Applicability. *CTES, LC*.
- Reinicke, K. M., Remer, R. J., & Hueni, G. (1987). Comparison of Measured and Predicted Pressure Drops in Tubing for High-Water-Cut Gas Wells. *SPE Production Engineering*, 2(03), 165-177. doi:10.2118/13279-PA
- Ros, N. C. J. (1961). Simultaneous Flow of Gas and Liquid as Encountered in Well Tubing. *Journal of Petroleum Technology*, 13(10), 1-037. doi:10.2118/18-PA
- Roullier, D., Karami, H., Pereyra, E., & Sarica, C. (2018). Existence of Slug Flow in Vertical Co-Current Two-Phase Flow. In *11th North American Conference on Multiphase Production Technology*. BHR Group.
- Sawai, T., Kaji, M., Kasugai, T., Nakashima, H., & Mori, T. (2004). Gas–Liquid Interfacial Structure and Pressure Drop Characteristics of Churn Flow. *Experimental Thermal and Fluid Science*, 28(6), 597-606. <https://doi.org/10.1016/j.expthermflusci.2003.09.003>.
- Schlegel, J. P., Sawant, P., Paranjape, S., Ozar, B., Hibiki, T., & Ishii, M. (2009). Void Fraction and Flow Regime in Adiabatic Upward Two-Phase Flow in Large Diameter Vertical Pipes. *Nuclear Engineering and Design*, 239(12), 2864-2874.
- Schoppa, W., Zabaras, G. J., Menon, R., & Wicks, M. (2013, May). Gaps and advancements for Deepwater Production and Remote Processing: Large Diameter Riser Laboratory Gas-Lift Tests. In *Offshore Technology Conference*. Offshore Technology Conference. doi:10.4043/23968-MS
- Sharaf, S., van der Meulen, G. P., Agunlejika, E. O., & Azzopardi, B. J. (2016). Structures in Gas–Liquid Churn Flow in a Large Diameter vertical Pipe. *International Journal of Multiphase Flow*, 78, 88-103. <https://doi.org/10.1016/j.ijmultiphaseflow.2015.09.005>.
- Shen, X., Hibiki, T., & Nakamura, H. (2015). Bubbly-to-Cap Bubbly Flow Transition in a Long-26 m Vertical Large Diameter Pipe at Low Liquid Flow Rate. *International Journal of Heat and Fluid Flow*, 52, 140-155. <https://doi.org/10.1016/j.ijheatfluidflow.2015.01.001>
- Shi, H., Holmes, J. A., Durlofsky, L. J., Aziz, K., Diaz, L., Alkaya, B., & Oddie, G. (2005). Drift-Flux Modeling of Two-Phase Flow in Wellbores. Society of Petroleum Engineers. doi:10.2118/84228-PA
- Shippen, M., & Bailey, W. J. (2012). Steady-State Multiphase Flow: Past, Present, and Future, with a Perspective on Flow Assurance. *Energy & Fuels*, 26(7), 4145-4157.
- Shoham, O. (2006). *Mechanistic Modeling of Gas-Liquid Two-Phase Flow in Pipes*. Richardson, TX: Society of Petroleum Engineers (Reprint).

- Sigaki Capovilla, M. (2018). *Two-Phase Flow Regime Map for Large Diameter Pipes and High-Velocity Flows*. [Louisiana State University]. https://digitalcommons.lsu.edu/gradschool_theses/4726
- SPE. (2015). Calculation of Worst-Case Discharge (WCD). Society of Petroleum Engineers.
- Taitel, Y., Bornea, D., & Dukler, A. E. (1980). Modelling Flow Pattern Transitions for Steady Upward Gas-Liquid Flow in Vertical Tubes. *AIChE Journal*, 26(3), 345-354. <https://doi.org/10.1002/aic.690260304>
- Tang, H., Bailey, W. J., Stone, T., & Killough, J. (2019). A Unified Gas/Liquid Drift-flux Model for All Wellbore Inclinations. *SPE Journal*. doi:10.2118/197068-PA
- Teles, F.B.X., Waltrich, P. J., Capovilla, M. S., Gupta, I., and Hughes, R. (2018). “Development and Improvement of Flow Models Applied to Multiphase Flows in Large-diameter Pipes and High-velocity Flows,” Report prepared under BOEM Award M17PX00030 by Louisiana State University, US Department of the Interior - Bureau of Ocean Energy Management. <https://www.boem.gov/sites/default/files/oil-and-gas-energy-program/Resource-Evaluation/Worst-Case-Discharge/Louisiana-State-University-Final-Report-08-29-18.pdf>
- Tornisiello, L. (2020). Development and Validation of a Simplified Transient Two-Phase Flow Model for Any Pipe Inclination. (Master’s Thesis, Louisiana State University). https://digitalcommons.lsu.edu/gradschool_theses/5045
- Turney, D. E., Kalaga, D. V., Ansari, M., Yakobov, R., & Joshi, J. B. (2018). Reform of the Drift-Flux Model of Multiphase Flow in Pipes, Wellbores, and Reactor Vessels. *Chemical Engineering Science*, 184, 251-258.
- Waltrich, P. J. (2012). Onset and Subsequent Transient Phenomena of Liquid Loading in Gas Wells: Experimental Investigation Using a Large Scale Flow Loop. Texas A&M University.
- Waltrich, P. J., Capovilla, M. S., Lee, W., de Sousa, P. C., Zulqarnain, M., Hughes, R., ... & Singh, J. (2019). Experimental Evaluation of Wellbore Flow Models Applied to Worst-Case-Discharge Calculations for Oil Wells. *SPE Drilling & Completion*. doi:10.2118/184444-PA
- Waltrich, P. J., Capovilla, M. S., Lee, W., Zulqarnain, M., Hughes, R., Tyagi, M., ... & Nguyen, H. (2017). Experimental Evaluation of Wellbore Flow Models Applied to Worst-Case-Discharge Calculations. In *SPE Health, Safety, Security, Environment, & Social Responsibility Conference-North America*. Society of Petroleum Engineers. doi:10.2118/184444-MS

- Waltrich, P. J., Falcone, G., & Barbosa Jr, J. R. (2013). Axial Development of Annular, Churn and Slug Flows in a Long Vertical Tube. *International Journal of Multiphase Flow*, 57, 38-48. <http://dx.doi.org/10.1016/j.ijmultiphaseflow.2013.06.008>
- Waltrich, P. J., Zhang, H., & Teodoriu, C. (2014). Remote Real-time Experimental Diagnostics for Well Challenges. In *SPE Annual Technical Conference and Exhibition*. Society of Petroleum Engineers. doi:10.2118/170953-MS
- Zuber, N., & Findlay, J. A. (1965). Average Volumetric Concentration in Two-Phase Flow Systems. ASME. *Journal of Heat Transfer*, 87(4), 453–468. <https://doi.org/10.1115/1.3689137>

Vita

Francisco Bruno Xavier Teles received his Bachelor's degree in Petroleum Engineering from Universidade Federal do Ceara (UFC). He was accepted into the Louisiana State University Petroleum Engineering program where he anticipates graduating with his Master's degree in May 2020.